A Numerical Wave Model for the Refraction and Diffraction of Irregular Waves, Part II.

Numerical Experiments of the Wave Model CREON

Werkdocument: RIKZ/OS-94.140x

Q. Gao
A.C. Radder
N. Booij

Ingenieursbureau SEPRA
Rijkswaterstaat, RIKZ
Delft University of Technology

A Numerical Wave Model for the Refraction and Diffraction of

Irregular Waves, Part II.

Numerical Experiments of the Wave Model CREON

Q. Gao[1]   A.C. Radder[2]   N. Booij[3]

Report to: RIKZ, Rijkswaterstaat

Project: Hydra, RKZ-003

Date: 2 August 1994

1.   Ingenieursbureau SEPRA
     Veursestraatweg 77, Leidschendam
     The Netherlands

2.   Ministry of Transport and Public Works, Rijkswaterstaat,
     RIKZ, Koningskade 4, The Hague,
     The Netherlands

3.   Delft University of Technology,
     Faculty of Civil Engineering,
     Group of Hydraulic Engineering, Stevinweg 1,
     Delft, The Netherlands

Abstract

The numerical wave model CREON is developed to predict the propagation and transformation of wave properties in shallow water. In Gao *et al.* (1993), which is referred to as Part I in the following, a description is given of the theoretical and numerical treatment of the model. In the present report, we present various computational results.

The model is applied to wave penetration behind breakwaters, to evaluate the combined effects of wave diffraction and directional spreading. The performance of the model in moving media such as currents is tested. The results of the model in case of a jetlike flow are discussed based upon the concept of ray theory. An extensive numerical investigation is carried out for the combined current-depth refraction in the tidal inlet of Texel. To assess the applicability to waves in a coastal area, two hindcasts are carried out in the Rhine estuary Haringvliet, where well-documented wave data are available for comparison.

The model has a wide range of applicability and the test results show that the model has a reasonably good performance in various situations. However, results of a comparison with the spectral models HISWA and SWAN in the tidal inlet of Texel show much lower wave heights in the CREON computations. No simple explanation could be found for this behaviour, and field data are needed to verify the various computational results.

2

Contents

1. Introduction

From October to early next year, severe storms frequently pass over the North Sea. They may enrage the sea state and excite destructive waves. Some parts of the coast of the Netherlands are especially vulnerable to perpetual onslaught of such waves. The breakwater is a structure intended to reduce the influence of waves. For consideration of safety and economical design, engineers want to know in advance the possible wave field behind the breakwater before it is built. A combined refraction-diffraction wave model shall be able to solve such a practical problem. In section two we describe the application of the model to different breakwaters and different incident waves.

Wave-current interaction is very important in engineering practice. Currents have various effects on waves, one of which is the well-known Doppler effect on velocity of the wave propagation. Waves propagating on currents undergo lengthening and shortening, increasing or dispersing wave energy. An important difference of waves on currents from the still-water case is that wave energy is not conserved, since wave energy is transferred between waves and currents through radiation stresses. However, Bretherton & Garrett (1968) showed that the total action of waves is conserved. Since then, numerous theories and laboratory studies have contributed to the description of wave-current interaction, c.f. Whitham (1974), Peregrine (1976). In section three, we first carry out a validation study of the model, then we devote attention to waves moving opposite to a jetlike stream in deep water. The wave-current interaction on oceanic scale has received several studies, c.f. Hayes (1980), Tolman (1992). But most reported accidents are those occurring near the Agulhas current. Mallory (1974) reported extensive damage or destruction of ships by giant waves on this current. However, only Smith (1976) and Peregrine & Smith (1979) have qualitatively estimated such giant waves through theoretical analysis. To date, no numerical modelling of such sea states has yet been reported, and this motivates us to investigate numerically such giant waves on a jetlike flow.

In the past three decades, ray methods are commonly used to obtain wave parameters in the coastal area. However, ray theory predicts singularities when currents are non-uniform and sea bottoms are irregular, for full discussion see Peregrine & Jonsson (1983). Ray methods fail in such cases and local remedy seems not to be able to solve the whole problem. The combined depth-current refraction is the most important part of the present study. In

the North Sea, tidal currents are the main subject for the study of wave-current interaction because the tidal currents are considered to have a uniform velocity profile along the depth, c.f. Vogel *et al.* (1988). In section four, we present numerical results of various wave conditions in the tidal inlet of Texel.

When waves enter a coastal area, wave conditions are dominated by a number of physical processes. Apart from refraction and diffraction, wave breaking and bottom friction can simultaneously reduce wave height, local wind can enhance the waves appreciably. Therefore, the model shall account for these effects and its applicability shall be assessed. In section five, two hindcasts of wave conditions are applied to the Rhine estuary Haringvliet, where wave data are available for comparison with the model results.

Finally, we draw conclusions in section six.

In this report, the term 'regular waves' has the same meaning as that of 'monochromatic waves', and 'irregular waves' means that the waves are composed of one frequency component and several directional components.

2. Wave field behind breakwaters

Waves behind breakwaters may induce sediment movement, to erode one part of the coast and to build land for the other part. Waves may enter a harbour basin, making loading or unloading of ships impossible. Recently, it is found that random in stead of regular incident waves cause different wave fields behind breakwaters, c.f. Goda (1985). In principle, semi-analytical solutions are possible for such wave fields, see Mei(1983, Chapter 10), Dalrymple & Martin (1992), but a numerical method seems more convenient to deal with practical situations.

We consider here two kinds of incident waves, i.e. regular and irregular waves. The directional spreading of the irregular waves is according to $\cos^4\theta$. Wave dissipation is not considered.

The depth is thought to be uniform, d=10m. The incident waves have height h_s=1m, period T=7s and length L=60m. The computational area is 1200*1200 m^2. The resolution in direction is 15^0, in space Δx=10m and Δy=5m. In the following we discuss wave fields corresponding to three different breakwaters.

Case one concerns waves passing over submerged obstacles. The wave height will be dramatically reduced through wave breaking

5

and reflection due to sudden decrease of depth. Behind the obstacle, wave breaking induces turbulence or eddies, which may further draw wave energy away. In the model these processes are simply modelled by a transmission coefficient. Fig.2.1 and Fig.-2.2 show two kinds of incident waves passing over a submerged obstacle, which has a width of 720m. The transmission coefficient is chosen to be 20 percent of the incident waves, and the wave heights on two cross sections x=480m and x=1080m are also plotted. The differences between the two kinds of waves are shown in Fig. 2.3.

Case two is a semi-infinite breakwater that is an example for protection of the coastal line. The breakwater is perpendicular to the direction of incident waves. The computational area is divided into two parts, one part is the so-called illuminated region and the other part the shadow region, which is behind the breakwater. Fig. 2.4 and Fig. 2.5 show the wave fields in the computational area. When the waves pass the breakwater, part of them is diffracted, causing the wave field in the illuminated region to oscillate. For the monochromatic waves the wave field in the shadow region is purely induced by wave diffraction. Waves decrease quickly with the increase of diffraction distance. The wave behaviour in the computational area is consistent with that of semi-analytical results of Mei (1983). The irregular waves can more directly penetrate into the shadow region. The differences between the two kinds of waves can be as high as 40 percent of the incident waves, as shown in Fig. 2.6.

Case three consists of waves passing through a gap of two breakwaters. Breakwaters for a sea harbour may be an example, a second example is that waves pass through a narrow strait and arrive at a wide water area on the other side, as will be seen in section four. The gap has width 120m, about 2 wave lengths. The wave fields are shown in Fig. 2.7 and Fig. 2.8. The monochromatic waves penetrate a longer distance in the illuminated region than the irregular waves, but the latter have wide spreading in the shadow region. The differences on the two cross sections are shown in Fig.2.9.

From above calculations we confirm that the two kinds of waves indeed induce different wave fields behind breakwaters, and the irregular waves are more effective to transmit energy into the shadow region than monochromatic waves. Case two and case three have been discussed numerically by a number of workers, and our computational results are consistent with that of Goda (1985) and Zhao & Anastasiou (1993).

3. Wave-current interaction

Following the common presumption, the scales of the currents are much larger than that of the waves. This leads to the consideration that currents are uniform and steady in local scale. When waves moving on such large scale currents, the changes of wave parameters can be described by the Doppler shift:

$$\omega = \sigma + K \cdot U \tag{3.1}$$

with

$$\sigma^2 = gk \tanh kd \tag{3.2}$$

where ω is the angular frequency in a fixed frame, and σ the frequency relative to the water moving with the current velocity, U the current velocity, K the wave number and d the water depth. From eq.(3.1) k can be solved numerically, e.g. using the well-known Newton-Raphson iterative method.

Analytical solutions exist only for a few simple cases, see Brevik (1980). Fig. 3.1 shows wave height versus wave propagation distance when waves moving upstream, Fig. 3.1(a), and downstream Fig. 3.1(b). The uniform currents only have velocity in x-direction, u=0 at x=0 and u= +/- 1 m/s at x=1000m. The numerical results are comparable with the analytical solution.

The changes in direction of the waves moving on a horizontal shear flow can also be tested. The linear shear flow is only in y-direction, with v=0 at x=0 and v=1m/s at x=500m. Waves propagate down- or upstream with a component parallel to the flow.

The analytical solution of wave direction in the linear shear flow can be derived from Snell's law:

$$\cos \theta = \frac{1}{\beta_0^2} (\beta_0^4 - \sin^2 \theta_0)^{1/2} \tag{3.3}$$

with

$$\beta_0 = (1 - \frac{v \cdot \sin \theta_0}{C_0}) \tag{3.4}$$

where θ_0 is the incident angle of waves at x=0 and C_0 the initial phase velocity. Fig. 3.2 shows waves propagating downstream initially at an incident angle 30° with x-axis and Fig. 3.3 waves propagating upstream initially at an angle -30°. Fig. 3.2(a) and

7

Fig. 3.3(a) show a correct transmission of the waves through both boundaries, without any distortion of the wave field.

The comparison is shown in Figs. 3.2(b) and 3.3(b). The figures also indicate that waves are refracted to weaker currents when waves have a downstream component and refracted into stronger currents when they have an upstream component. In Part I, we have fully discussed depth refraction by an elliptical shoal. The computations of the model are compared with the observations from a hydraulic model. The pure current refraction will be discussed in the rest of this section.

Peregrine (1976) and Peregrine & Jonsson (1983) fully discussed the incapability of the simple refraction theory in dealing with non-uniform currents. When waves move upstream on a jetlike flow, waves are refracted into the main stream and the ray method predicts singularities, which are so-called caustics, as shown in Fig.3.4. Recently, so-called combined spectral-refraction models are widely used to calculate waves riding on currents, see Vogel et al.(1988), Tolman (1992). Because of neglecting wave diffraction, it is questionable whether the spectral-refraction models can correctly solve the problem of wave-current interaction.

The wave behaviour near caustics has been treated in several studies, c.f Smith (1976) and Peregrine & Smith (1979). On a jetlike flow it is found that waves near caustics have the behaviour of Airy function. This means that waves vary rapidly along transverse section. But these studies are far from the engineering practice. The combined refraction-diffraction model enables us to investigate fully the wave properties on caustics. We assume here the flow independent of x-direction, in y-direction the flow has the form

$$u = u_0 (1 - y^2), \quad with \quad -1 \leq y \leq 1. \tag{3.5}$$

Following the large scale assumption, the flow has width 5000m, with maximum velocity at y=2500m; water depth d=100m; incident wave height h_s=1m and mean direction θ=0. We calculate both regular and irregular waves. The latter have the same directional spreading and resolution as in section two. Again, wave dissipation is not considered, although wave breaking may become significant near caustics.

Fig. 3.5 to Fig. 3.7 show the incident waves, with period T=10s, moving upstream on a jetlike flow, which has maximum velocity in the main stream of u_0=-2m/s. Along the cross sections waves do vary rapidly and the large waves occupy very tiny width comparing with that of the flow, as shown in Figs. 3.6(b) and 3.7(b). The

8

theoretical analysis indicates that waves along a transverse section have the behaviour of Airy function, however, our numerical results indicate that along the main stream, waves, as shown in Fig. 3.6(a)-3.7(a), Fig.3.8-3.10, also behave like Airy function. Wave height increases monotonously until a maximum height, then decreases dramatically and wave pattern oscillates with the distance. Wave intensity caused by energy convergence is noticeable and important. The height amplification has a factor of 4.8 and 2.6 respectively for monochromatic and irregular waves. The former is comparable with the theoretical estimate of a factor 4 (Smith, 1976).

No:	type	$H_{s,max}$	T	U_0	wind	dis.
1	reg.	4.80m	10s	-2m/s	no	no
2	irreg.	2.62m	10s	-2m/s	no	no
3	reg.	4.45m	10s	-2.4m/s	no	no
4	irreg.	2.50m	10s	-2.4m/s	no	no
5	reg.	5.2m	10s	-1.6m/s	no	no
6	irreg.	2.95m	10s	-1.6m/s	no	no
7	reg.	4.46m	7s	-2.0m/s	no	no
8	irreg.	2.64m	7s	-2.0m/s	no	no
9	reg.	6.86m	10s	-2.0m/s	20m/s	no
10	irreg.	4.20m	10s	-2.0m/s	20m/s	no

Table 3.1 maximum wave height in different situations. reg: regular waves; irreg: irregular waves; dis: dissipations.

According to the concept of caustics of the ray theory, the successive crossing points of rays form the curves known as caustics. In the smoothly varying refractive medium, two caustics can only begin with a cusp, see Fig. 3.4(b). In the cusp one finds waves reaching their maximum height, then it separates into two caustics and one will find two equal maxima. Because waves are refracted to the caustics, waves in the main stream are reduced drastically as the distance between the two caustics increase, as shown in Fig. 3.6-3.12. These results indicate that the computations are well consistent with the concept of the ray theory. In principle, irregular waves have the same behaviour as monochromatic waves, as shown by Fig. 3.7(a), but the former may be more complicated. Fig. 3.7(b) shows along the cross sections that there are three near equal maxima, but 1000m further they are

reduced to two maxima with increase of the width. The edges of the flow form a good example of a wave guide, as waves are indeed trapped in the current.

Fig. 3.8 shows waves in the case of 20 percent increase in the current velocity, i.e. u_0= -2.4m/s. Comparing with Fig. 3.6 and Fig. 3.7, waves travel a shorter distance before they reach their maximum. Fig. 3.9 shows that waves travel a longer distance in a current with smaller velocity, u_0=-1.6m/s. Fig. 3.10 gives an incident wave with period T=7s. The above examples indicate that changes in current velocities do not much affect the maximum wave heights if the currents do not stop waves, see table 3.1.

Fig. 3.11 and Fig. 3.12 show results for a wind with a velocity 20m/s in the wave direction. Waves on two sides of the flow are clearly sucked into the main stream, leading to an increase of maximum wave heights, which reach about 7m and 4m respectively for regular and irregular waves.

Above computations confirm that current refraction can cause significant amplification in wave height, or so-called giant waves. One of the distinct differences of the current refraction from the pure depth refraction in Part I is that the irregular waves also undergo a strong energy convergence. For regular waves the calculated maximum amplifications are comparable with the theoretical estimate. The computed wave behaviour is consistent with the concept of the ray theory. Only combined refraction-diffraction can trustworthily be used to predict such wave conditions. Sturm (1974) indicated that current refraction not only leads to large wave height, but also to a steep wave profile on the forward face. Such combined effects can cause hazardous conditions for shipping.

4. Combined current-depth refraction in the tidal inlet of Texel

The tidal inlet connects the North sea on the west side and the Wadden sea on the other side. The area is characterized by complicated depth and current features, see Fig. 4.1. In the entrance of the inlet a shoal prevents most waves from entering, therefore only waves, which propagate from southwest on an ebb current, are considered in the following computations. The computational area is shown in Fig. 4.2. Further we will discuss the wave behaviour on several lines where wave heights are plotted. The depths on these lines are shown in Fig. 4.3 and the velocities of the currents in Fig. 4.4. The lines roughly represent the following regions:

The Shoal (SH) region is indicated by lines 1 and 2, along which waves pass over an underwater hill and the current increases gradually with the wave propagation distance; wave shortening and energy convergence behind the shoal may be the dominating processes.

The Refraction (RF) region is marked by lines 5, 6 and two transverse lines. The area has a deep trough with extreme steepness, the tidal currents are strongest. Lines 7 and 8 clearly show a jetlike flow.

The Wadden sea (WD) region is shown by lines 9 and 10. Waves become weaker with the propagation distance.

The model is run for several cases, which are listed as follows:

case	H_s	T	Type	wind	dir.	Cur.	level
I	1.0m	7s	irreg.	no	sw	no	3.1m
II	1.0m	7s	irreg.	no	sw	ebb	3.1m
IV	1.0m	10s	irreg.	no	sw	ebb	3.7m
V	1.0m	7s	reg.	no	sw	ebb	3.1m
VII	1.0m	7s	irreg.	20m/s	sw	ebb	3.1m

Table 4.1 The cases used for the running of the model. T is mean period; irreg.: irregular waves; reg: regular waves; Dir: wave direction; Cur: tidal current; level: water level to datum (NAP).

These cases are a selection of eight cases, intended for comparison of wave models for the tidal inlet of Texel.

The computations take an area 20000 * 13500 m^2, the step size is Δx=12m and Δy=6m. The irregular waves have the same direction spreading and resolution as in section two. The dissipation effects such as wave breaking and bottom friction are included in the computations.

Case I is pure depth refraction and the model results are shown in Fig. 4.5. Along the forward face of the shoal in SH region, the decrease of wave heights due to bottom friction is partly compensated by the shoaling. With the increase of depth the wave pattern becomes irregular. In the RF region waves are modulated by the complicated bathymetry. Waves decrease with the propagation distance, part of them is refracted into the coastal line

11

and dissipated there. Line 7 indicates that there may be two energy convergence areas.

The decrease of wave height along line 9 in the WD region is partly due to refraction to the coastal line of Texel and partly due to direct transmission to the shadow region in the south. This explains why the waves increase along line 10, which is located in the shadow region.

Case II is an example of combined depth-current refraction, and the model results are shown in Fig. 4.6. In the SH region the waves begin to feel the effect of the current. The modulation of wave height is very strong in the RF region. Generally the depth and current modulate the wave heights in the different locations. The two types of refraction effects counteract each other and the maximum height is reduced. The cross lines (line 7 and line 8) also show the possible locations of energy convergence.

In the WD region waves on line 9 decrease faster than in case I. The waves may be refracted into the current along the south of the Texel coast where currents are strong. In the shadow region along line 10 the waves increase due to direct transmission. The differences between case I and case II, ($\Delta H = H_i - H_{ii}$) are shown in Fig. 4.7. Fig.4.7(c) is the most indicative one, the positive value on shallow water and negative one on deep water show the effect of the current in the tidal inlet.

The model result for case IV is shown in Fig. 4.8. This case shows that the longer waves are strongly modulated by the depth. In the SH region, the increase of wave energy due to shoaling surpasses the friction dissipation. Behind the shoal, a strong energy convergence takes place. In the RF region, waves are reduced dramatically, one hardly finds the effect of current and only a tiny fraction of the incident waves enter the Wadden sea. Most waves, before their arriving at the Wadden sea, are refracted to shallow areas or coastal lines and dissipated there. The difference between case IV and case II ($\Delta H = H_{iv} - H_{ii}$) is shown in Fig. 4.9. Again, along line 7 and line 8 of Fig. 4.7(c) one finds the depth modulation for longer waves. From this example we confirm that for longer waves the bottom refraction is the dominant effect.

The regular wave case V is shown in Fig.4.10. One can find a strong modulation of wave heights due to depth-current refraction along line 1, 5, 6, 7, 8. Waves are refracted into the main stream where they have maximum amplification. Comparison with case II is shown in Fig. 4.11, $\Delta H = H_v - H_{ii}$, from which one finds that the regular and irregular waves modulate height in different

locations. The energy on the two sides of the flow is sucked into the flow and the wave amplification is noticeable. In the WD region, refraction is also very important. The incident waves decay rapidly with distance as shown in line 9; on the contrary, the waves in the shadow region increase in height.

Case VII is shown in Fig. 4.12, where the wind has a velocity 20m/s in the direction of the incident waves. If the incident waves are small, local winds can enhance the waves considerably. The effect is most important in the Wadden Sea where existence of the waves mainly depends on local winds. Again, the current refraction can appreciably increase the maximum wave heights. The differences ($\Delta H = H_{vii} - H_{ii}$) are shown in Fig. 4.13.

The maximum amplification of wave heights for irregular waves amounts to a factor of 1.4 to 1.5 in case of pure depth refraction and 1.8 to 2.0 in case of combined depth-current refraction. This factor may be higher than 3.5 in case of regular waves. But comparing to the pure current refraction in the previous section, they are obviously smaller because of the counteracting effect of the depth refraction. The incident waves of high frequency have stronger interaction with currents and the longer waves are dominated by the effect of the bathymetry. The local winds play an important role in the Wadden Sea, which is shadowed by the narrow entrance of the tidal inlet.

The comparison of the model CREON with other models in this area for case I is shown in Fig. 4.14. The incident wave height is 2m and the period 7s. The wave heights are plotted along a straight line through the area, following the axis of the main channel. For the first 8km the results of CREON (C) agree quite well with those of the fully spectral model SWAN (S). Between 8-15 km the two spectral models HISWA (H) and SWAN have close agreement, but differ from the CREON results. Behind 15km the results of the three models again come closer. The ray model (R) contains no dissipative effects. Between 0-8km and behind 15km the bathymetry is relatively simple in the computational area. However, the bathymetry between 8-15km is very complicated and strong refraction occurs, the results from the spectral models and CREON differ significantly and the ray model obviously fails in this region (see Fig. 4.14). Although the spectral models and the model CREON treat wave propagation with different numerical methods considering different physical processes, we have no definite explanation for the discrepancy between the two kinds of models and we have to wait for observations to verify the computational results.

5. Hindcast of waves in the Haringvliet

To assess its applicability in real situations, two hindcasts are performed in the area of the Rhine estuary where wave data from a measurement campaign during the autumn of 1982 (Dingemans, 1983) are available.

The bathymetry of the area and the locations of the wave sensors and gauges are shown in Fig. 5.1(a). Fig. 5.1(b) shows the computational area that can be roughly divided into three regions: offshore, shoal and inshore. The offshore region is one with nearly straight depth isolines; the shoal is called Hinderplaat, which falls partly dry during low tide; the inshore region has a relatively complicated bathymetry.

The computations are carried out in an area of 13000*10000 m^2 for hindcast number one (HN1) and 13000*8000 m^2 for number two (HN2), with step size Δx=10m and Δy=5m. Each hindcast is applied to two wave conditions, i.e. regular and irregular waves. For irregular waves we have the same direction spreading function and direction resolution as in previous sections. To assess the influence of the nonlinearity on waves, each wave condition is computed with 'h_n' effect (p_v=1) and without 'h_n' effect (p_v=0) (the definition of 'h_n' can be found in part I).

To test the applicability of the model, we have the following considerations:

A: to assess the model performance with different periods of the incident waves.

B: to assess the model performance with different water levels.

Therefore we select two of the six sets of measurements during 14-15 October 1982. In HN1 we use the first set of data (at 17:00 Oct.14, 1982) and in HN2 the second set (at 22:00 Oct.14, 1982). A directional wave buoy WAVEC (WA) provides wave parameters as input for the upwave boundary condition, the wave riders and gauges in various locations, as shown in Fig. 5.1, provide the wave heights for verification of model results. We show computational results along two lines for further discussion, as shown in Fig. 5.1(b). Fig. 5.2 shows the depths along these two lines (the water level is zero to NAP). In order the computational results to be fully plotted, the lines are roughly divided into three regions: offshore (OF), shoal (SH) and inshore (IN) region. In the following we only plot the results without 'h_n' effect in

the computations.

The input parameters for HN1 at WA are H_s =2.58m, T=6s, θ=320°, the wind has the same direction as the waves and the wind speed is w=16m/s. The water level is -0.1m below NAP.

Fig. 5.3 and Fig. 5.4 give the results for regular and irregular waves respectively. In the offshore region, the isolines of wave height are nearly parallel to those of the bottom, but waves rapidly decrease in the shoal region. Behind the shoal waves are regenerated. In the computational area, wave dissipation due to bottom friction and breaking play a dominant role and wind becomes only important behind the breaking zone.

No:	Name	Measur.	I	I*	II	II*
1	WA	2.58	-	-	-	-
2	WR1	2.34	2.52	2.43	2.50	2.50
3	WR2	2.21	2.11	2.07	2.08	2.06
4	WR3	2.21	2.04	2.06	2.04	2.02
5	WR4	0.4	0.26	0.26	0.28	0.26
6	WR5	0.66	0.75	0.49	0.71	0.67
7	WR6	1.16	1.24	1.24	1.08	1.16
8	E-75	0.61	0.59	0.42	-	0.47
rms			0.09	0.10	0.08	0.10

Table 5.1 Comparison of wave heights between model and measurements for hindcast number one (HN1). I is the case of regular and II the case of irregular waves, superscript * indicates computations without 'h_n' effect. rms is root-mean-square error.

Along line 1 one finds that in the first part of the offshore region the decrease in wave height is compensated by the shoaling and wind input. When waves enter the 10m bottom isoline, the balance is broken down and wave heights decrease drastically to zero on the shoal. Behind the shoal waves grow under influence of the wind. Along line 3, waves decrease earlier than along line 1, but they can freely enter the inshore region through the south of the Hinderplaat. In the inshore region wave pattern become irregular in response to the complicated bathymetry. Fig. 5.5 gives the differences of the two kinds of waves, $\Delta H = H_{irreg} - H_{reg}$. In the offshore region there is hardly a difference. In the inshore

15

region, wave directionality has an important influence on the wave behaviour, as shown in Fig. 5.5c. The positive and negative differences indicate that wave heights induced by strong refraction are smoothed out by the directional spreading of the irregular waves. The height modulation due to depth refraction seems more important than wind enhancement.

The computational results in the measurement locations are shown in Table 5.1. Four computations are carried out for one set of wave measurements, where rms (root-mean-square error) is also given for each computation. The performance of the model is reasonably good. The use of effective depth has a positive influence on the accuracy of the calculations.

When the water level becomes extremely low, the computation for irregular waves with effective depth fails because of too large growth rate due to shoaling. Therefore one is advised to use smaller p_v ($0 < p_v < 1$) for very shallow water.

For HN2 the input wave parameters at WA are $H_s = 3.38m$, $T=7s$ and $\theta=320^0$, the wind has the same direction as the waves and $w=17m/s$. The water level is +0.85 above NAP. Figs. 5.6 and 5.7 show the model results. From the plots we find that the waves have the same behaviour as in HN1, waves decrease rapidly when they enter the 10m depth isoline.

In the shoal region waves are strongly dissipated, and behind the shoal enhanced by the wind. When the waves reach about 1m depth, the height modulation due to bottom becomes more important than wind, since the growth due to wind is counteracted by strong dissipation. The directionality of waves is important in the inshore region, as shown by Fig. 5.8. Table 5.2 gives the computational results at the measurement points. As in HN1 the influence of the directional spreading can be found at WR6 and E-75. But the use of the effective depth is important for the accuracy in the whole region.

The above results indicate that the model has a reasonably good performance in real situations. Generally, the use of the effective depth improves the accuracy of the calculation. While the directional spreading of the waves is important in the inshore region, too little field data are available for verification in this region.

16

No:	Name	Measur.	I	I*	II	II*
1	WA	3.38	-	-	-	-
2	WR1	2.90	3.27	3.19	3.22	3.23
3	WR2	2.58	2.62	2.58	2.59	2.56
4	WR3	2.68	2.54	2.56	2.54	2.49
5	WR4	0.62	0.40	0.42	0.42	0.41
6	WR5	1.05	1.11	0.79	1.12	0.98
7	WR6	1.60	1.59	1.66	1.46	1.57
8	E-75	0.95	0.77	0.64	0.65	0.62
rms			0.11	0.13	0.11	0.12

Table 5.2 Comparison between model and measurements for hindcast number two (HN2). The notations are the same as Table 5.1.

In locations WR1, WR2, WR3, WR5 and WR6 we have a satisfactory accuracy. Comparing with the measurements, we find that wave propagation and wave growth due to wind are reasonably modelled before waves undergo strong dissipation. The relatively large differences between the model results and the measurements in WR4 and E-75 have been extensively discussed by Dingemans (1983). The discrepancies are explained as follows: behind a breaking zone the mean wave period changes and wind enhance waves considerably. The use of one representative period in the present model leads to too large dissipation due to bottom friction and too low growth rate, since the rate of wave growth is inversely proportional to the phase speed of waves.

6. Conclusions

The wave model CREON is intended to simulate the combined effects
of refraction and diffraction for an irregular wave field. The
model can be considered as an extension of the model CREDIZ (for
a description and verification of this model, see Radder 1979;
Booij 1981; Dingemans 1983; Vogel et al. 1988).
The latter model is extended in two respects:
 (i) the effect of directional spreading is added, to simulate
the behaviour of irregular waves,
 (ii) perfect lateral boundary conditions are applied, to prevent
undesirable side effects of these (artificial) boundaries.
For a description of the model CREON, see Gao et al. (1993). In
the present report, various computational results are presented.

It is shown that the combined effects of wave diffraction and
directional spreading behind breakwaters are significant, leading
to large differences between regular and irregular wave fields
(cf. Goda 1985).

Current refraction can cause the occurrence of cusps and caust-
ics, in particular in case of a jet-like flow (giant waves, cf.
Mallory 1974). For regular waves, the computed maximum wave
height is comparable with the theoretical estimate (cf. Smith
1976); irregular waves also undergo strong convergence effects.
Although there are no measurements to verify the results in this
case, the computed wave behaviour is consistent with the concept
of the ray theory.

In the tidal inlet of Texel, strong depth- and current variations
influence the wave field. While depth refraction and (ebb) current
refraction have opposite effects in the inlet, a convergence of
wave energy ('tunneling') occurs first, afterwards leading to a
decrease of wave height. The results of five selected cases of
computation confirm this complicated behaviour. A comparison of
CREON with three other wave models has been made (cf. Fig.4.14):
a ray model (R), the fully spectral model SWAN (S), and the para-
meterized spectral model HISWA (H). The results of the spectral
models and those of CREON (C) differ significantly, requiring
further verification with field data.

The hindcasts in the Haringvliet indicate that the model has a
reasonably good performance. The use of effective depth improves
the accuracy of the calculations and the directionality of the
incident waves influences the wave field considerably in the
inshore region with complicated bathymetry.

Whereas we may conclude that the model CREON has a wide range of applicability and reasonably good performance in various situations, a fundamental problem remains to be solved. It is known that one representative period cannot properly model waves behind a breaking zone (Haringvliet) or at steep bottomslopes or current gradients (Texel), where theory and measurements indicate that the mean wave period changes considerably due to generation of lower and higher harmonics. It is clear that a fully spectral wave model, which includes effects of nonlinear wave-wave interactions in shallow water, is needed for a better performance in such situations.

References

Booij, N. 1981. Gravity waves on water with non-uniform depth and current. *Rep. No. 81-1, Delft Univ. Tech.*

Bretherton, F.P. and Garrett, C.J.R., 1968. Wave trains in inhomogeneous moving media. *Proc. Royal. Soc. London*, Vol. A302, No. 1417, 529-554.

Brevik, I., 1980. Flume experiment on waves and currents II, Smooth bed. *Coastal Eng.* vol. 4, No. 2, 89-110.

Dalrymple, R.A. and Martin, P.A., 1992. Perfect boundary conditions for parabolic water-wave models. *Proc. Royal Soc. London.* A437, 41-54.

Dingemans, M.W., 1983. Verification of numerical wave propagation models with field measurements, CREDIZ verification Haringvliet. *Delft Hydraulics Lab.*, Report W488, Dec. 1983.

Gao, Q., Radder, A.C. and Booij, N., 1993. A numerical wave model for the refraction and diffraction of irregular waves, Description of the wave model CREON. Report 5-93, *Faculty of Civil Engineering, Delft University of Technology.*

Goda, Y., 1985. Random seas and design of maritime structures. *University of Tokyo Press*, Japan, 1-323.

Hayes, J.G., 1980. Ocean current-wave interaction study. *J. Geoph. Res.* Vol. 85, No. C9, 5025-5031.

Mallory, J.K., 1974. Abnormal waves on the south east coast of South Africa. *Inter. Hydro. Rev.* Monaco, Vol. LI, No. 2, 99-129.

Mei, C.C., 1983. *The Applied Dynamics of Ocean Surface Waves.* New York, Wiley-Interscience.

Peregrine, D.H., 1976. Interaction of water waves and currents. *Adv. Appl. Mech.* 16, 9-117.

Peregrine, D.H. and Smith, R. 1979. Nonlinear effects upon waves near caustics. *Phil. Trans. Royal Soc. London*, England, Series A, Vol. 292, No. 1392, 341-370.

Peregrine, D.H. and Jonsson, I.G., 1983. Interaction of Waves and Currents. CERC report No. 83-6, March 1983.

Radder, A.C., 1979. On the parabolic equation method for water-wave propagation. *J. Fluid Mech.* 95(1), 159-176.

Smith, R., 1976. Giant Waves. *J. Fluid Mech.* 77, 417-431.

Sturm, H., 1974. Giant waves. *Ocean*, 2(3), 98-101.

Tolman, H.L., 1992. Effects of the Gulf Stream on wind waves in SWADE. *Proc. 23th Int. Conf. on Coastal Eng. ASCE*, 712-725.

Vogel, J.A., Radder, A.C. and de Reus, J.H., 1988. Verification of numerical wave propagation models in tidal inlets. *Proc. 21th Int. Conf. on Coastal Eng.* ASCE, 433-447.

Whitham. G.B., 1974. *Linear and nonlinear waves.* New York, Wiley-Interscience.

Zhao, Y. and Anastasiou, K., 1993. Economical random wave propagation modelling taking into account nonlinear amplitude dispersion. *Coastal Eng.* 20, 59-83.
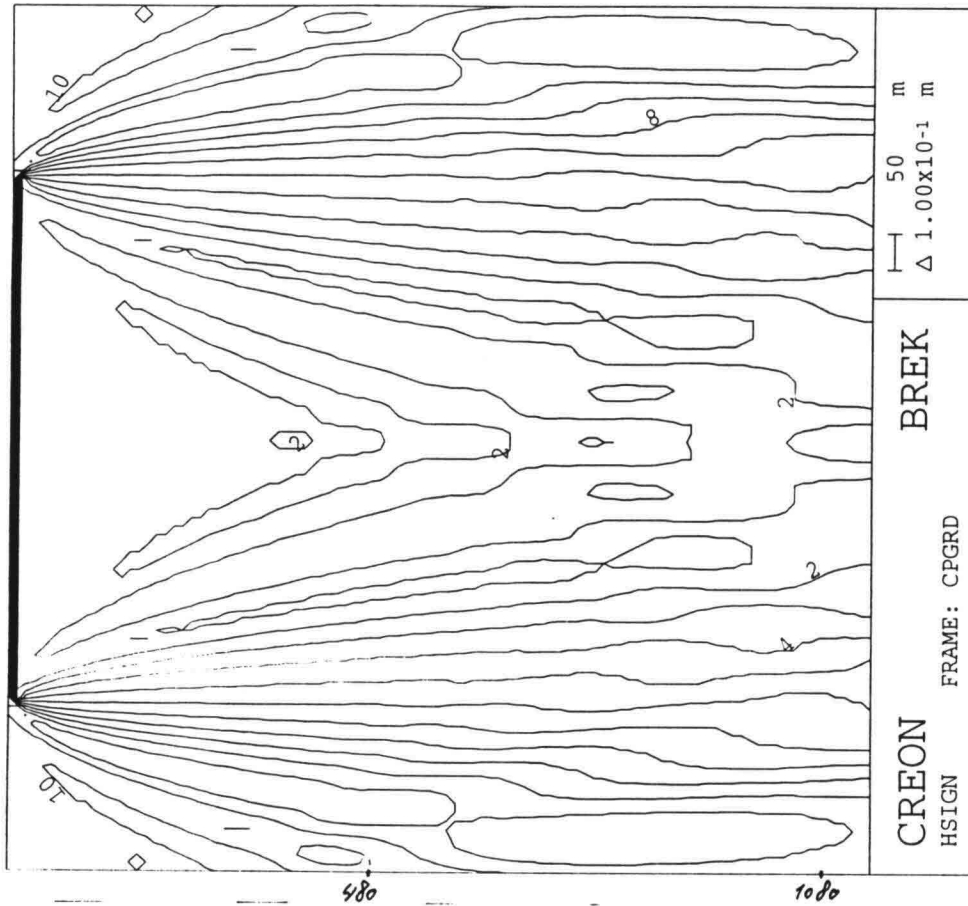
(a)
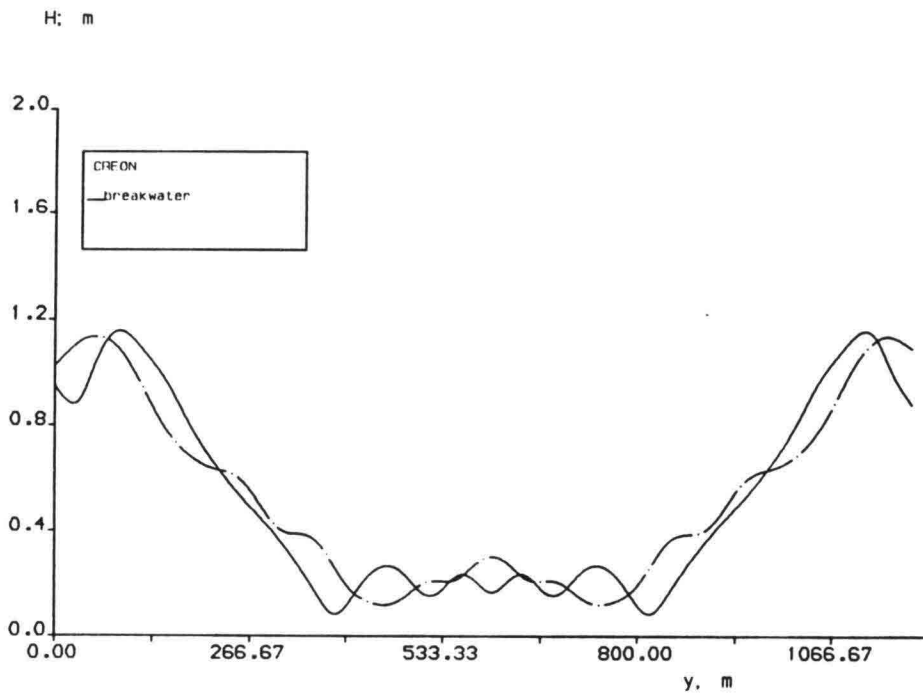
(b)

Fig. 2.1. Regular waves passing a submerged obstacle.
(a) Isolines of wave height; incident wave height 1.0 m.
(b) Wave height along two cross lines, ——: x = 480 m, —.—:
x = 1080 m.
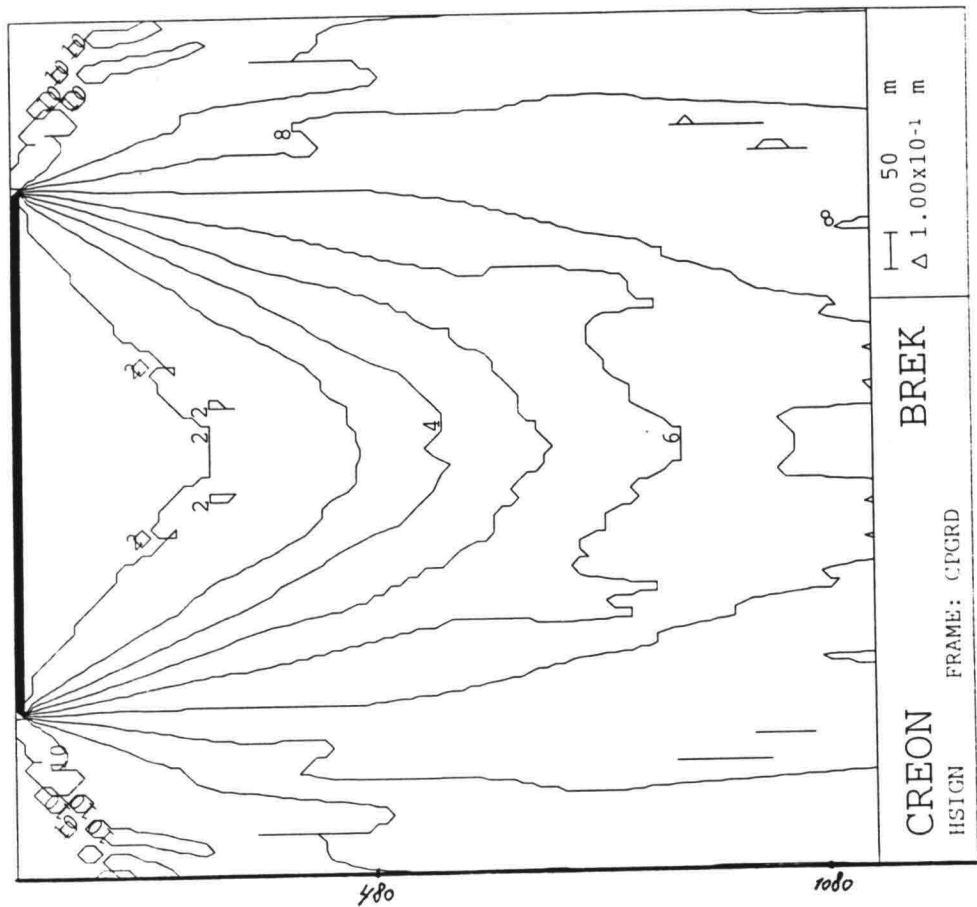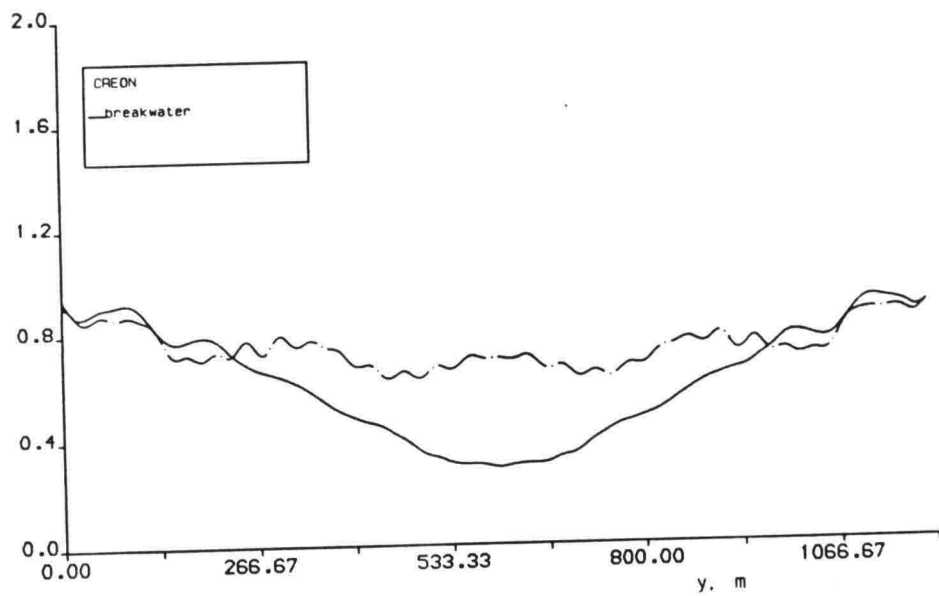
Fig. 2.2. Irregular waves passing a submerged obstacle. (a), (b) see fig. 2.1.

23
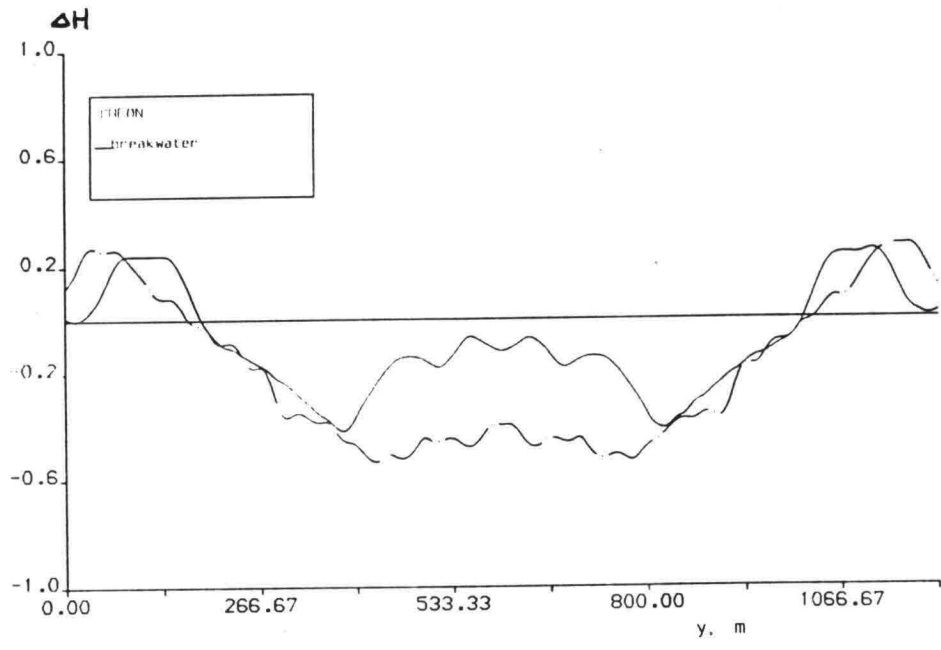
Fig. 2.3. The differences between regular and irregular waves along the two cross lines. ΔH.
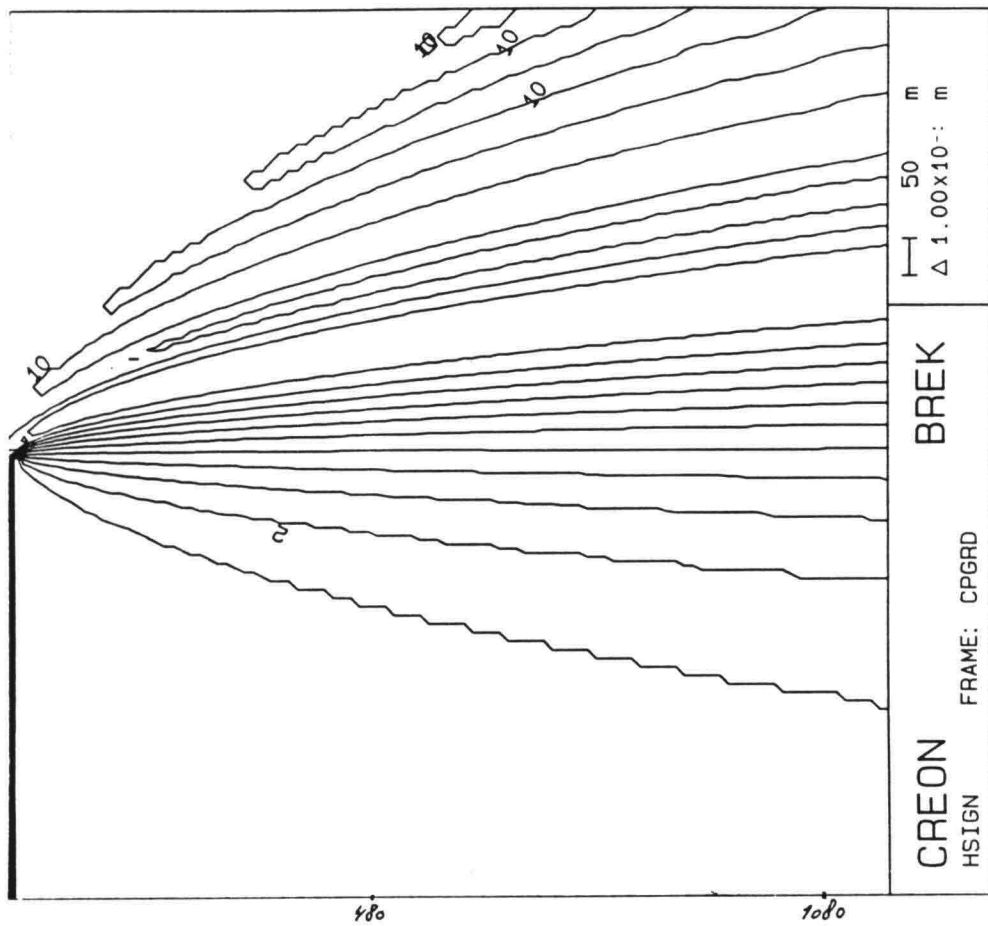
(a)
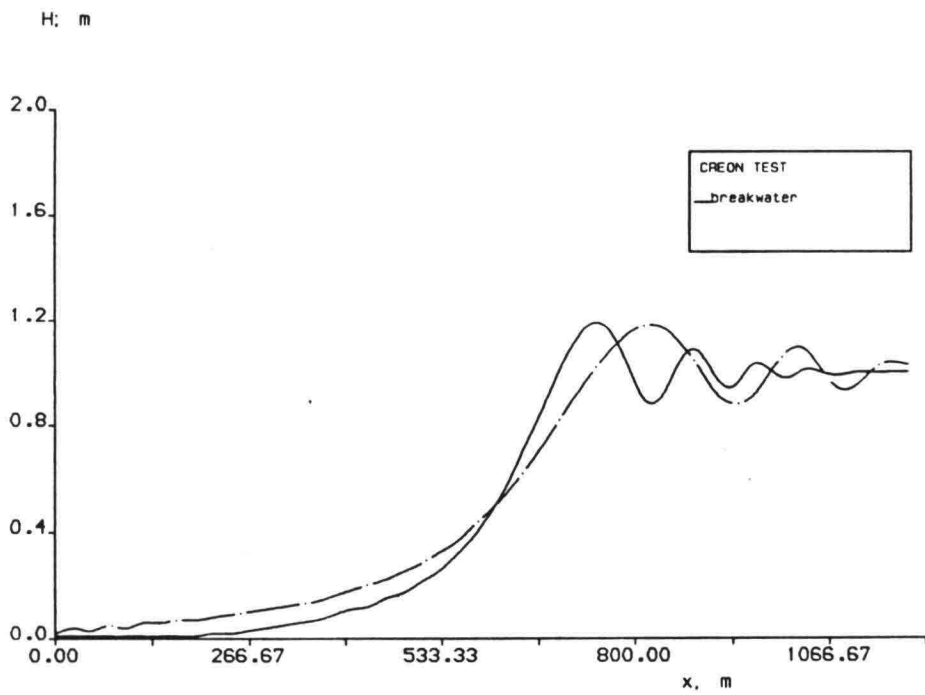
(b)

Fig. 2.4. Regular waves behind a semi-infinite breakwater.
(a), (b) see fig. 2.1.

25
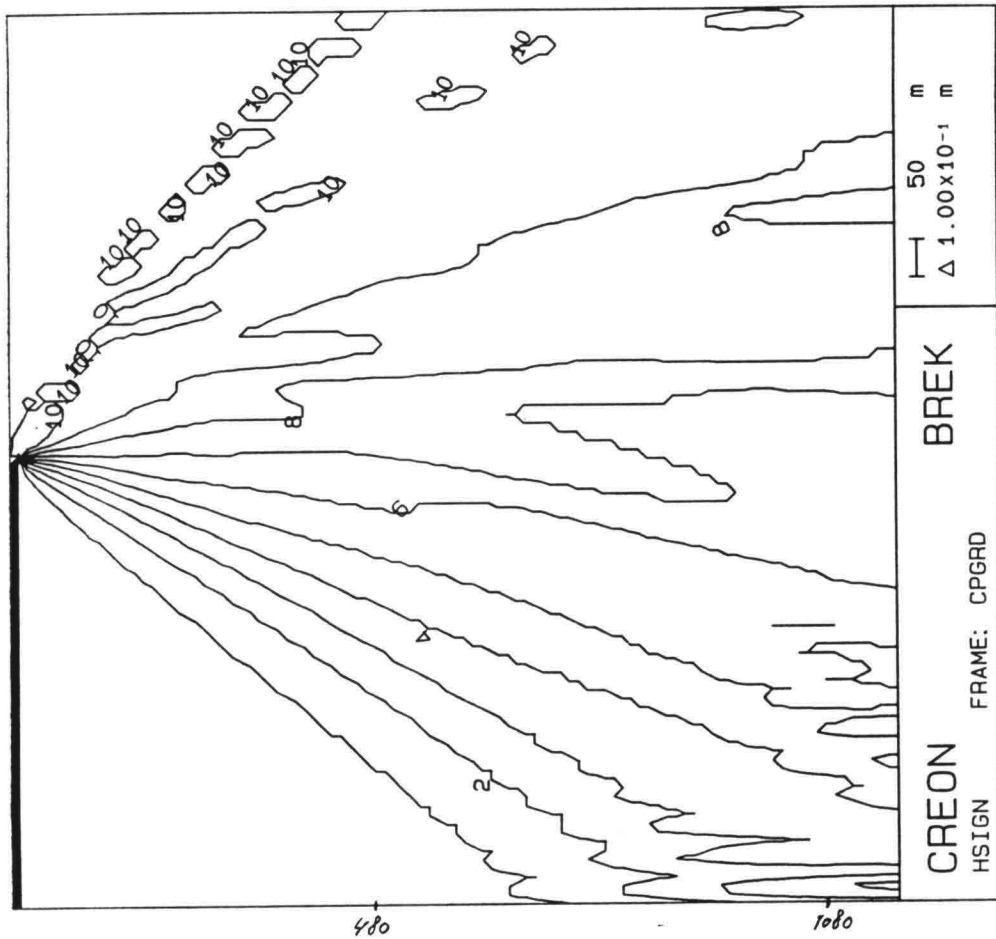
(a)
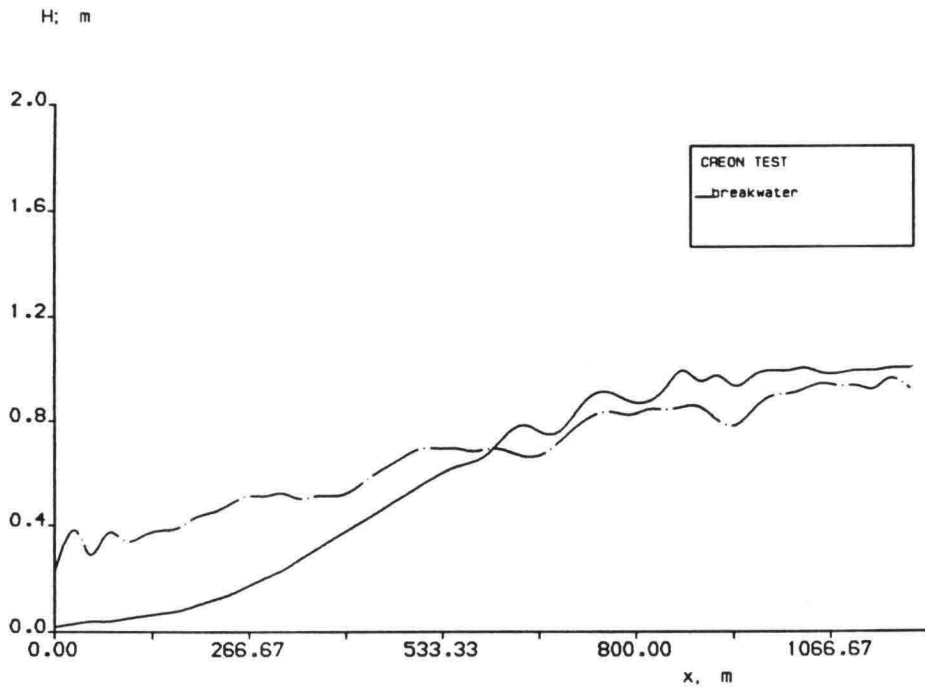
(b)

Fig. 2.5. Irregular waves behind a semi-infinite breakwater. (a), (b) see fig. 2.1.

∠H: m
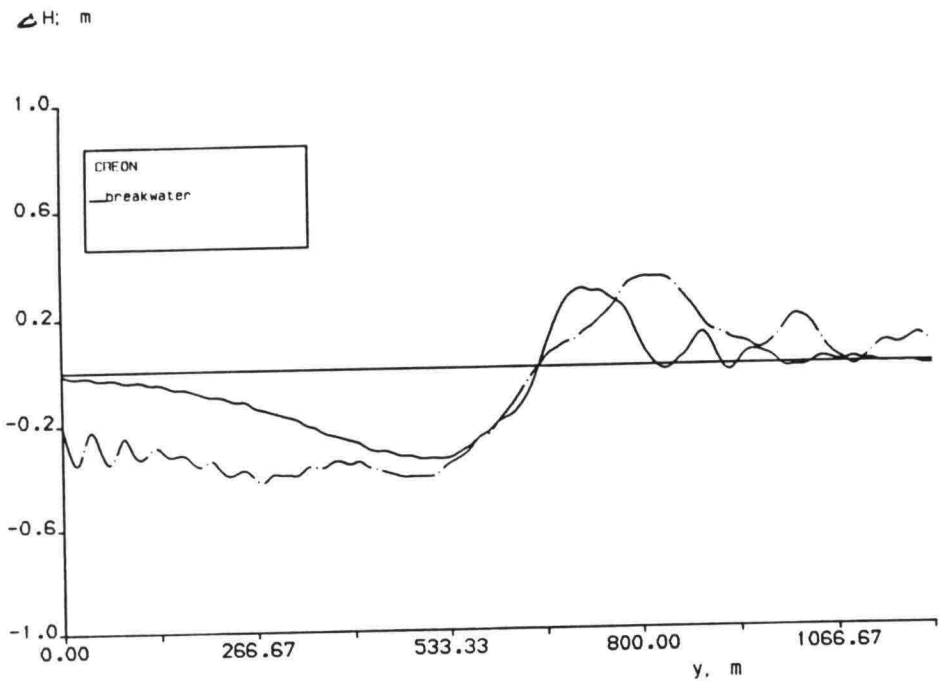
Fig. 2.6 The same as Fig.2.3 for semi-infinite breakwater.

(a)

CREON   BREK   m   m
HSIGN   FRAME: CPGRD   50
                       ⫿ Δ 1.00x10⁻¹

480   1080

H: m

(b)

CREON TEST
— breakwater
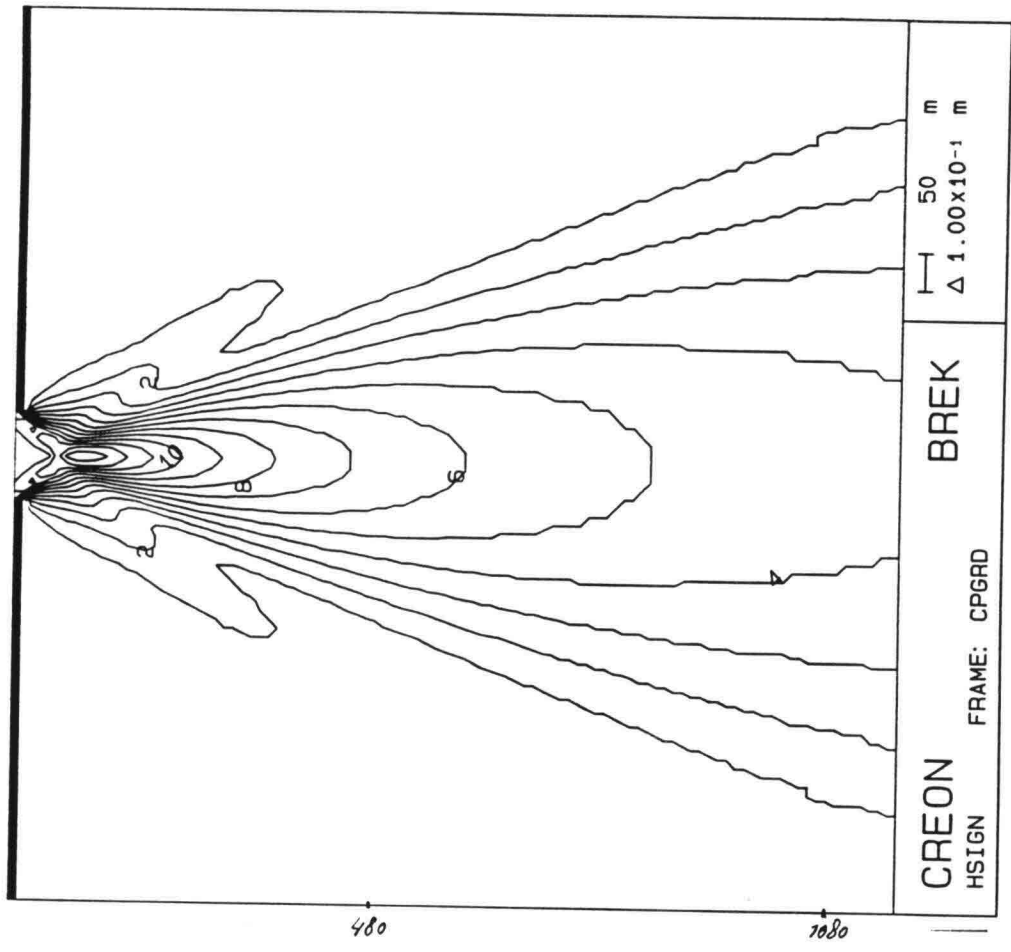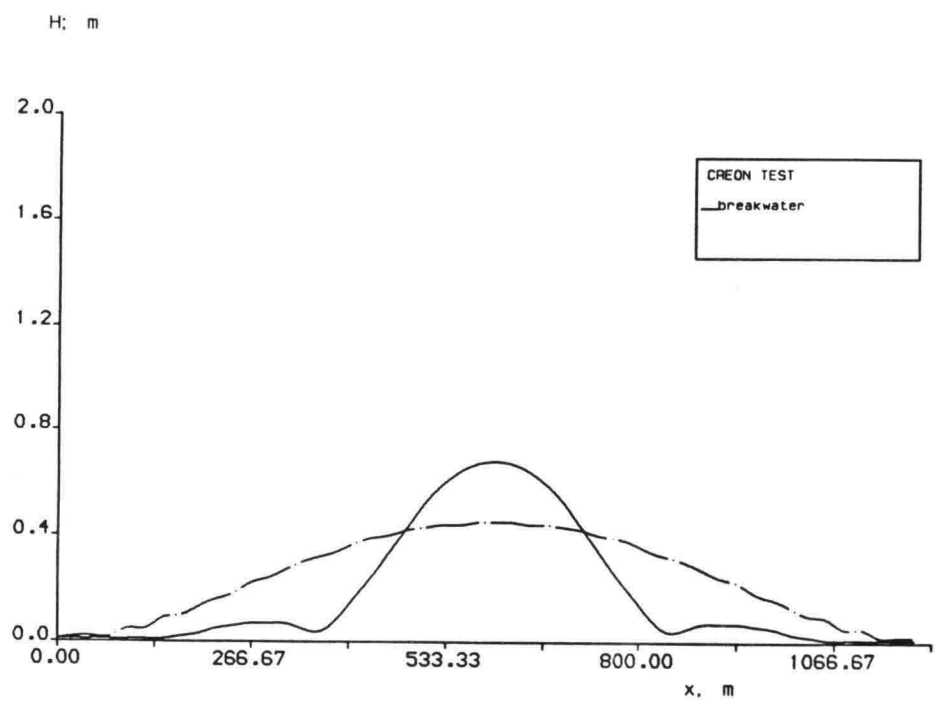
Fig. 2.7.   Regular waves behind two breakwaters.
(a), (b) see fig. 2.1.
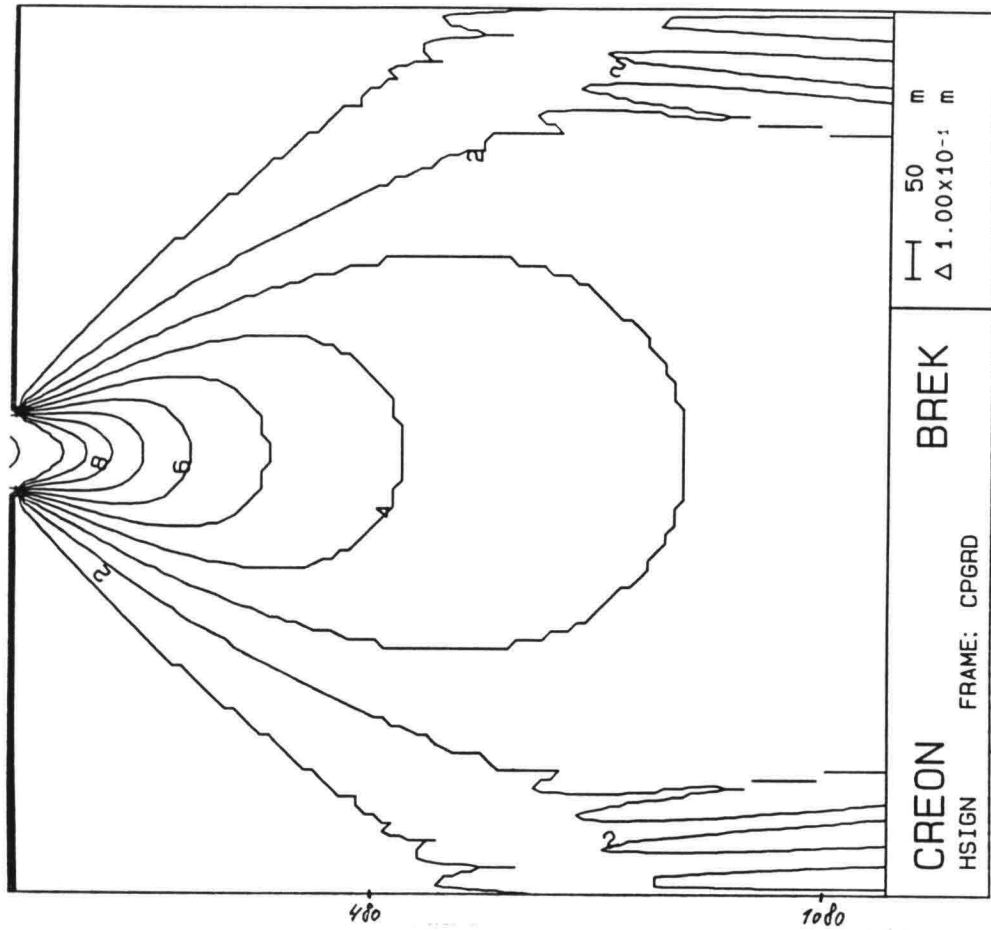
(a)
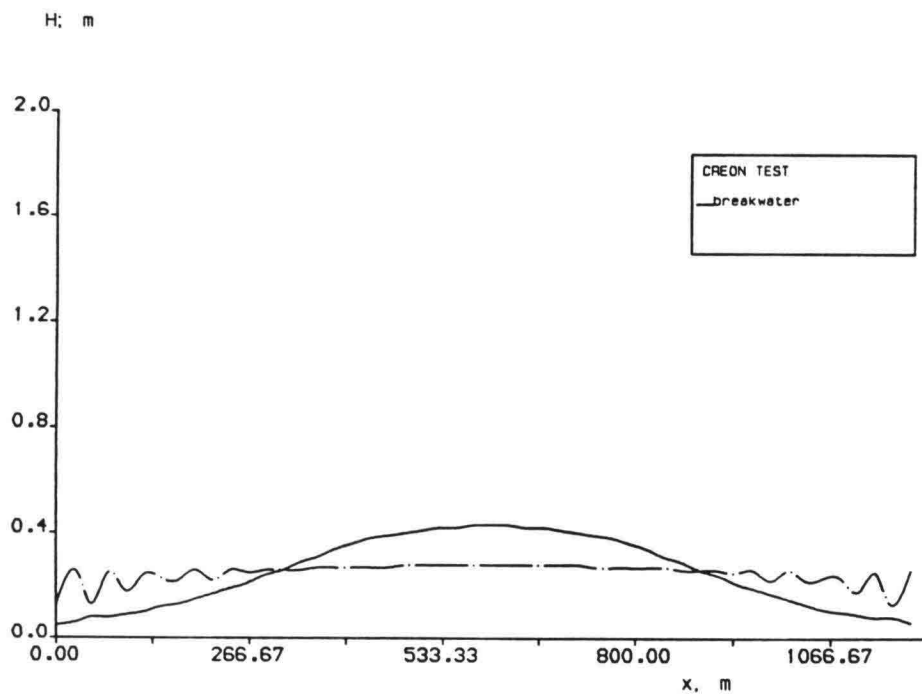
(b)

Fig. 2.8. Irregular waves behind two breakwaters.
(a), (b) see fig. 2.1.
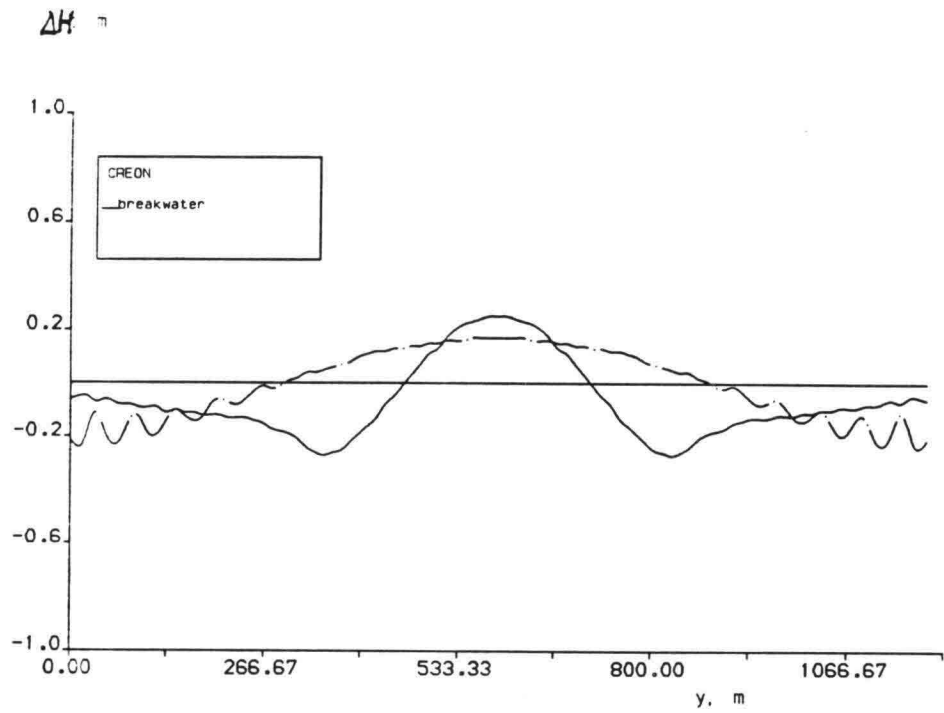
Fig. 2.9 The same as Fig. 2.3 for two breakwaters.
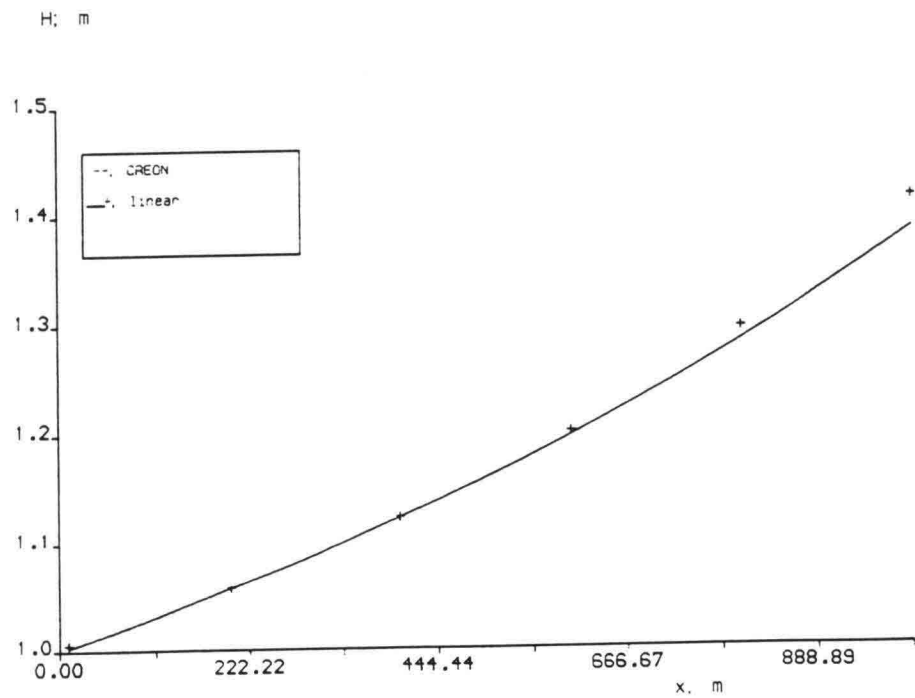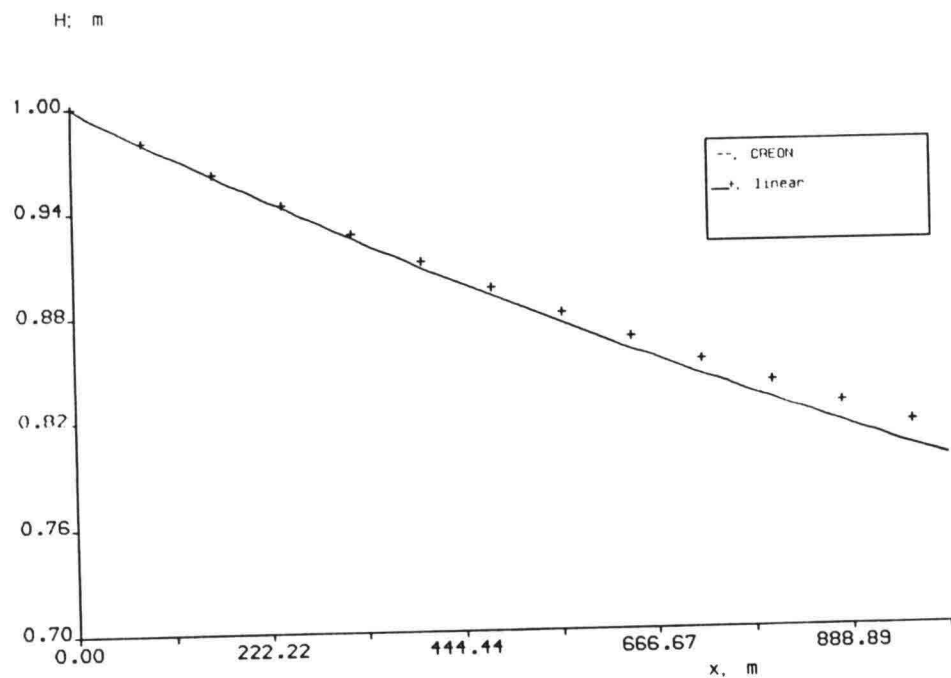
Fig. 3.1 Waves propagating parallel to *non*-uniform flow. a) in upstream direction. b) in downstream direction. The incident wave H_s=1.0m. ──── : the model's result; +: from linear theory.

(a)

x: m   *(wave field)*

(b)
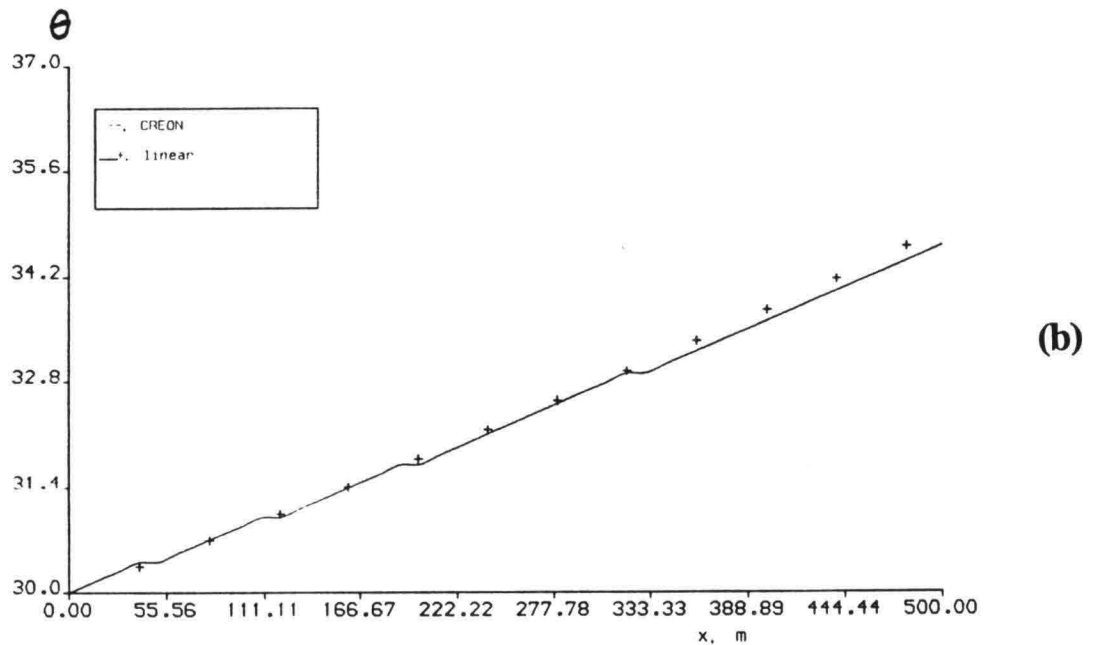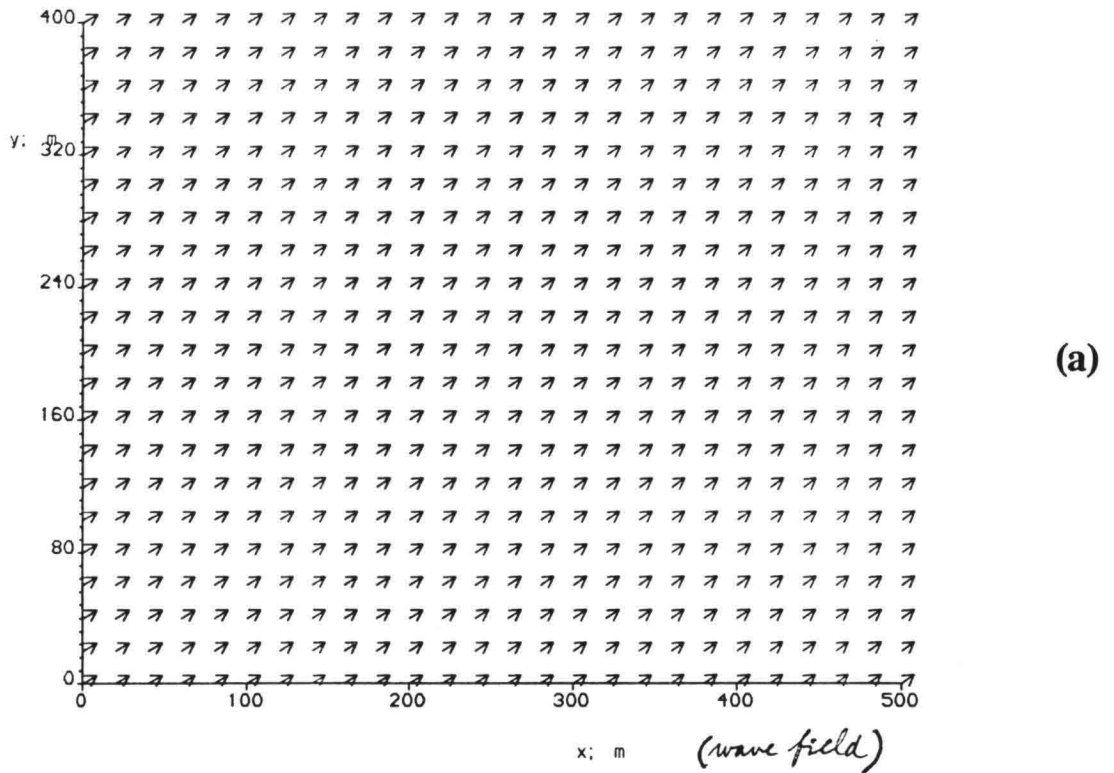
Fig. 3.2 Waves propagating at an angle to the shear flow. a) waves have a component parallel to downstream direction. The incident angle $\theta_0=30^0$ to x-axis. b) the comparison between linear theory (+) and model's results (———).

(a)

(b)
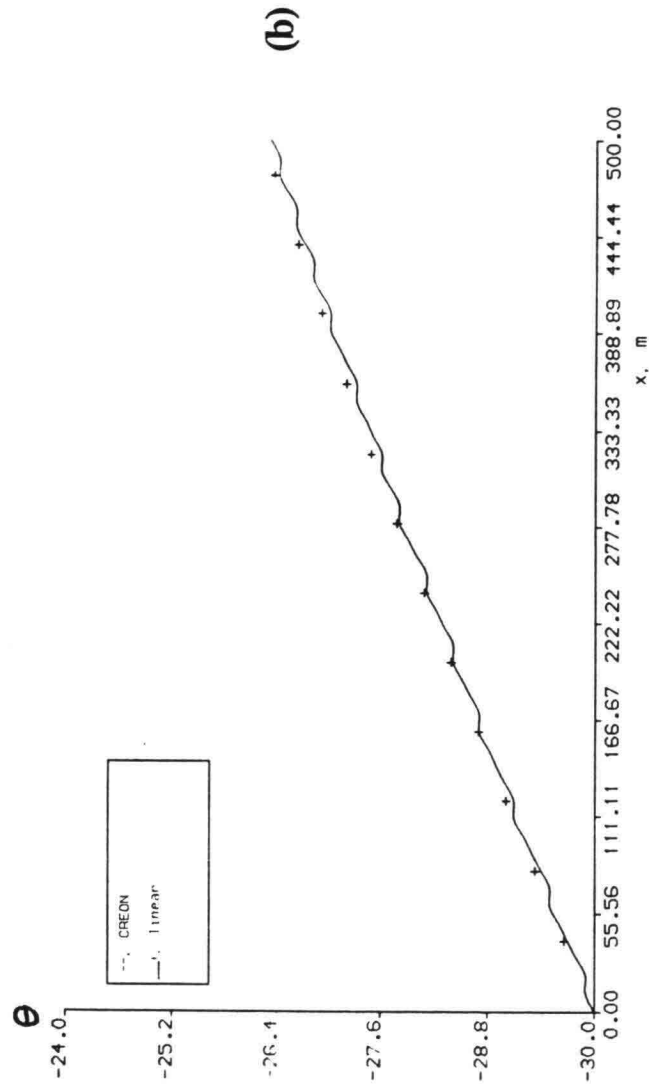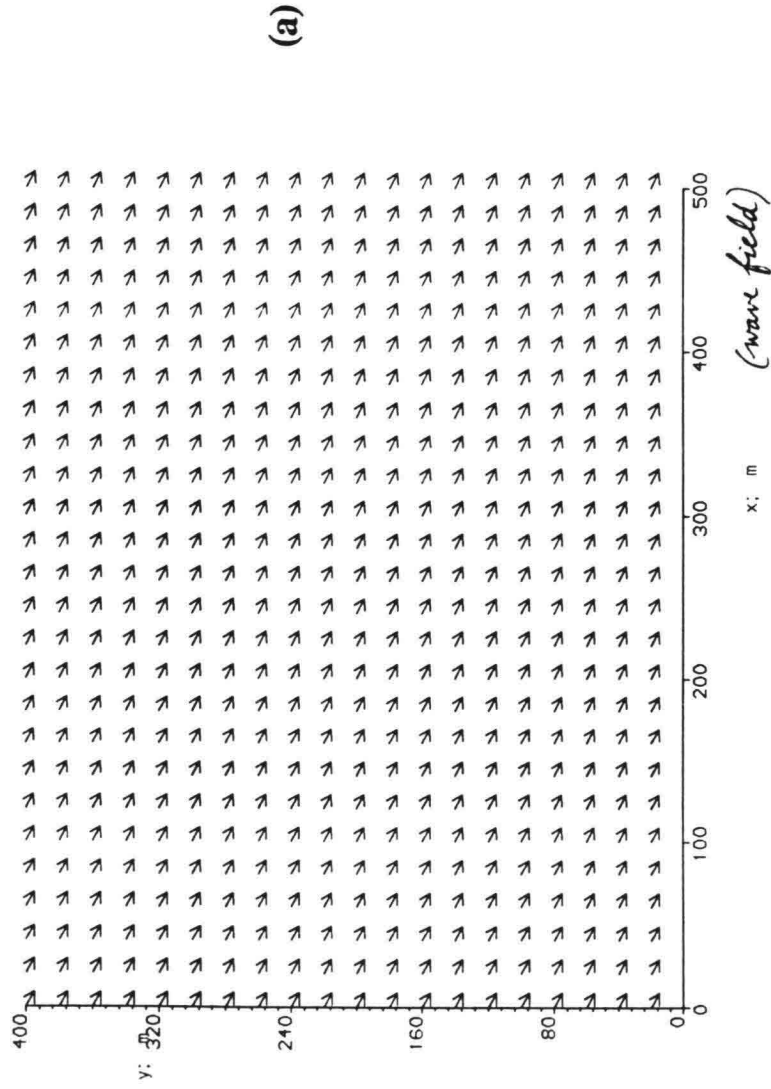
Fig. 3.3 a) waves have a component parallel to upstream direction. The incident angle $\theta_0 = -30^0$ to x- axis. b) the comparison between linear theory (+) and model's results (———).

33
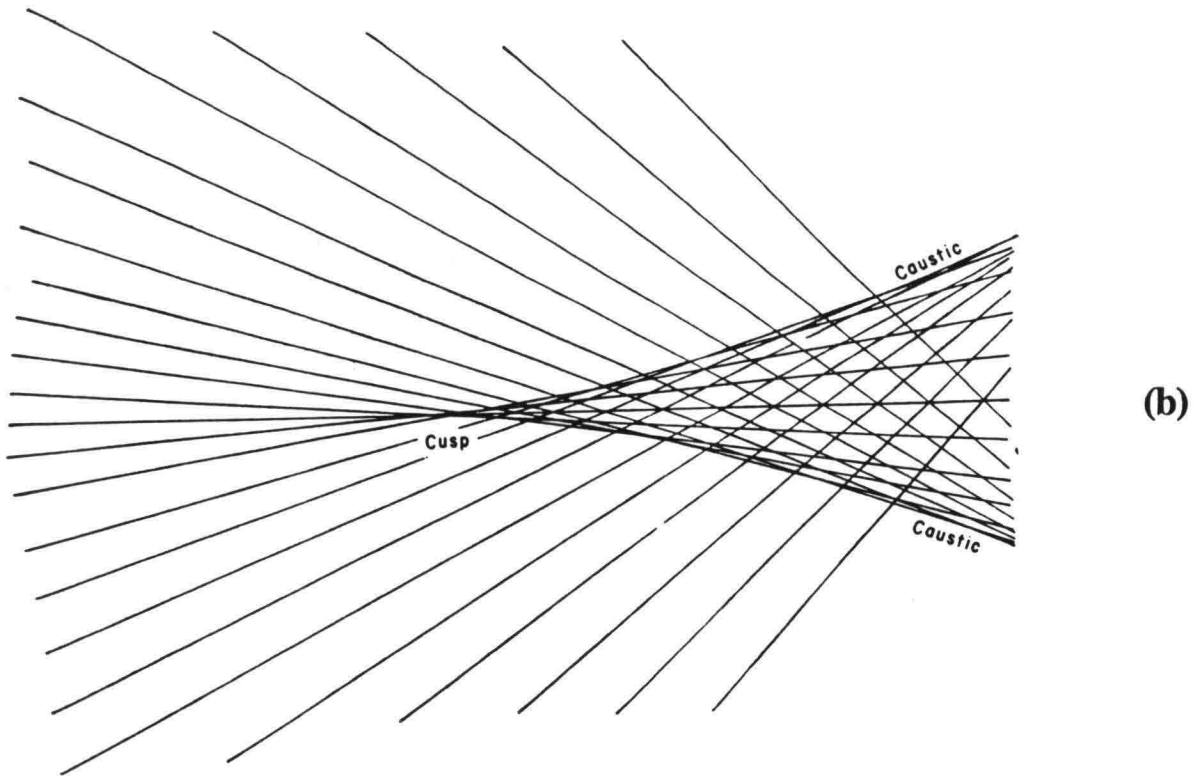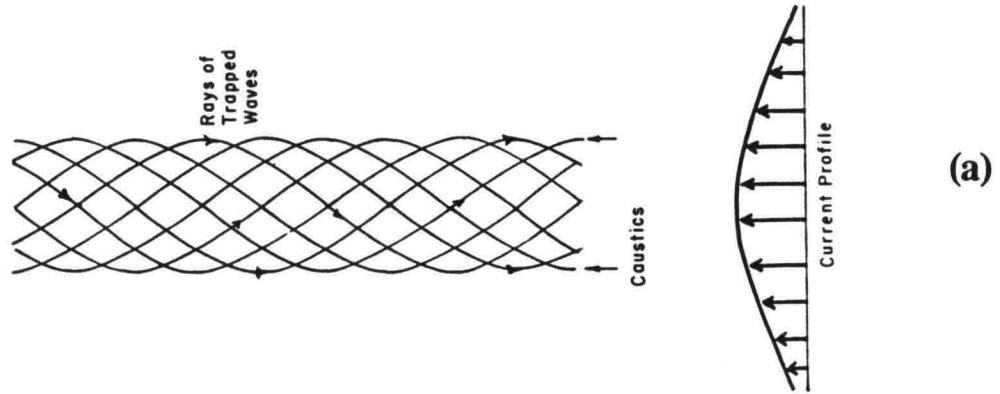
Fig. 3.4.   a) wave rays in a jetlike flow.
            b) rays focusing at a cusp.
            (From Peregrine & Jonsson 1983)

(a)
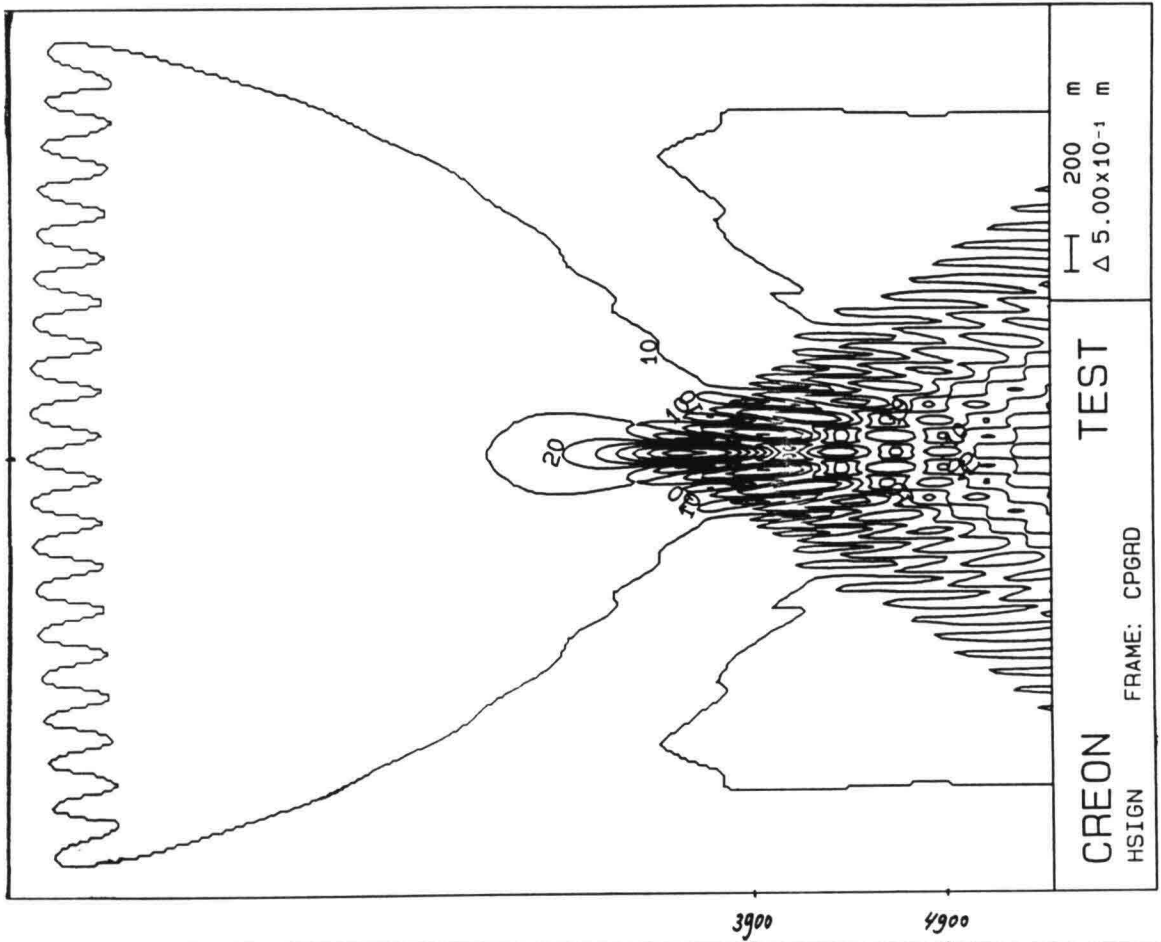
(b)
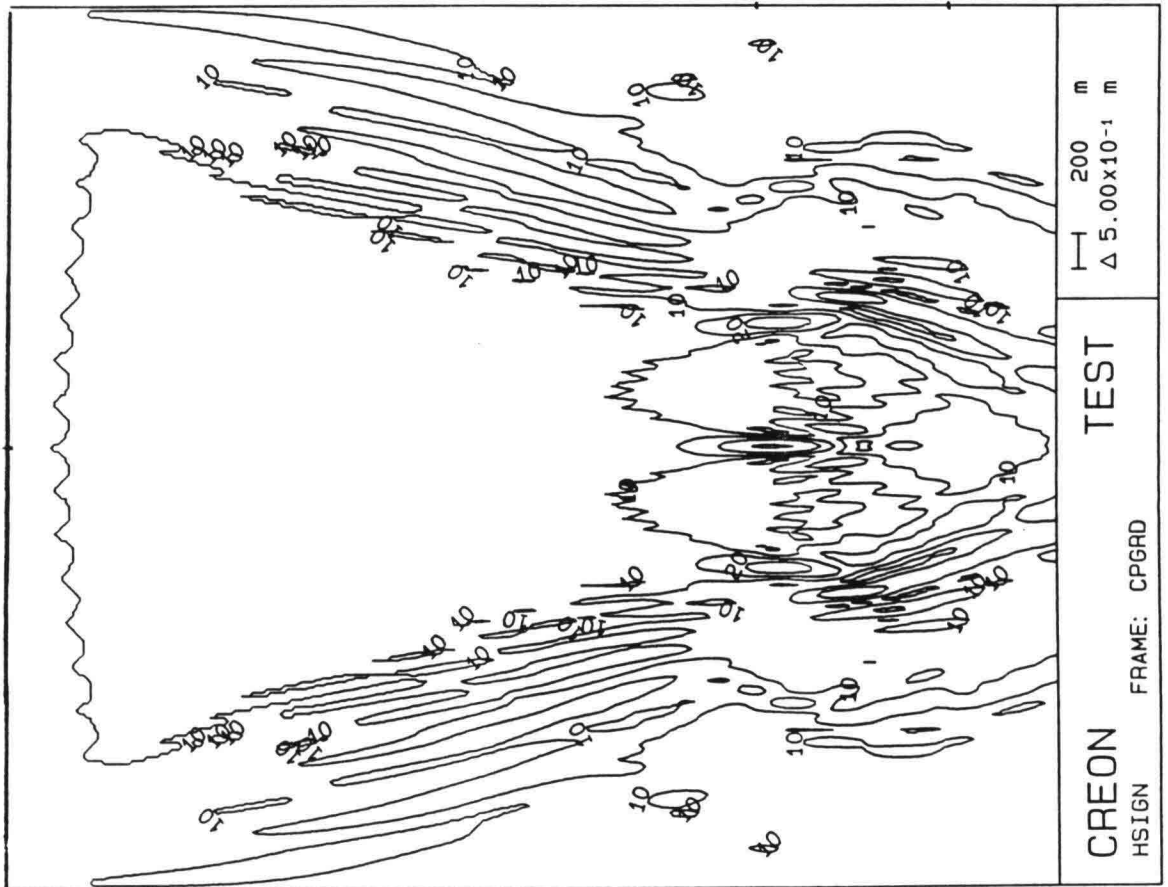
Fig.3.5 Wave fields on a jetlike flow with a maximum velocity
$u_0=-2m/s$. Waves propagate from left to right in upstream direc-
tion, the incident wave $H_s=1m$, $T=10s$. a) monochromatic waves.
b) irregular waves.

35

(a)

H: m

(b)

H: m
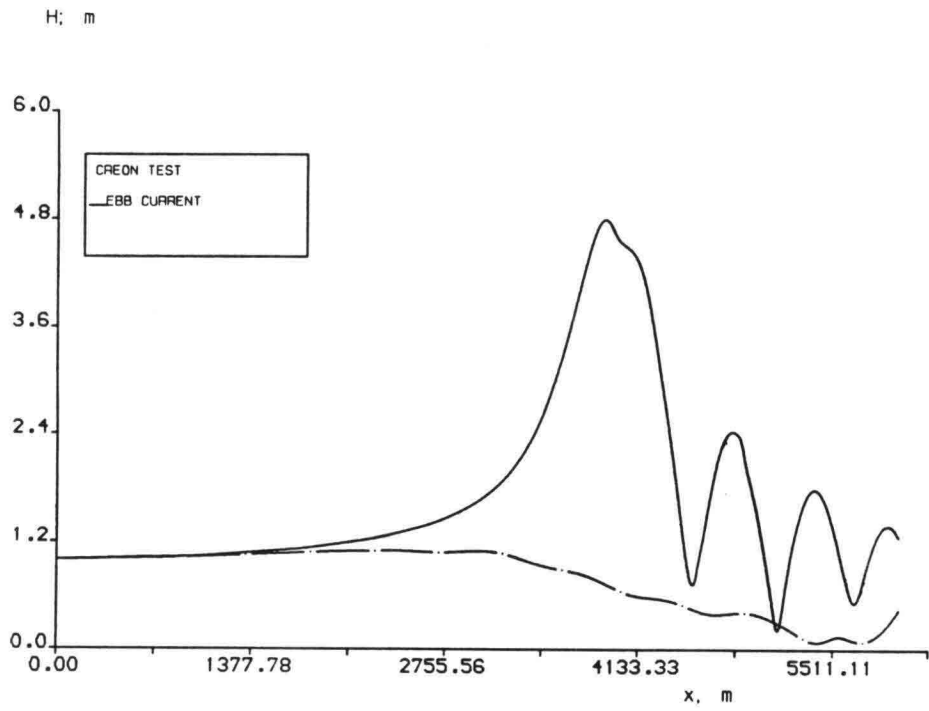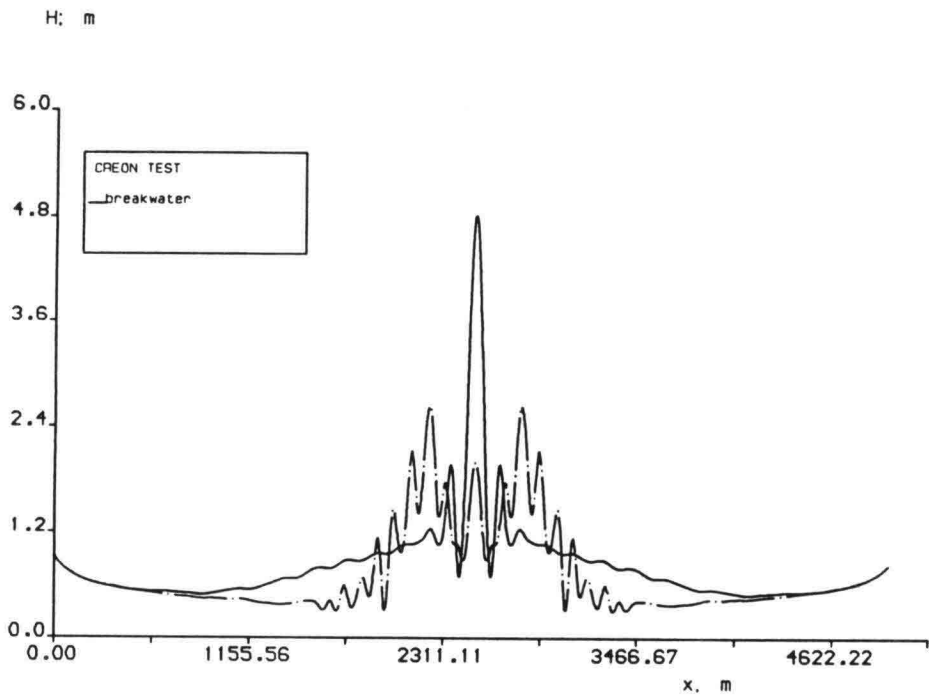
Fig 3.6 a) the height of monochromatic waves on the longitude sections. ———— : y=2500m, ——•—— y=1500m from lateral boundary. b) wave height on the cross sections, ————: x=3900m, ——•—— x=4900m. from upwave boundary.

(a)

H: m

CREON TEST
___EBB CURRENT

(b)

H: m

CREON TEST
___breakwater
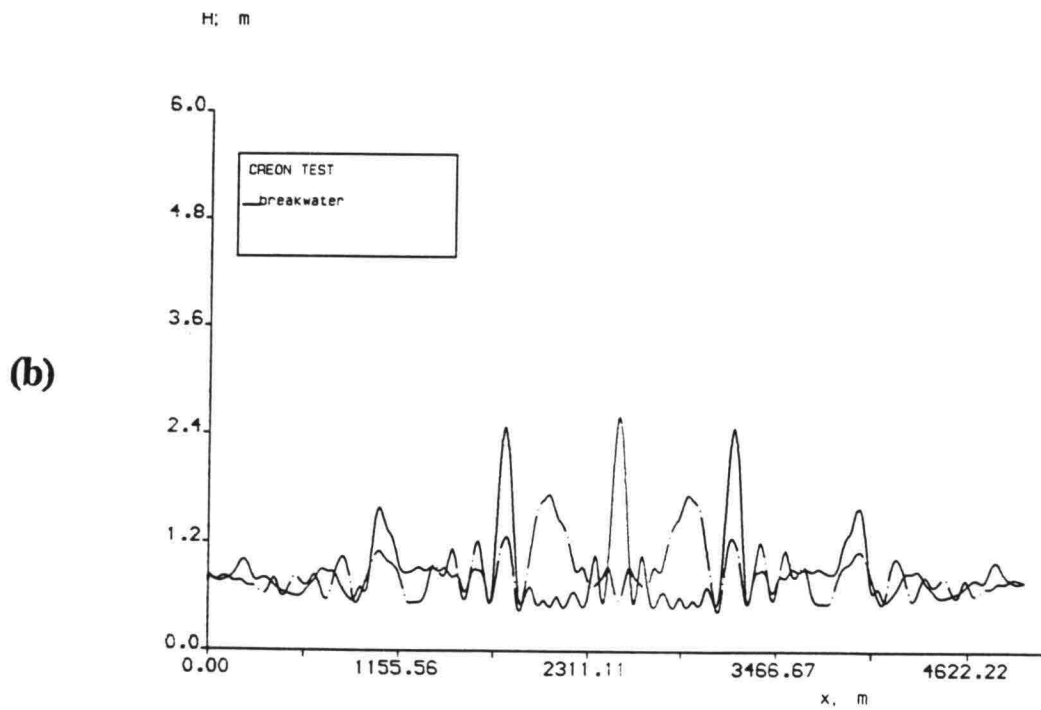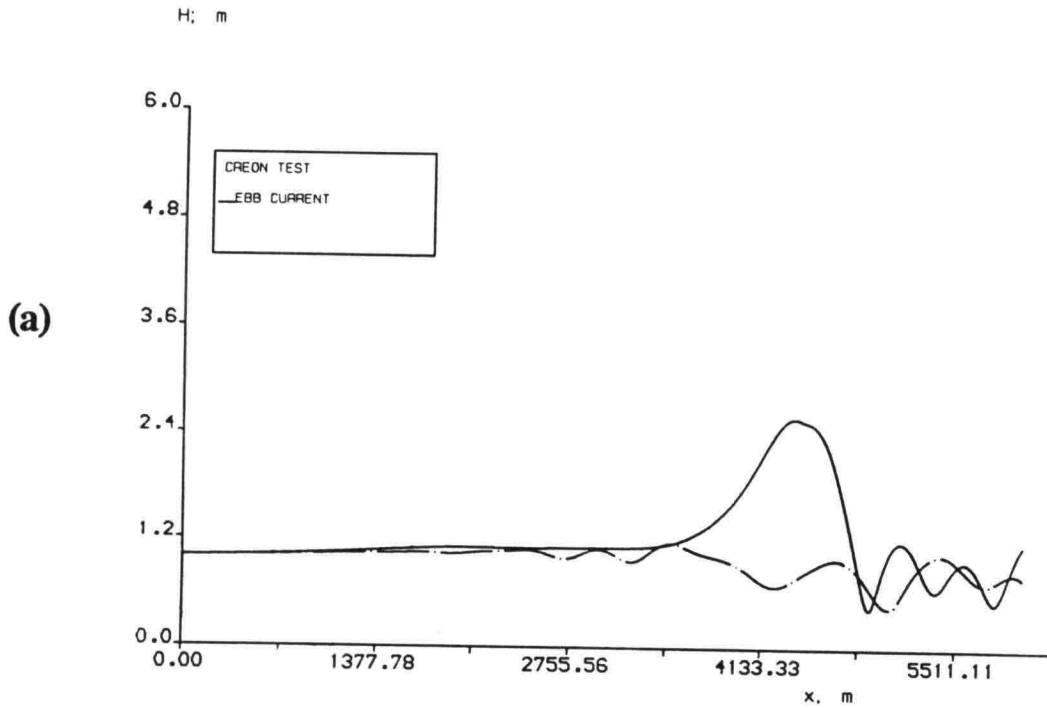
Fig 3.7 a) the height of *irregular* waves on the longitude sections. ————: y=2500m, ——•—— y=1500m from lateral boundary. b) wave height on the cross sections, ———— : x=4400m,——•.—— x=5400m from upwave boundary.

(a)
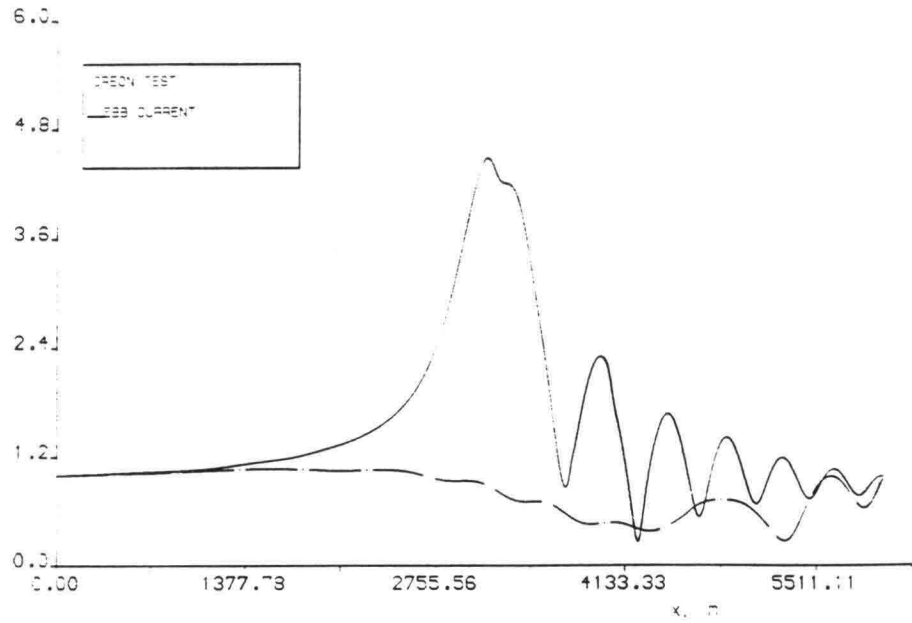
(b)
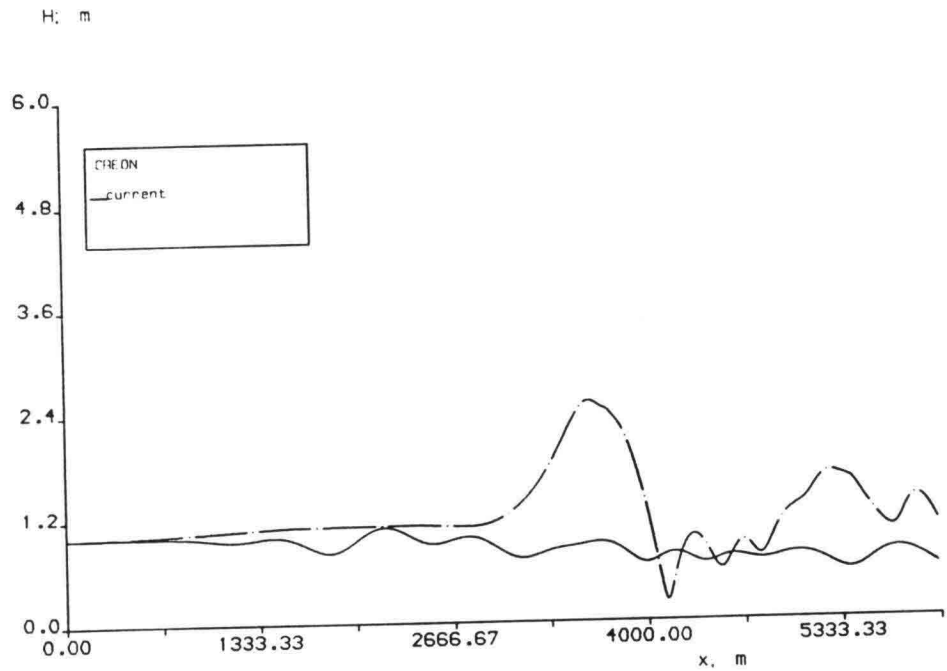
Fig.3.8 Waves propagate on a jetlike flow with a maximum velocity
u_0=-2.4m/s. The incident waves have H_s=1m, T=10s. a) monochromatic
waves, b) *irregular* waves on longitude sections as Fig. 3.6(a).

H: m

(a)

CREON TEST
EBB CURRENT

H: m

(b)

CREON TEST
EBB CURRENT
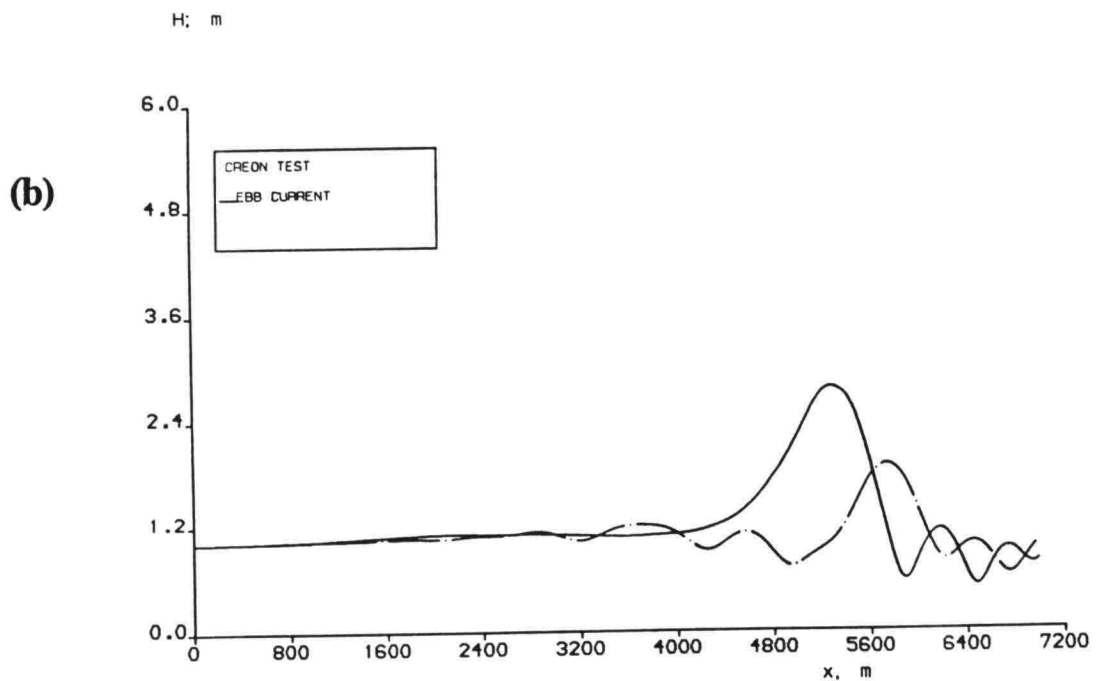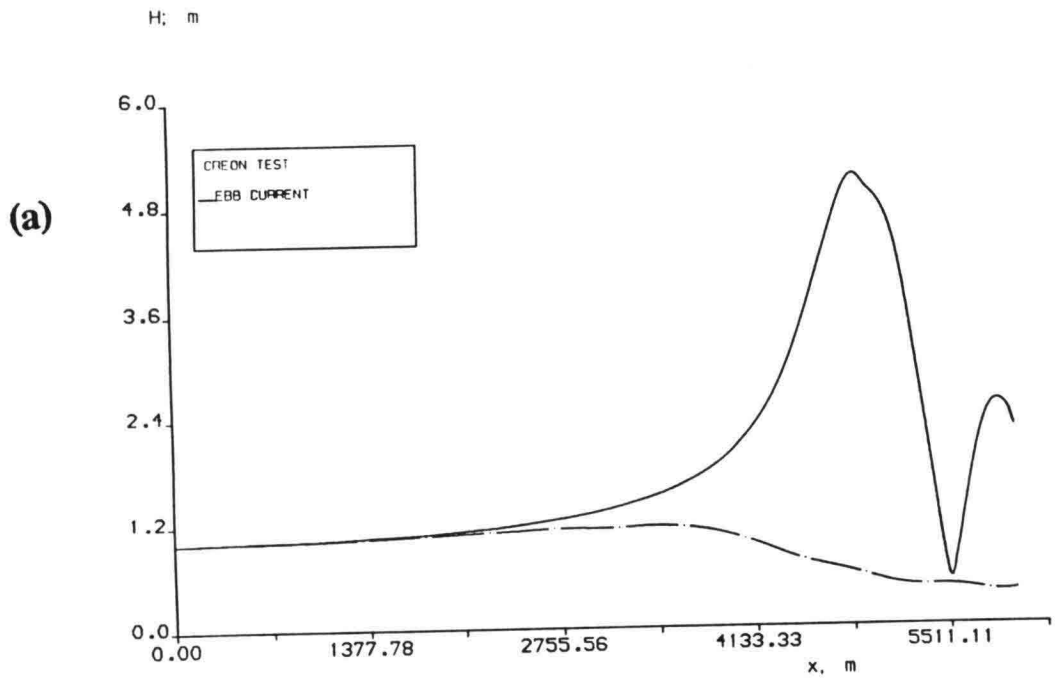
Fig.3.9 Waves propagate on a jetlike flow with a maximum velocity
$u_0=-1.6$m/s. a) monochromatic waves, b) *irregular* waves   on the
longitude section as Fig. 3.6(a)

39
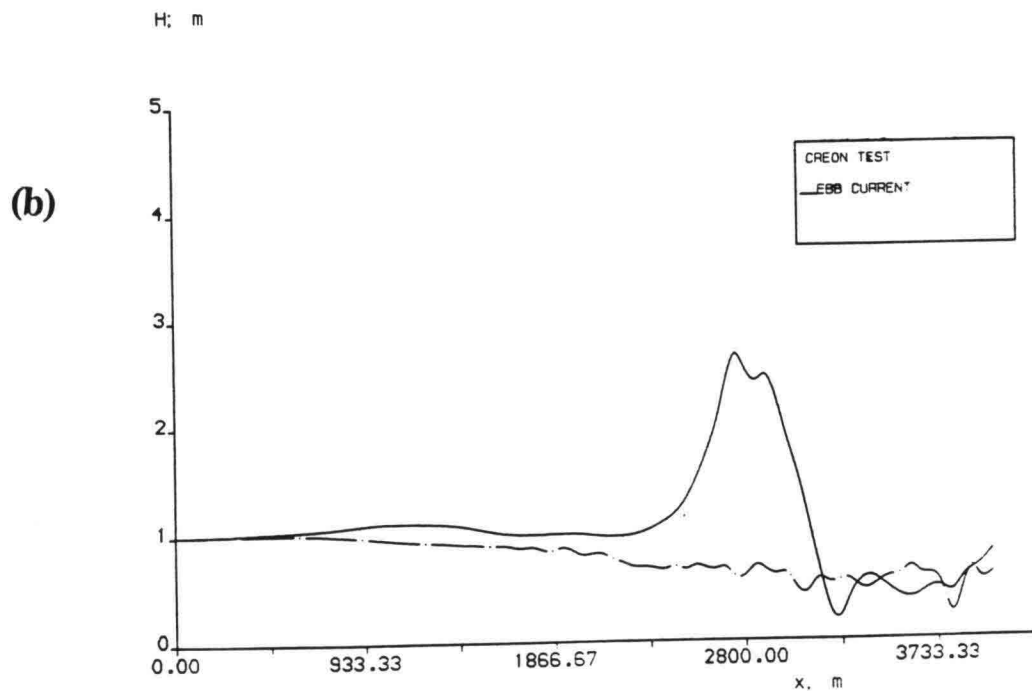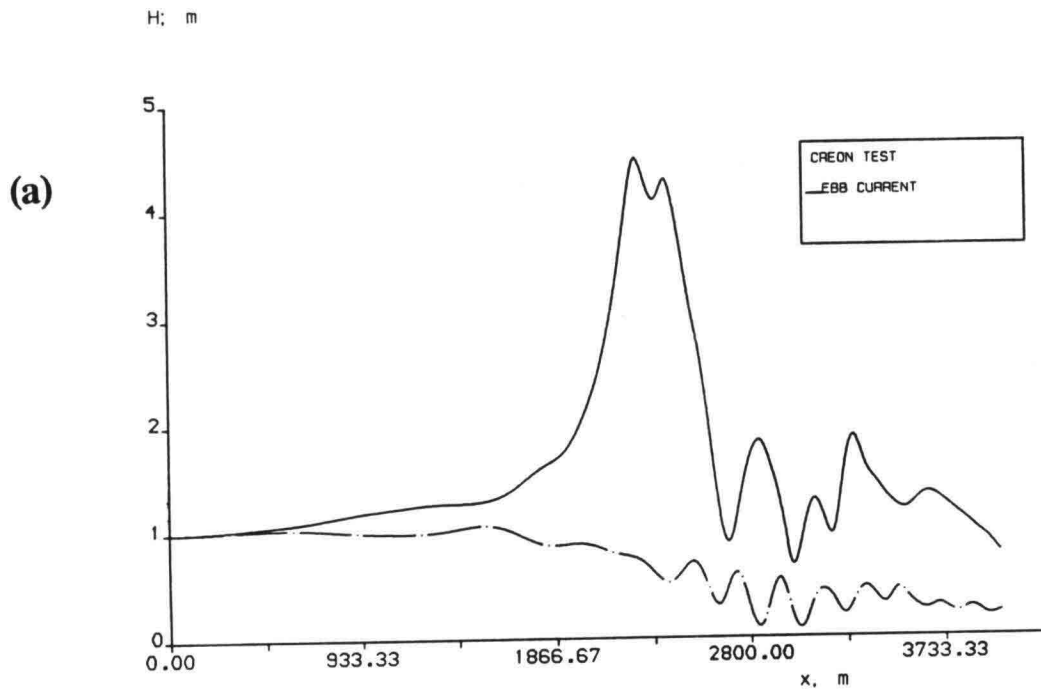
Fig. 3.10 Waves propagate with period T=7s, H_s=1m. a)monochromatic waves, b) *irregular* waves on longitude section as Fig. 3.6(a).

H: m

(a)

(b)
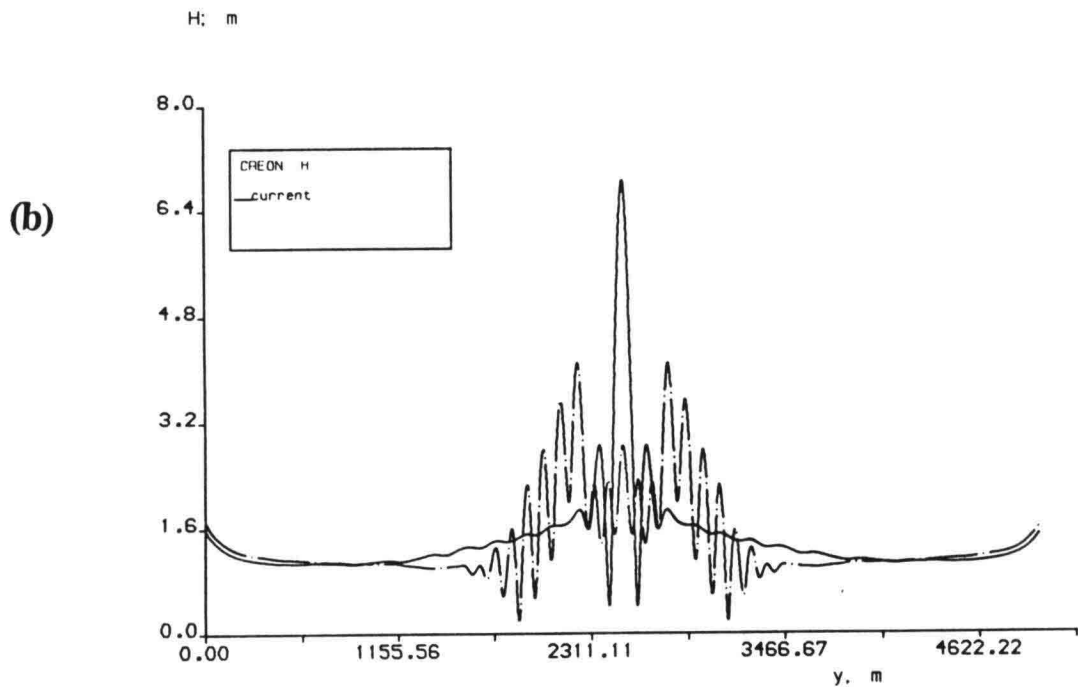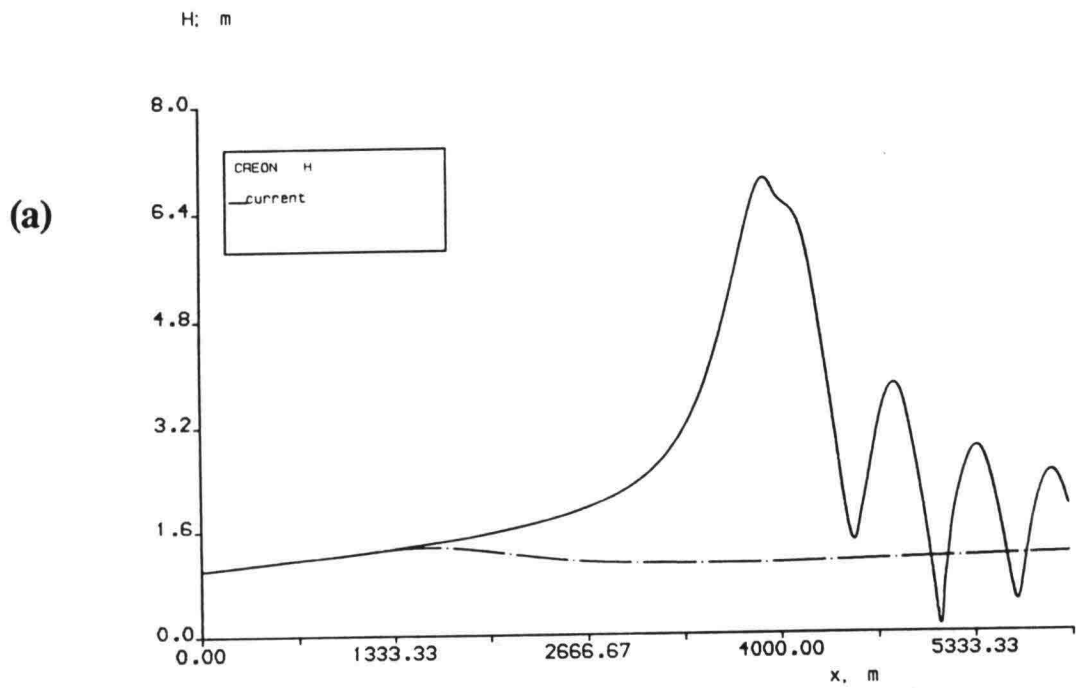
Fig. 3.11 wind with speed w=20m/s *blowing* over the flow in the direction of incident waves. a) the monochromatic waves on the longitude sections as Fig.3.6(a), b) wave height on the cross sections as Fig.3.6(b).

41

H: m

(a)

H: m

(b)
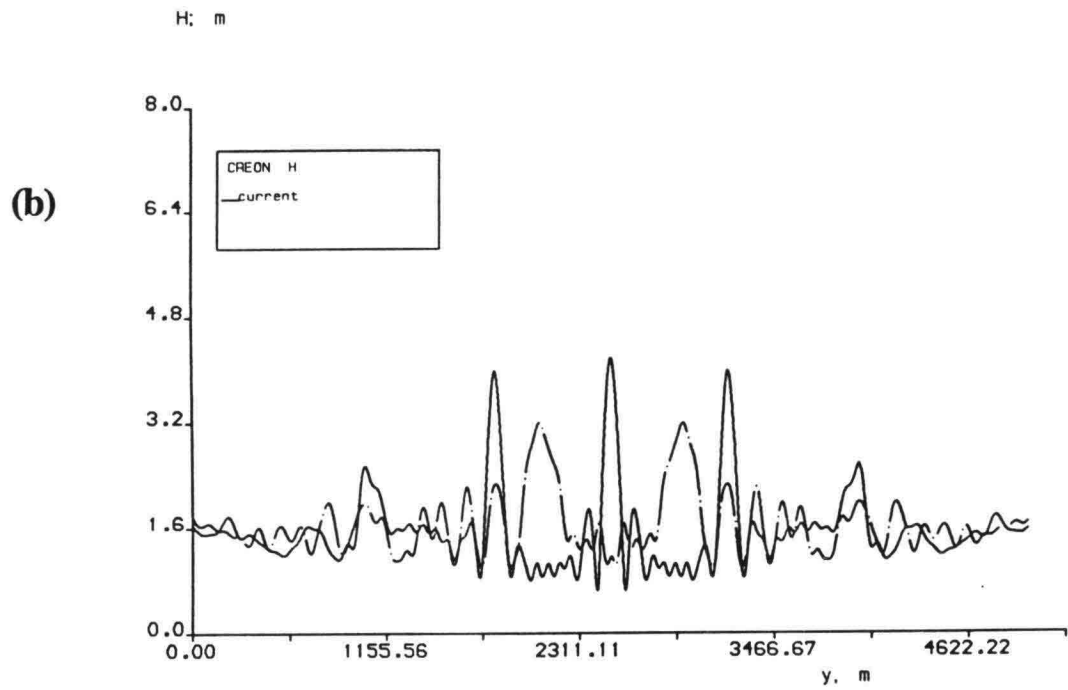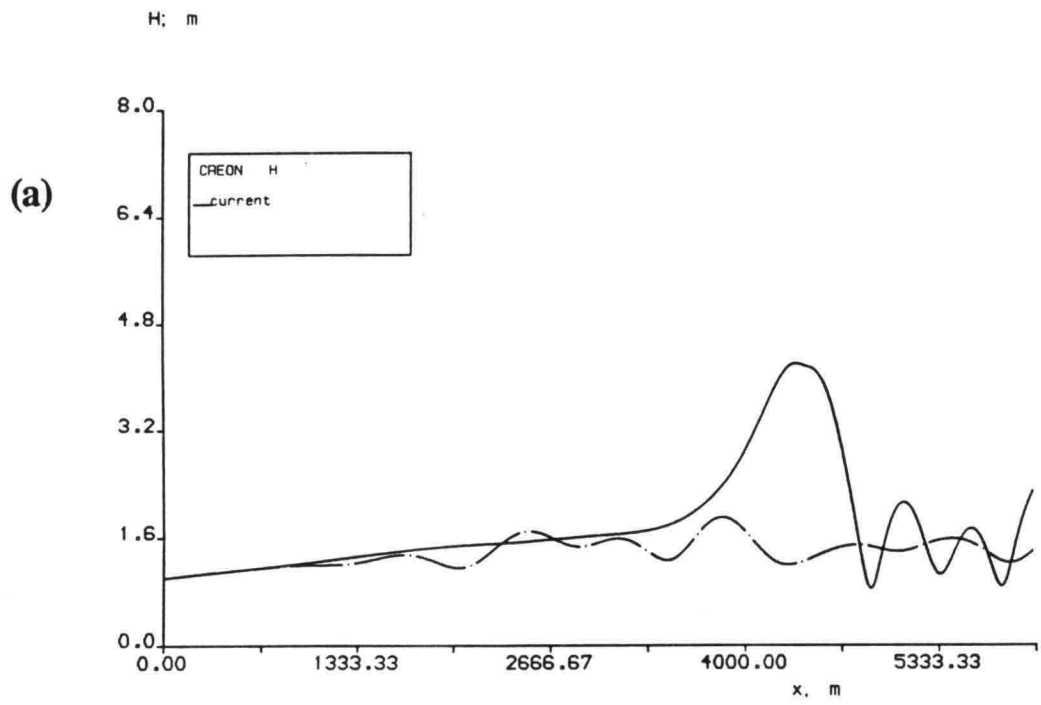
Fig 3.12 the same as Fig. 3.11 for *irregular* waves. a) longitude
sections as Fig.3.7(a), b)cross sections as Fig. 3.7(b).

42

(a)
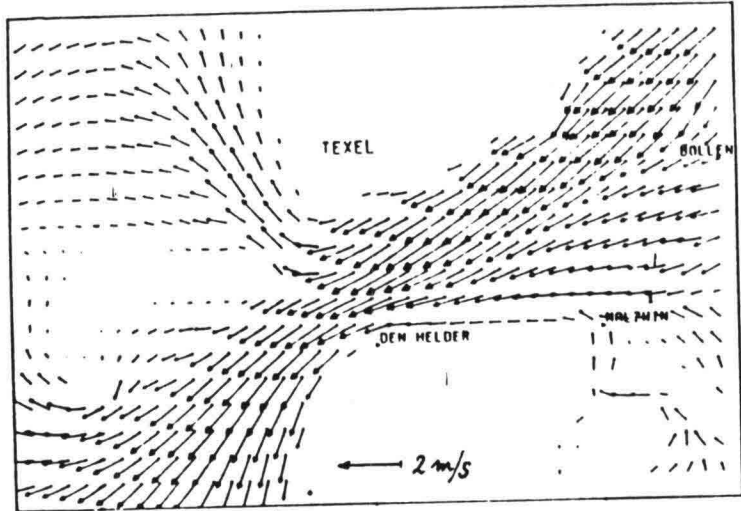
(b)
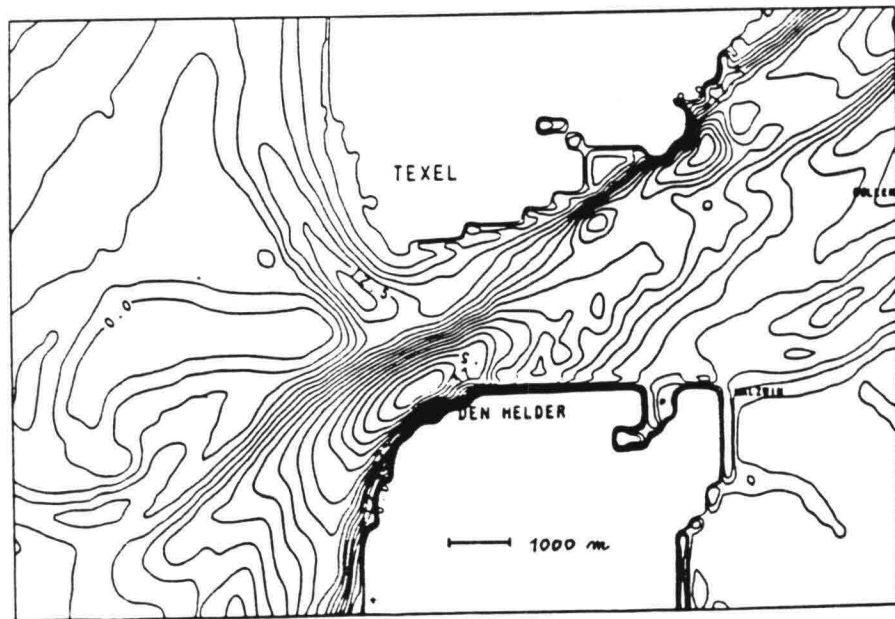
Fig. 4.1 a) ebb currents in the area of tidal inlet Texel, b) depth isolines.
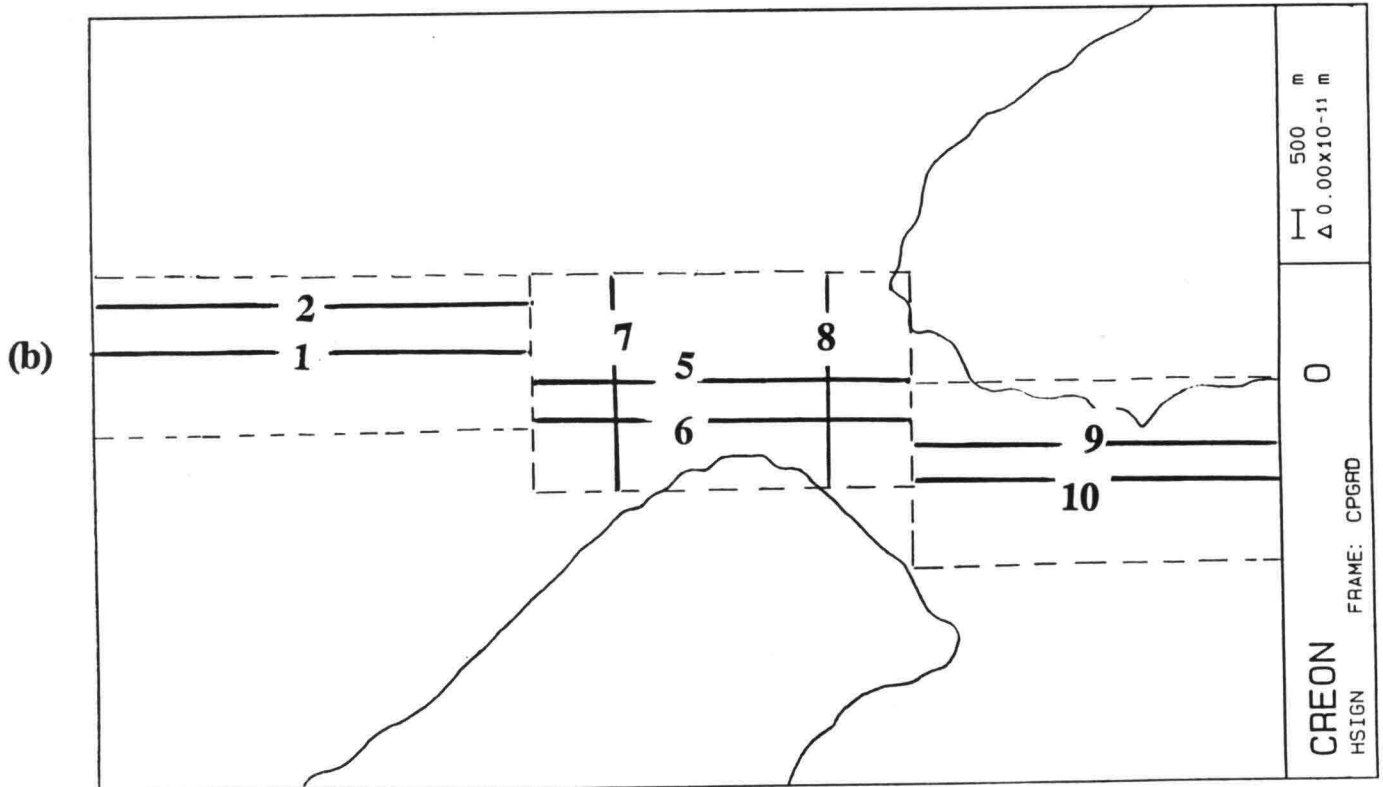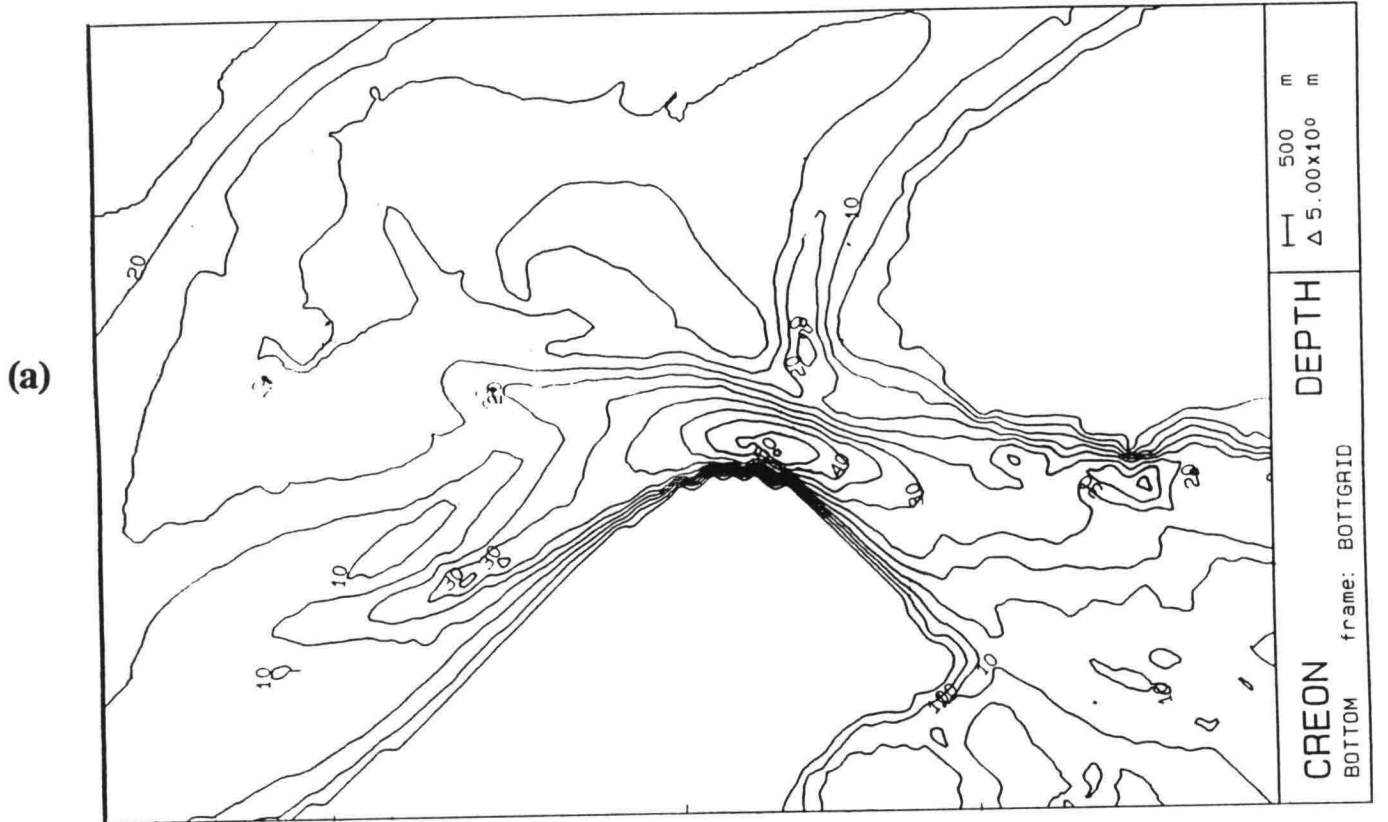
Fig. 4.2 a) computational area and depth isolines. b) output lines
in the computational area.

(a)

(b)
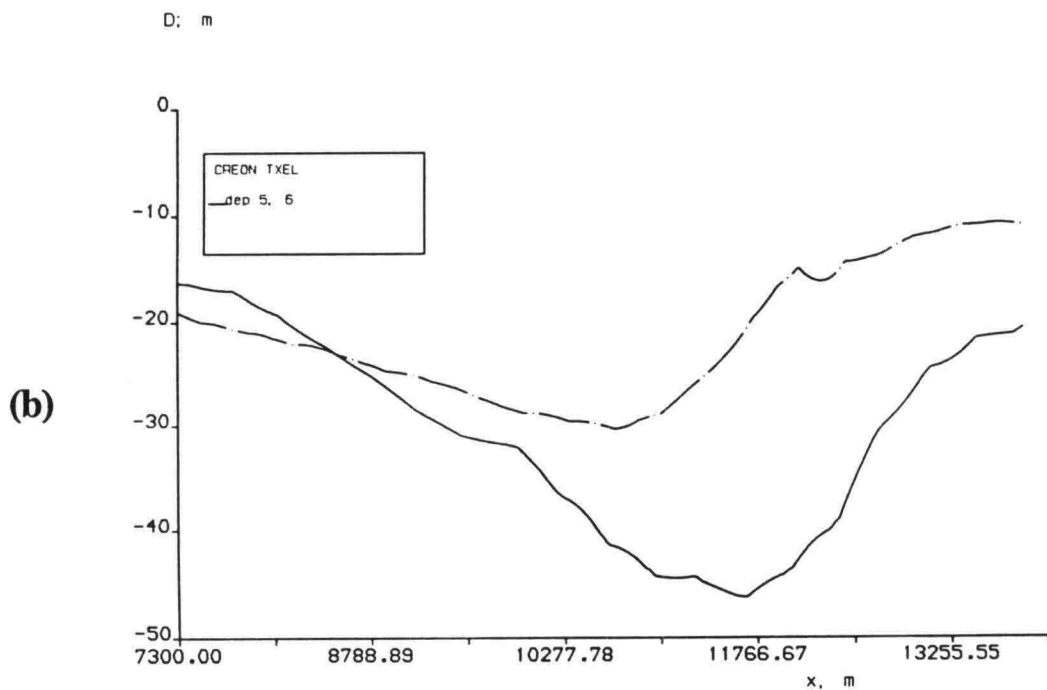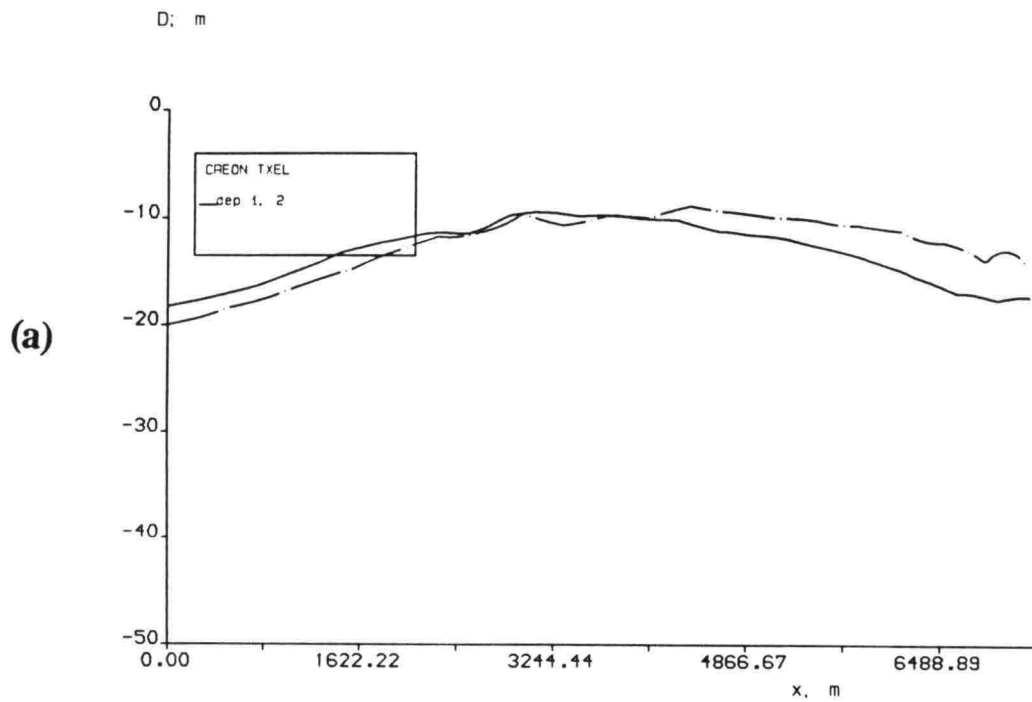
Fig. 4.3 Depth along the output lines.
a) —————: line 1; ——•——: line 2
b) ——•——: line 5; —————: line 6.

(c)

D: m

(d)

D: m.
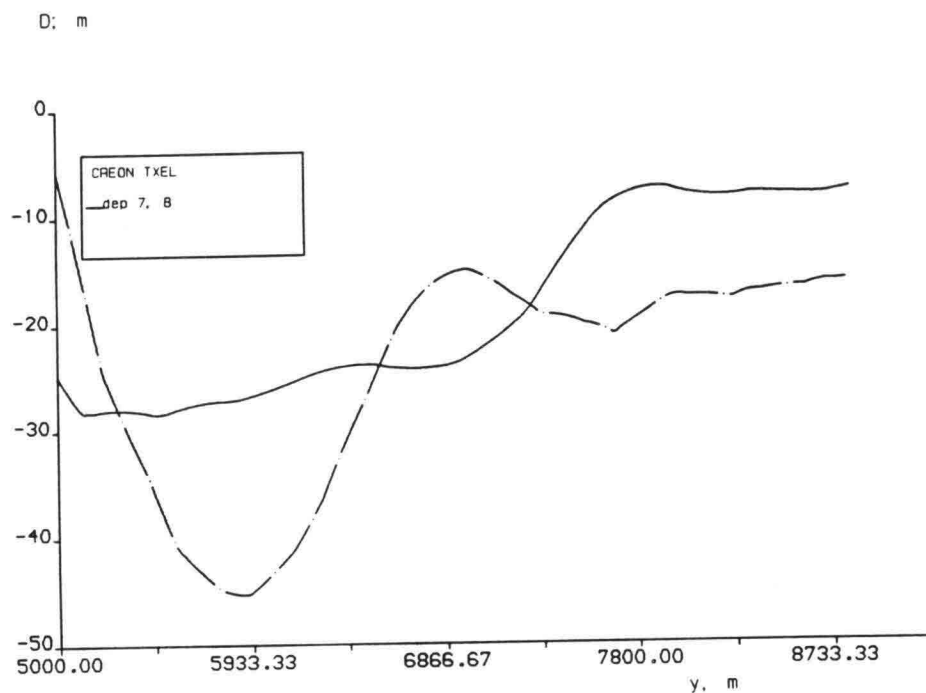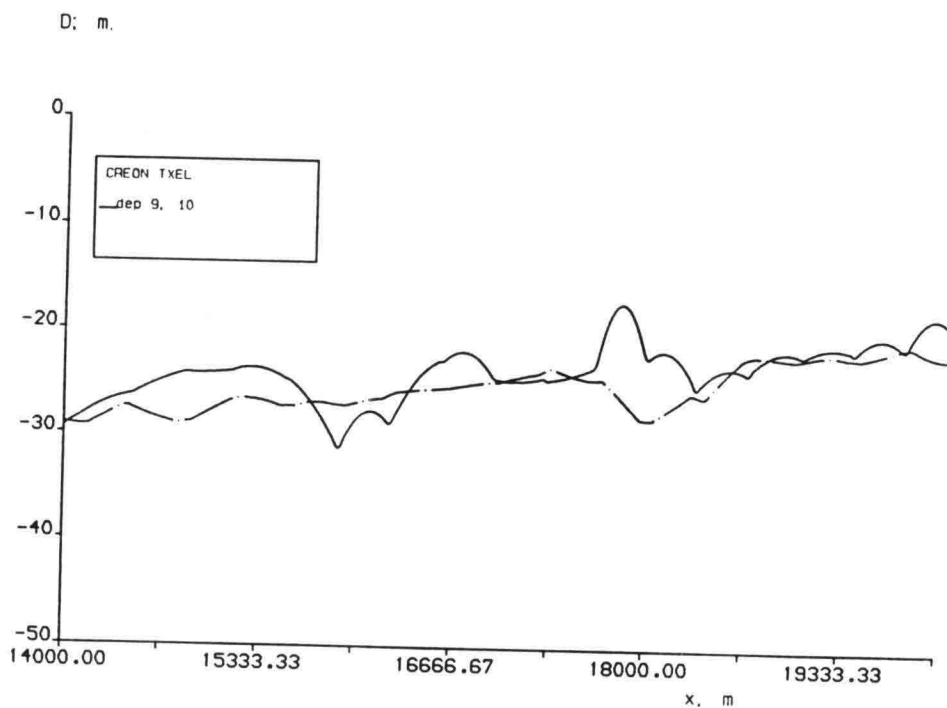
Fig. 4.3 (continued) c) ――――― : line 7; ――•――: line 8
d) ――――: line 9; ―•――: line 10.

U: m/s

(a)

U: m/s

(b)
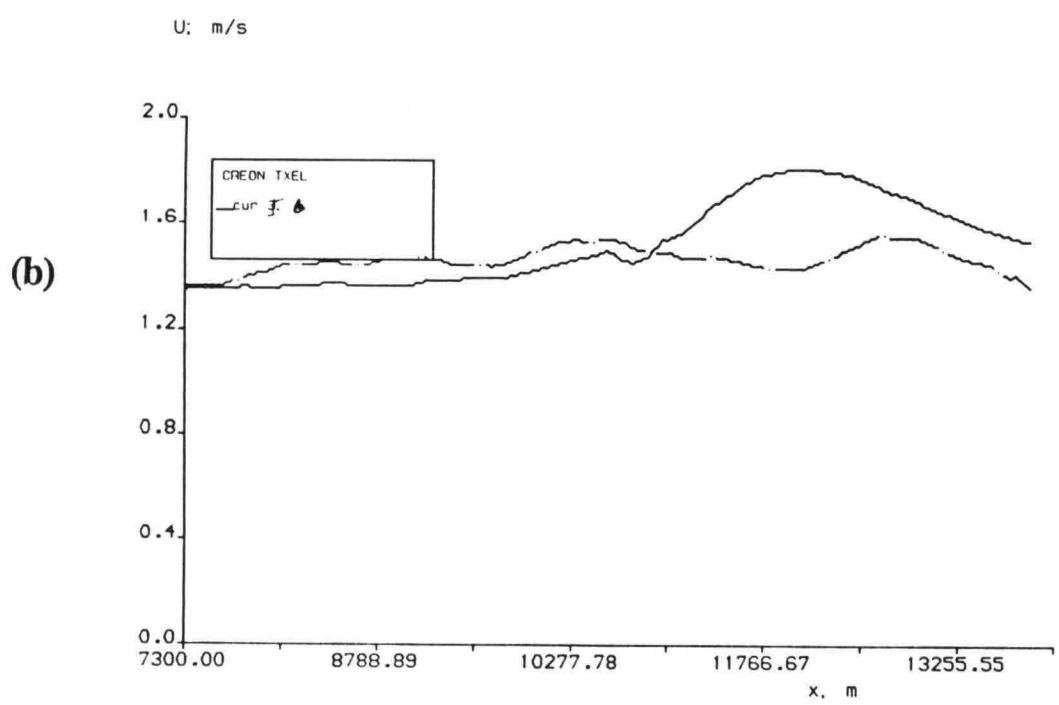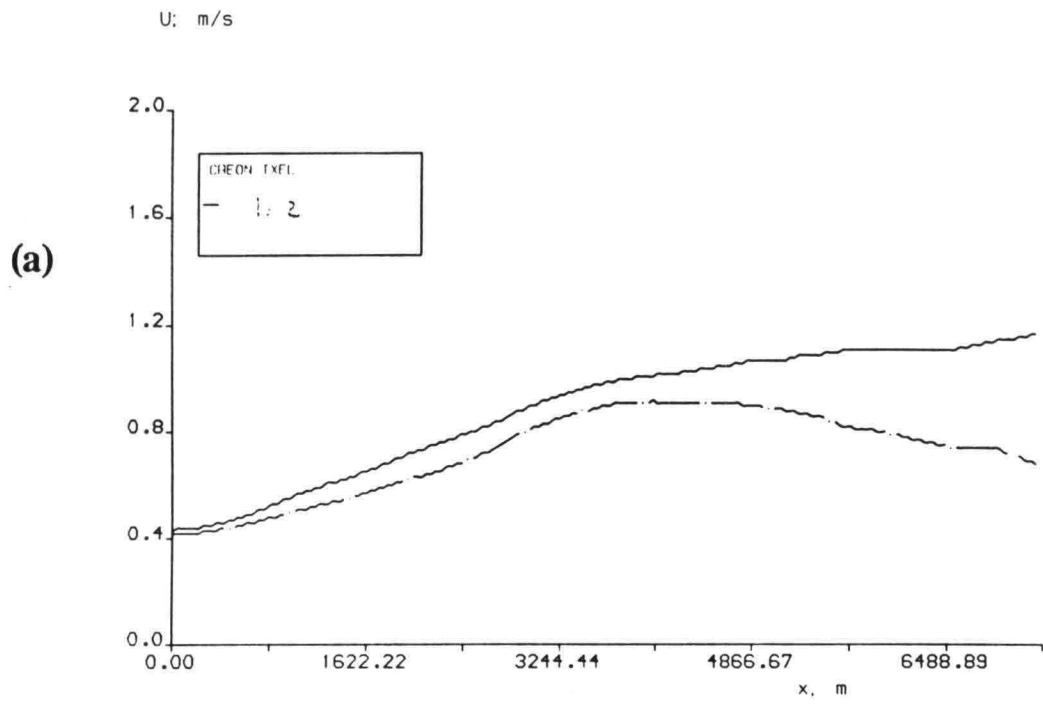
Fig. 4.4 velocity along the output lines. The notations of lines
are the same for the wave height output in the following computa-
tions.
a) ————: line 1; —·——: line 2
b) —·——: line 5; ————: line 6.

(c)

(d)
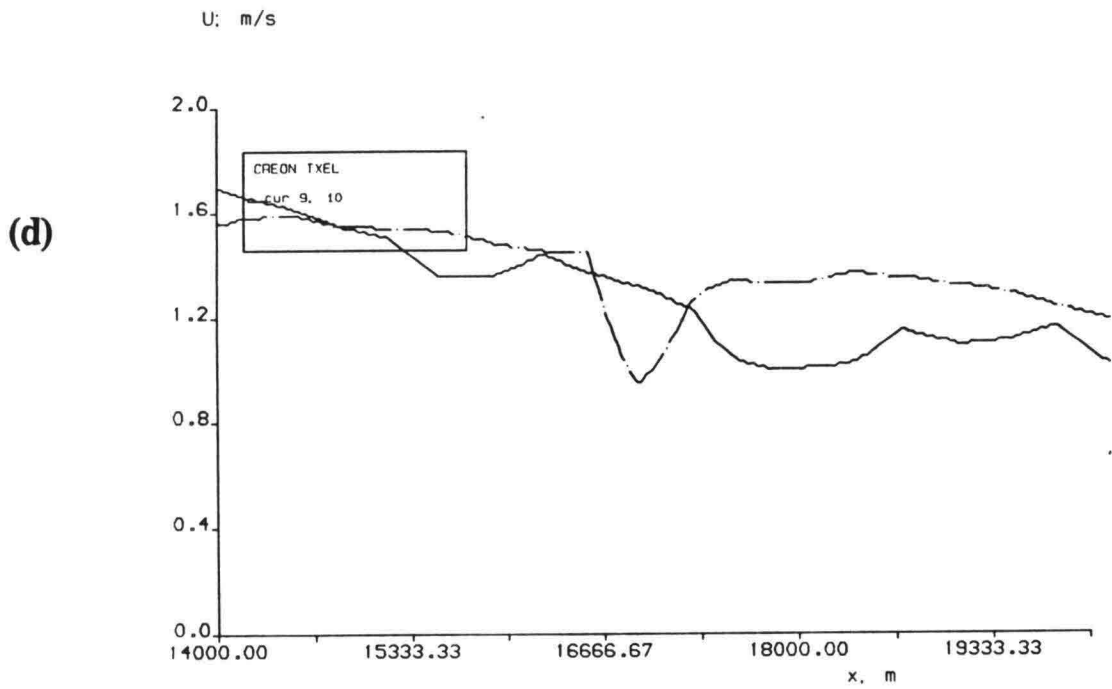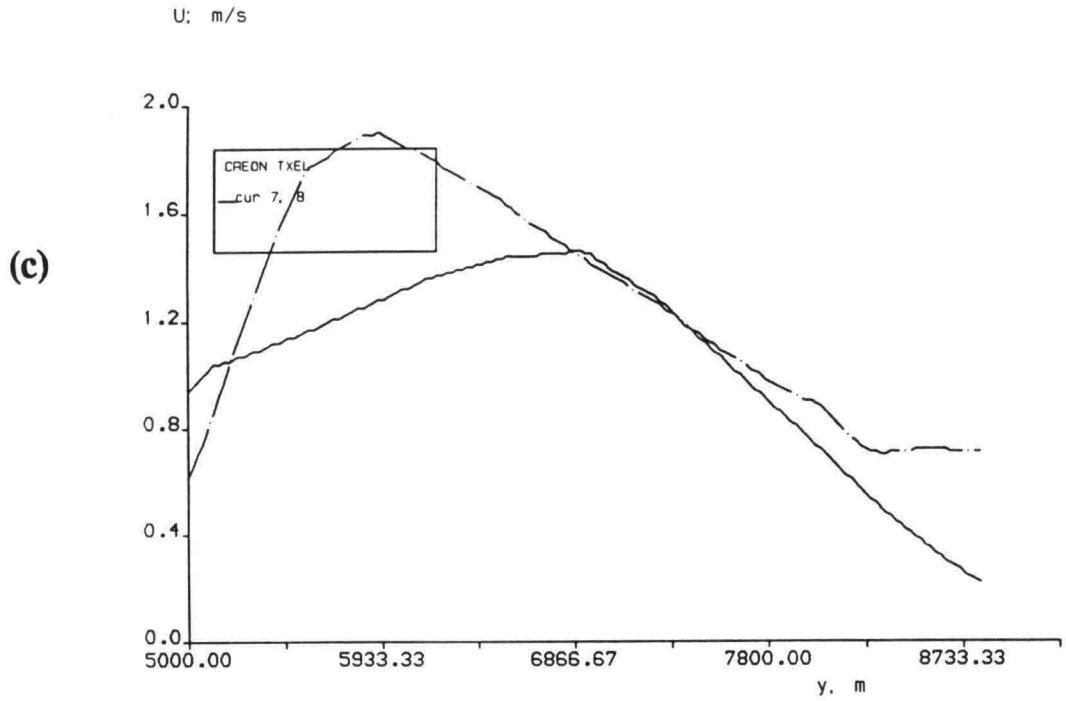
Fig. 4.4 (continued) c) ———: line 7; ——●——: line 8
d) ———: line 9; ——●——: line 10.

(a)

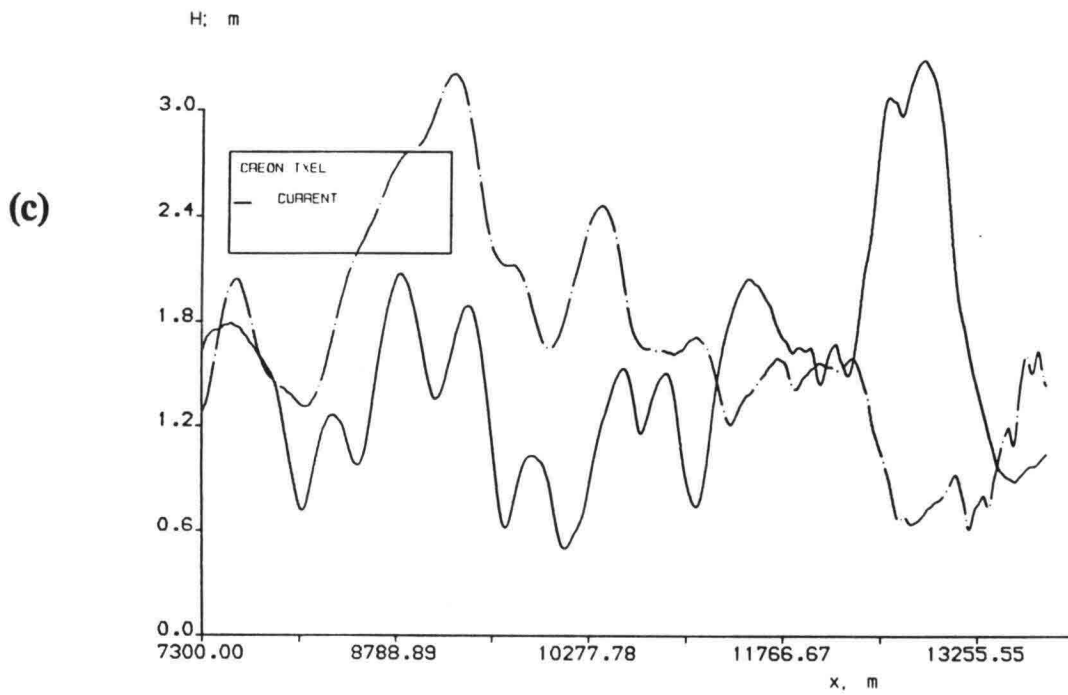Fig. 4.5   computed waves of case I, a) wave field, *isolines*
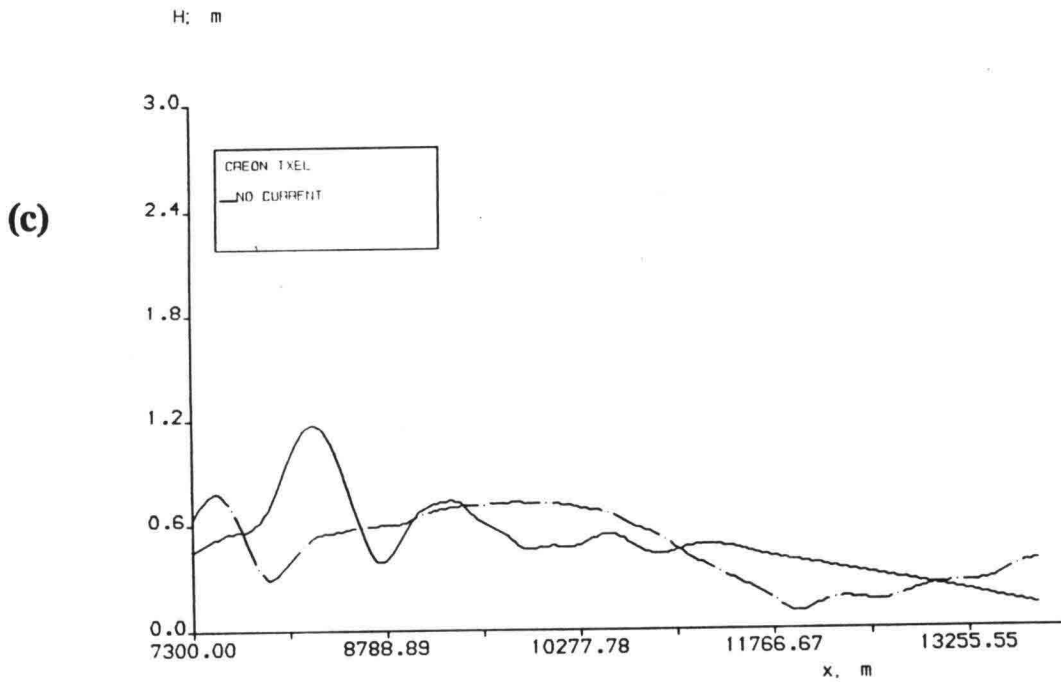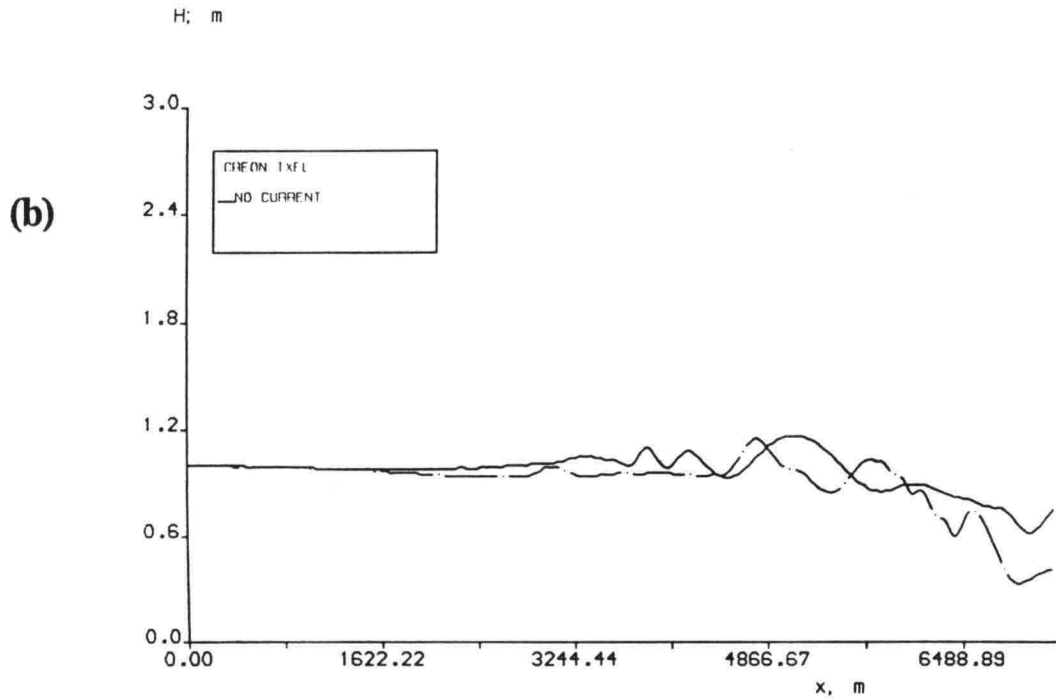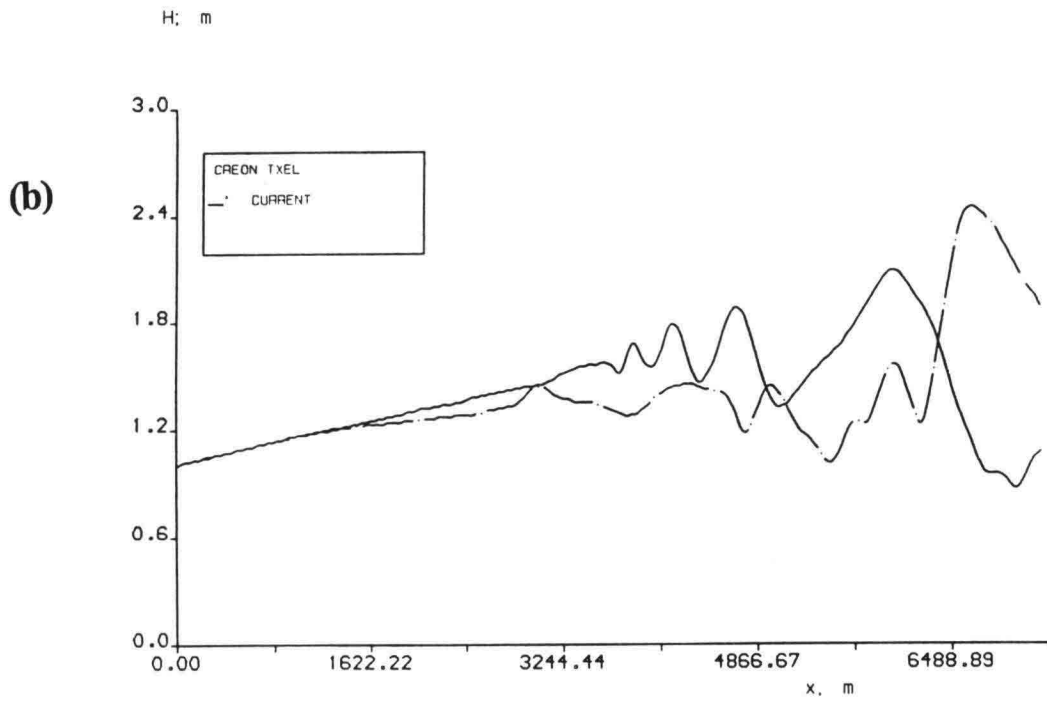
Fig. 4.5(continued) b) wave heights along line 1 and line 2, c) wave heights along line 5 and line 6.
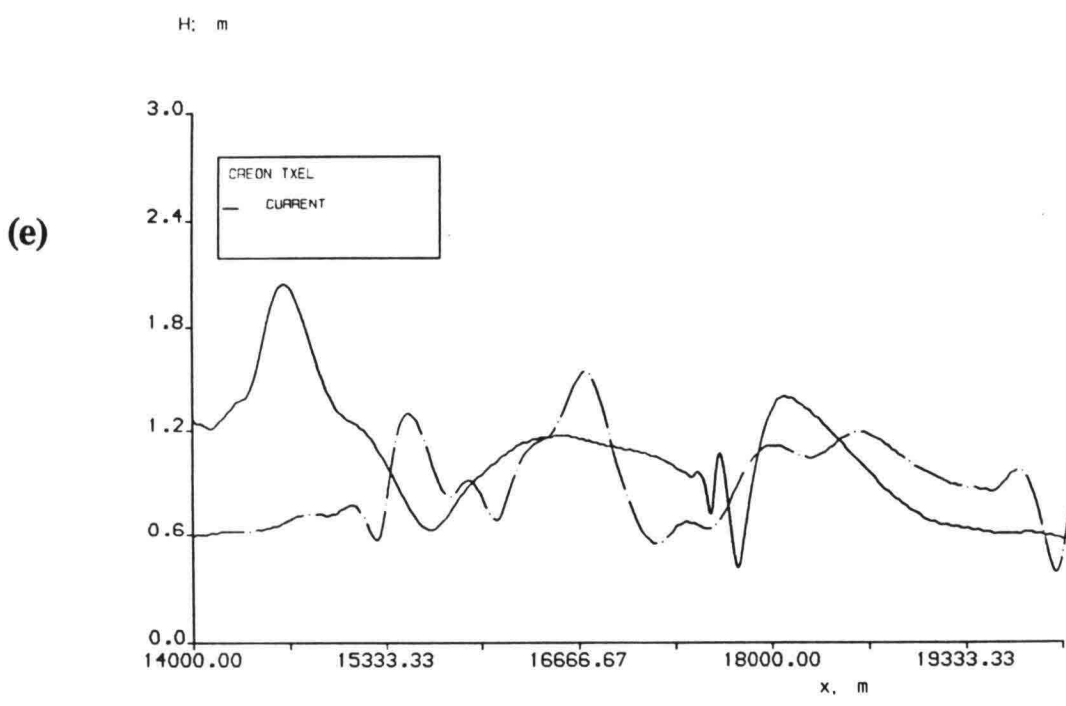
(d)

(e)
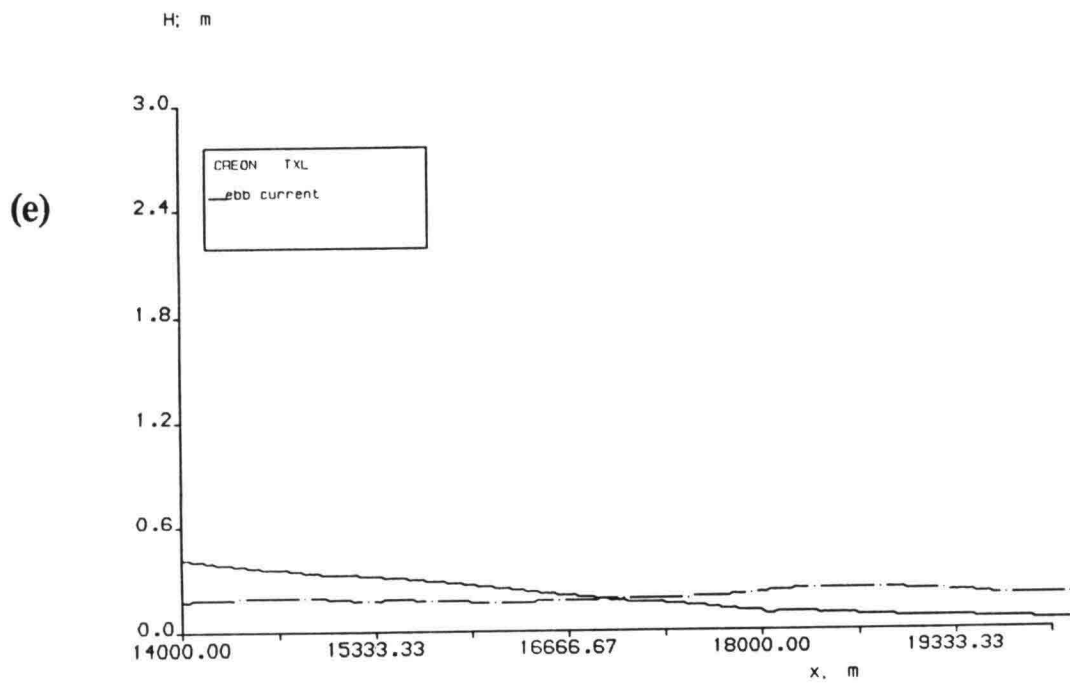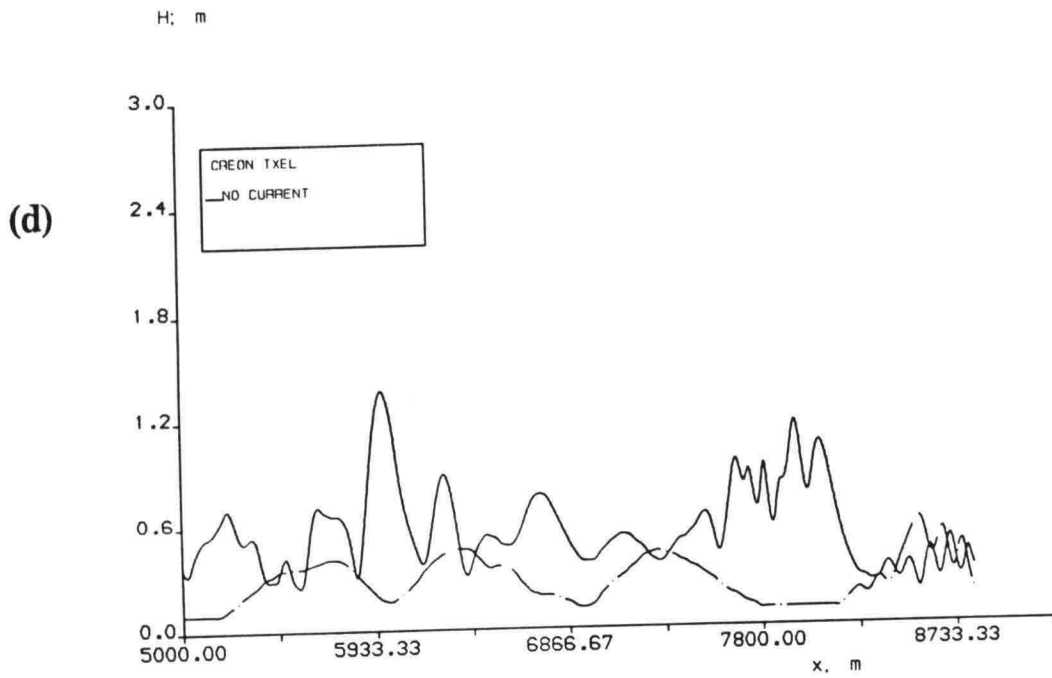
Fig. 4.5(continued) d) wave heights along line 7 and line 8, e)
wave heights along line 9 and line 10

(a)

Fig. 4.6   computed waves of case II, a) wave field, *isolines*

(b)

H: m

3.0

2.4

CREON TXEL

EBB CURRENT

1.8

1.2

0.6

0.0

0.00   1622.22   3244.44   4866.67   6488.89

X. m

(c)

H: m

3.0

2.4

CREON TXEL

EBB CURRENT

1.8

1.2

0.6

0.0

7300.00   8788.89   10277.78   11766.67   13255.55

x. m
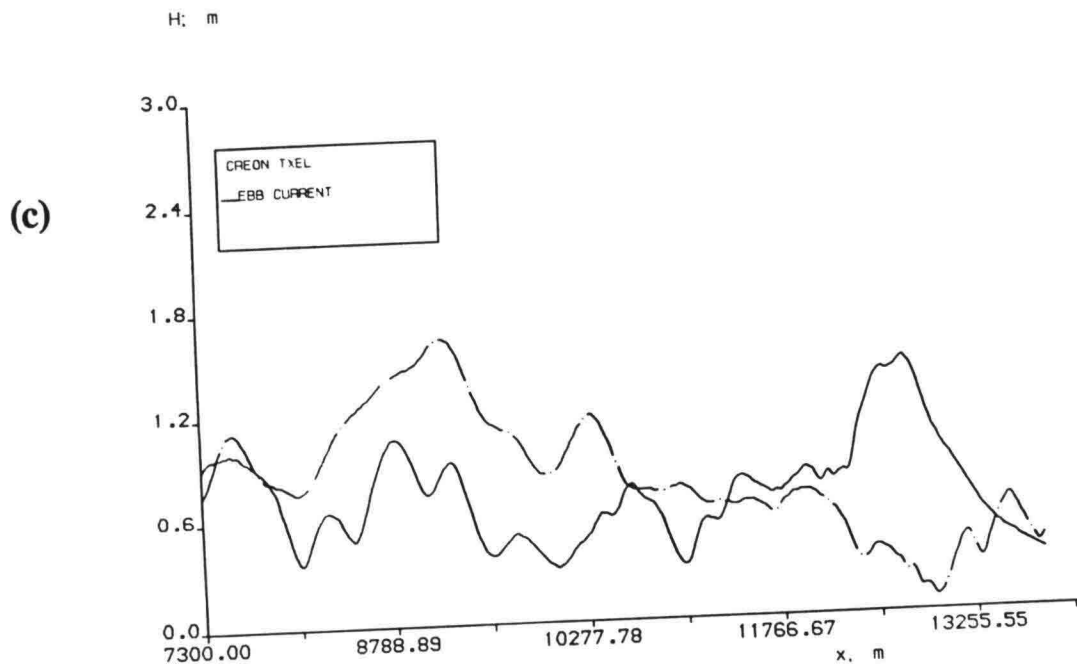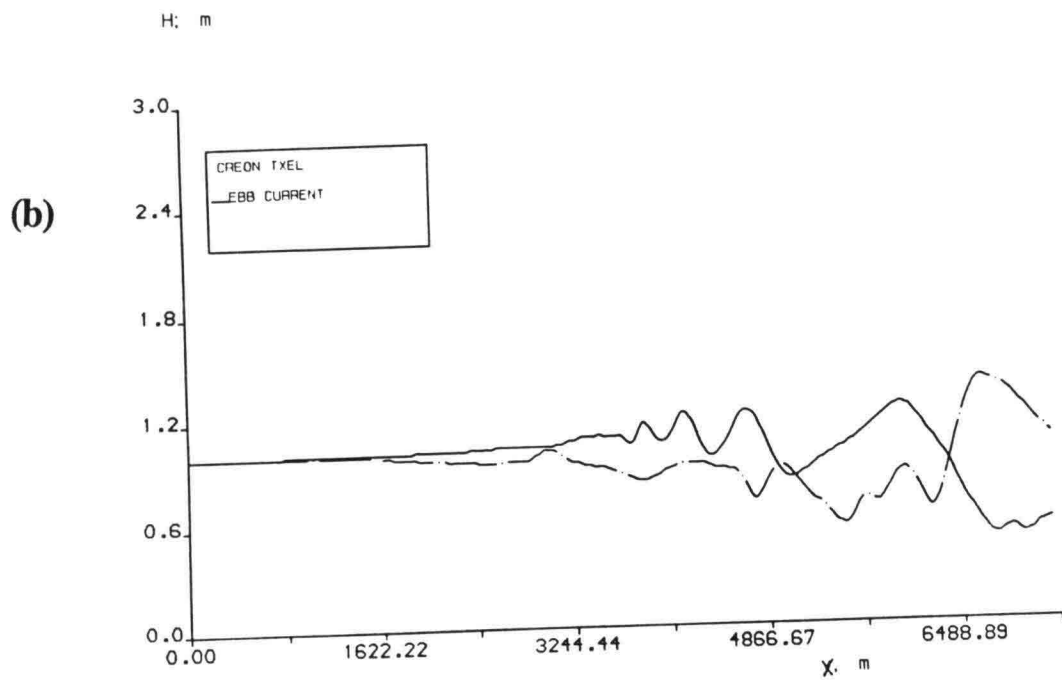
Fig. 4.6(continued) b) wave heights along line 1 and line 2, c) wave heights along line 5 and line 6.

53

(d)

(e)

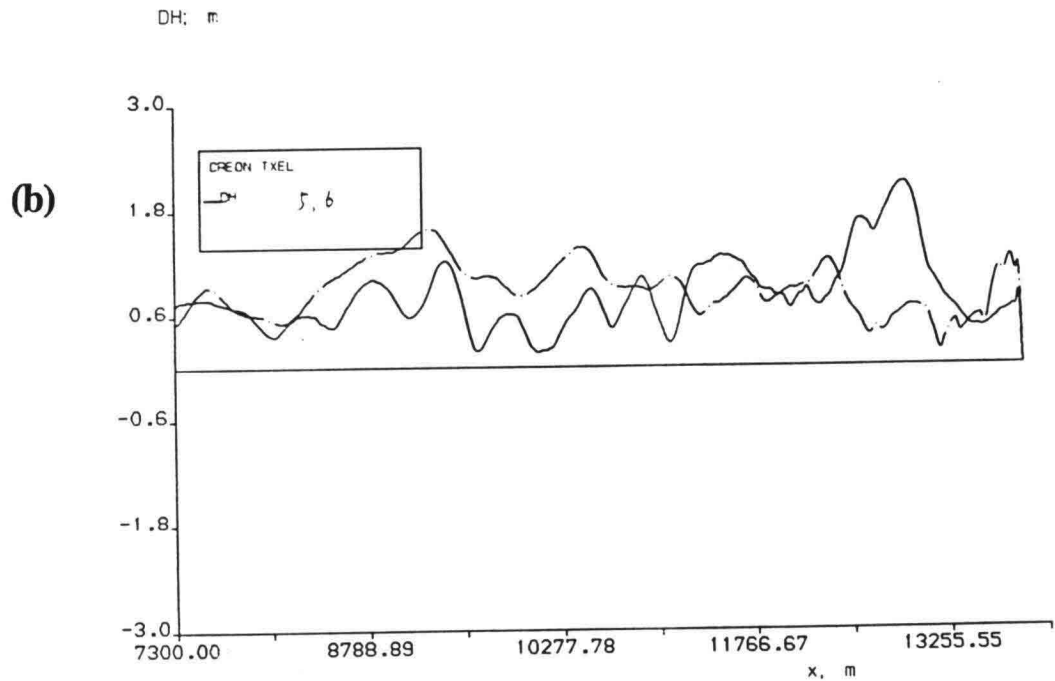Fig. 4.6(continued) d) wave heights along line 7 and line 8, e)
wave heights along line 9 and line 10

DH: m

3.0

(a)

1.8

CREON T·EL

DH 1, 2

0.6

-0.6

-1.8

-3.0

0.00   1622.22   3244.44   4866.67   6488.89

x, m

DH: m

3.0

(b)

1.8

CREON T·EL

DH   5, 6

0.6

-0.6

-1.8

-3.0

7300.00   8788.89   10277.78   11766.67   13255.55

x, m
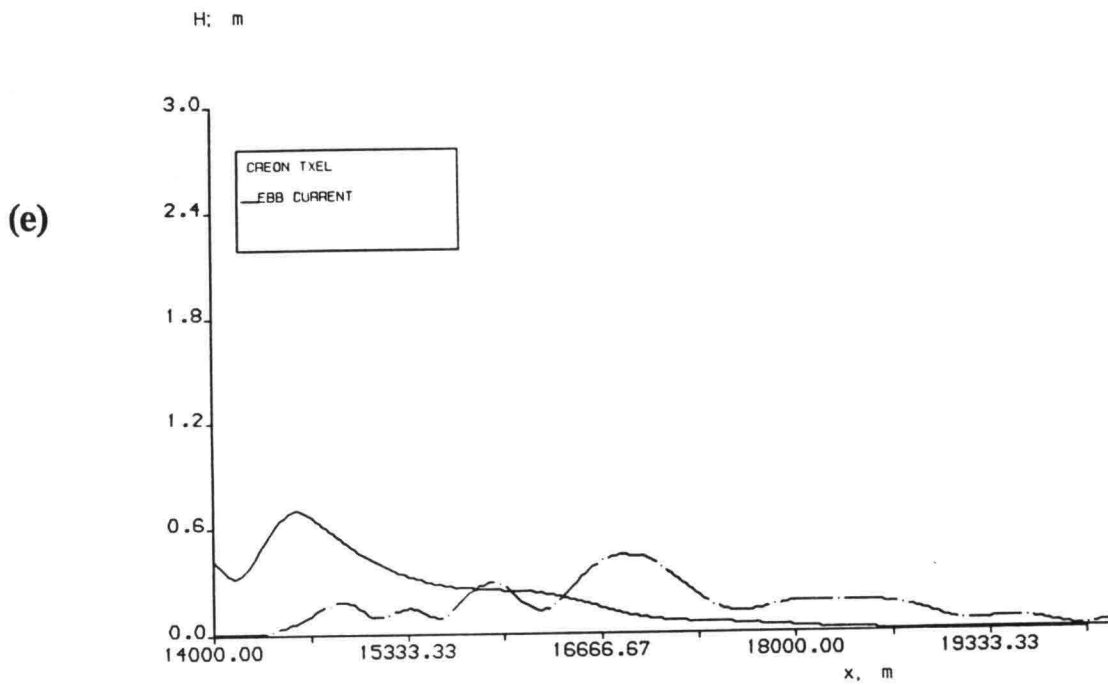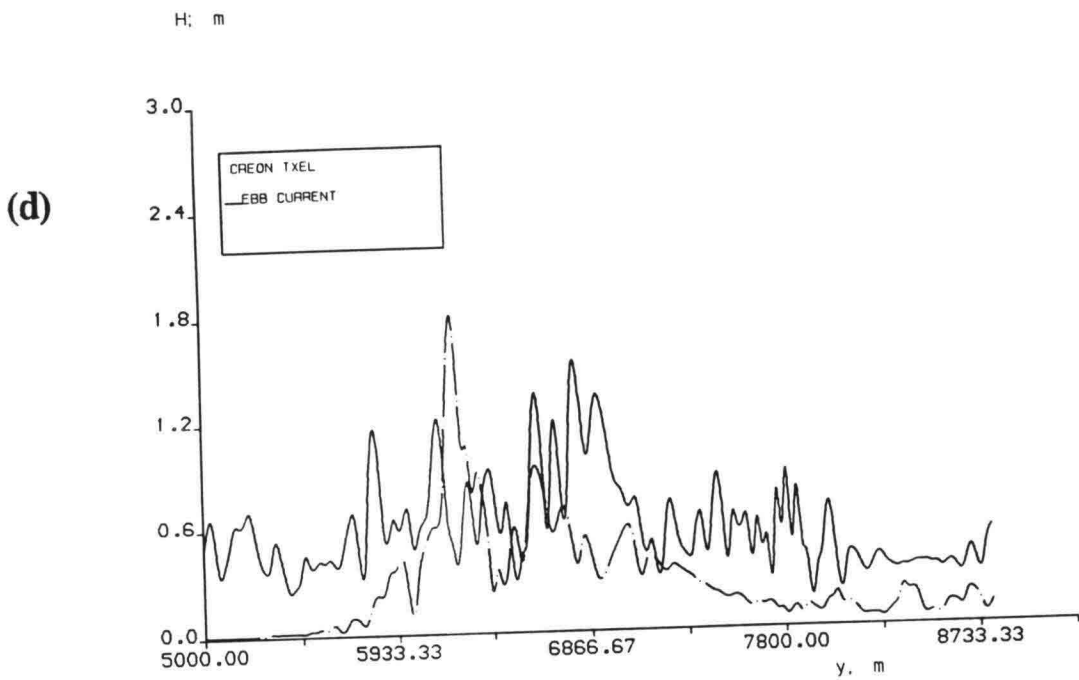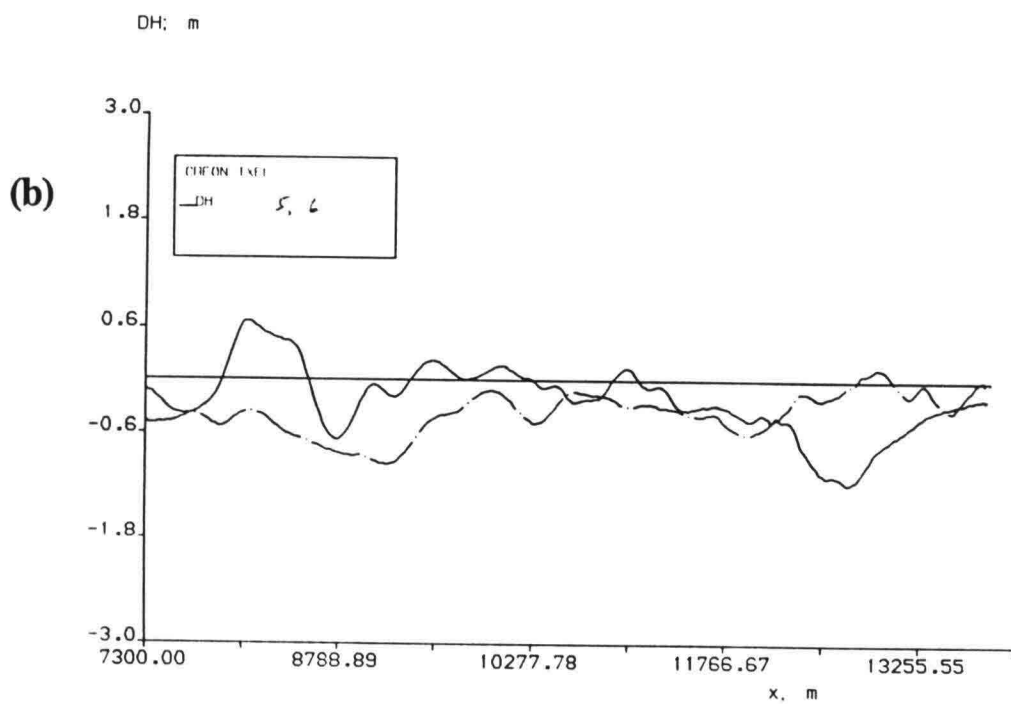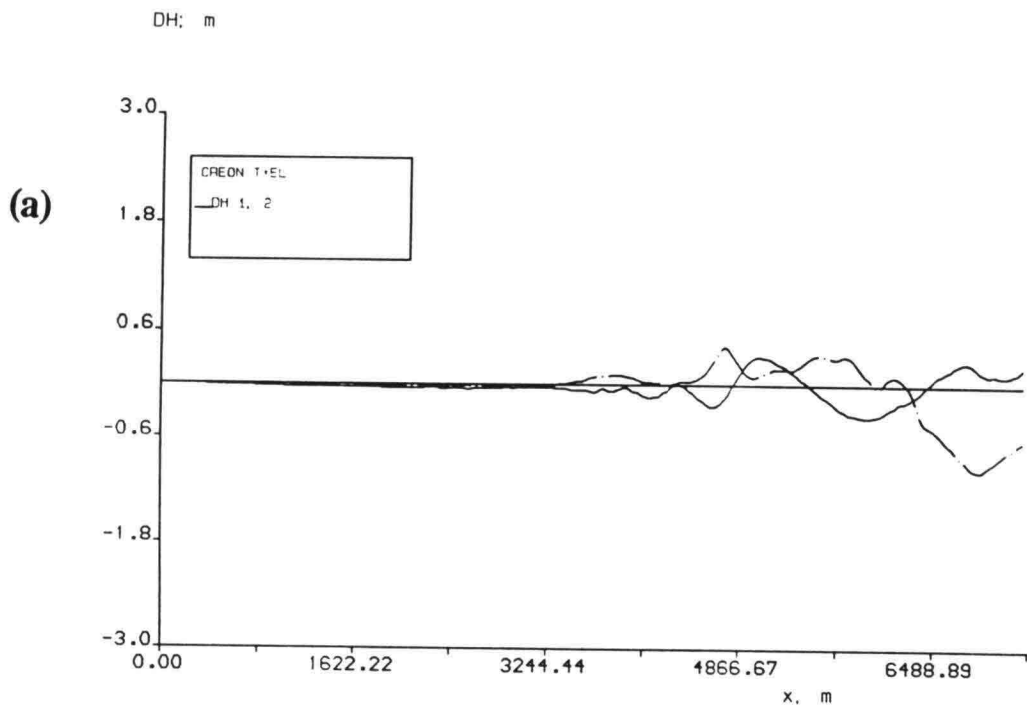
Fig. 4.7 The difference of wave heights between case I and case II. $\Delta H = H_i - H_{ii}$. a) the differences along line 1 and line 2, b), along line 5 and line 6.
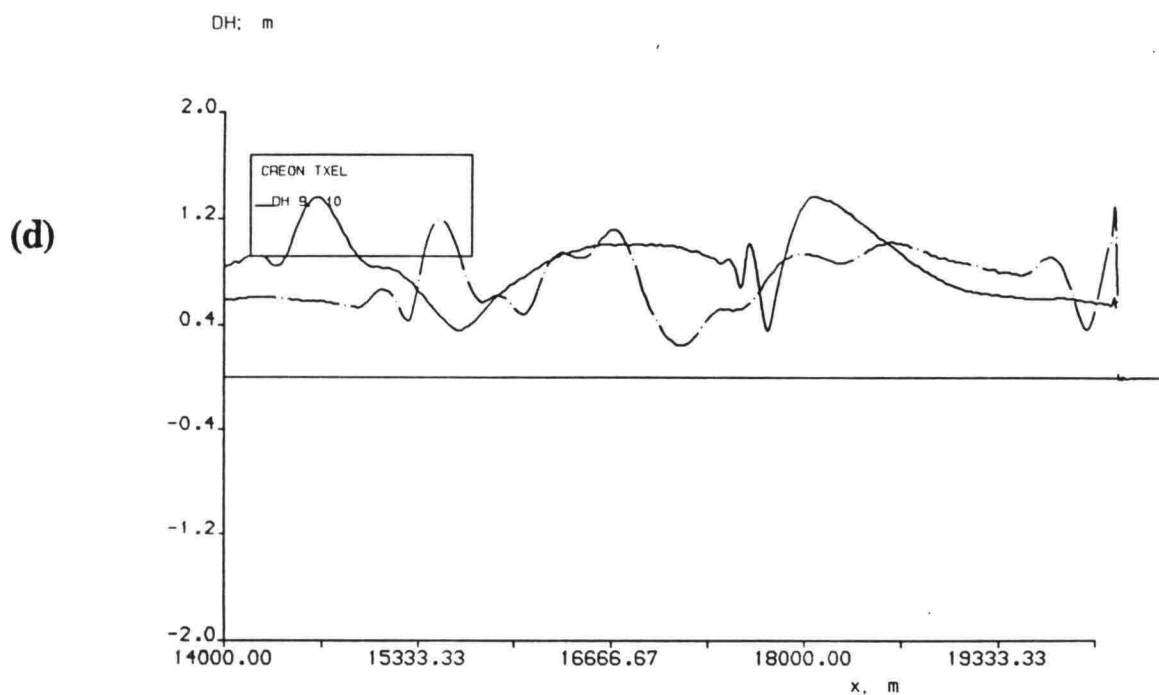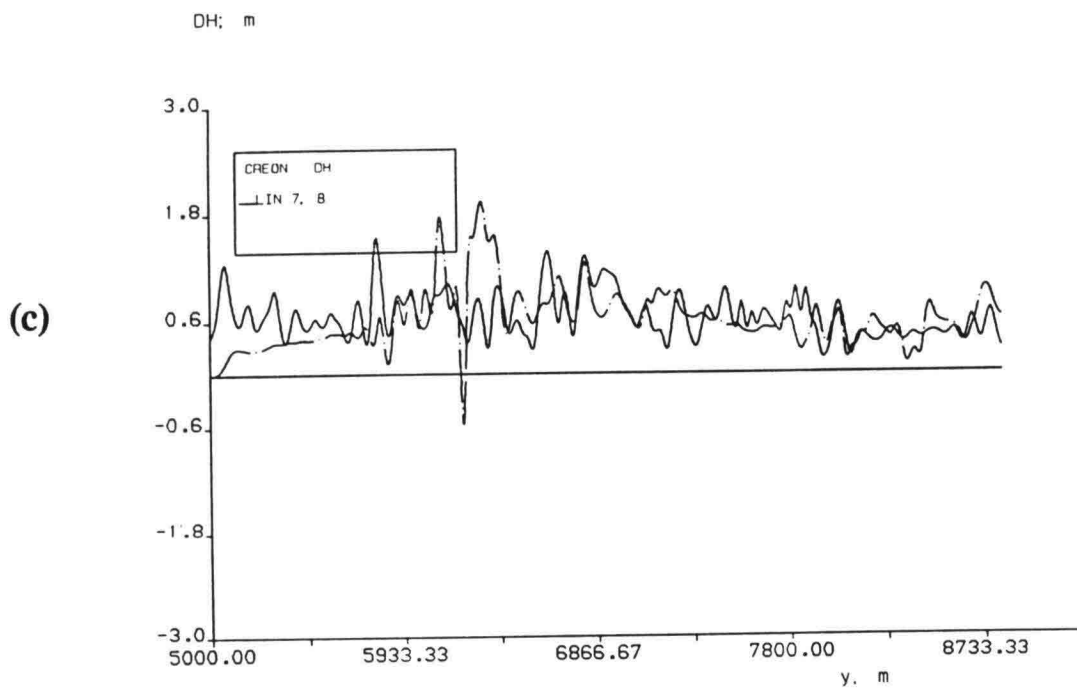
55
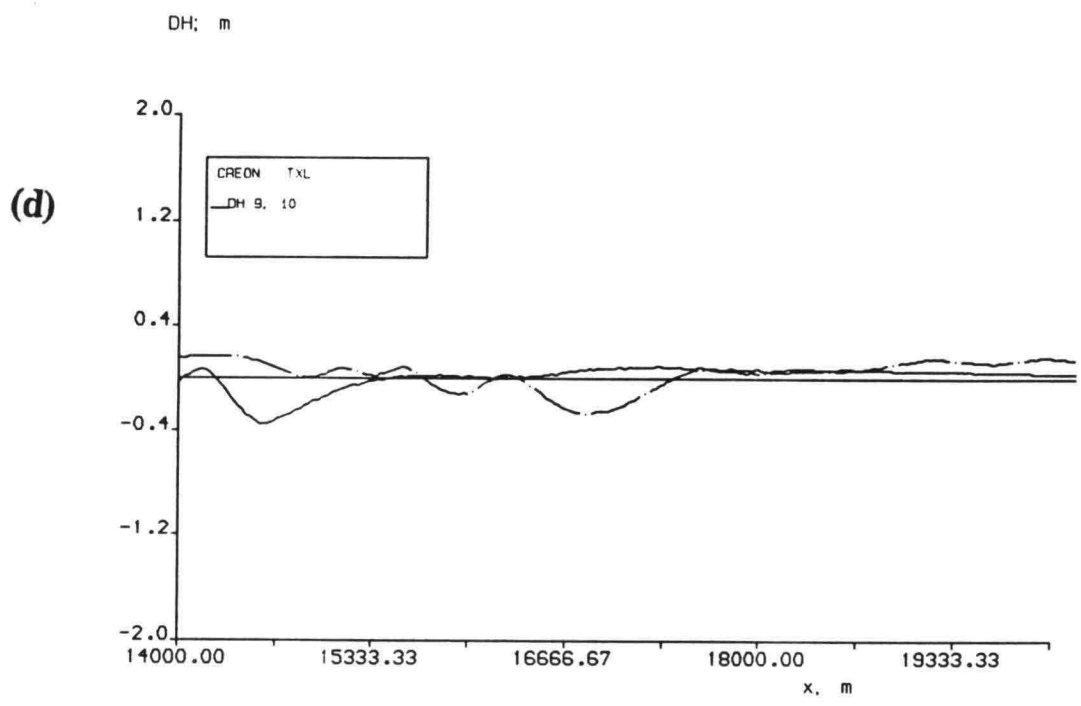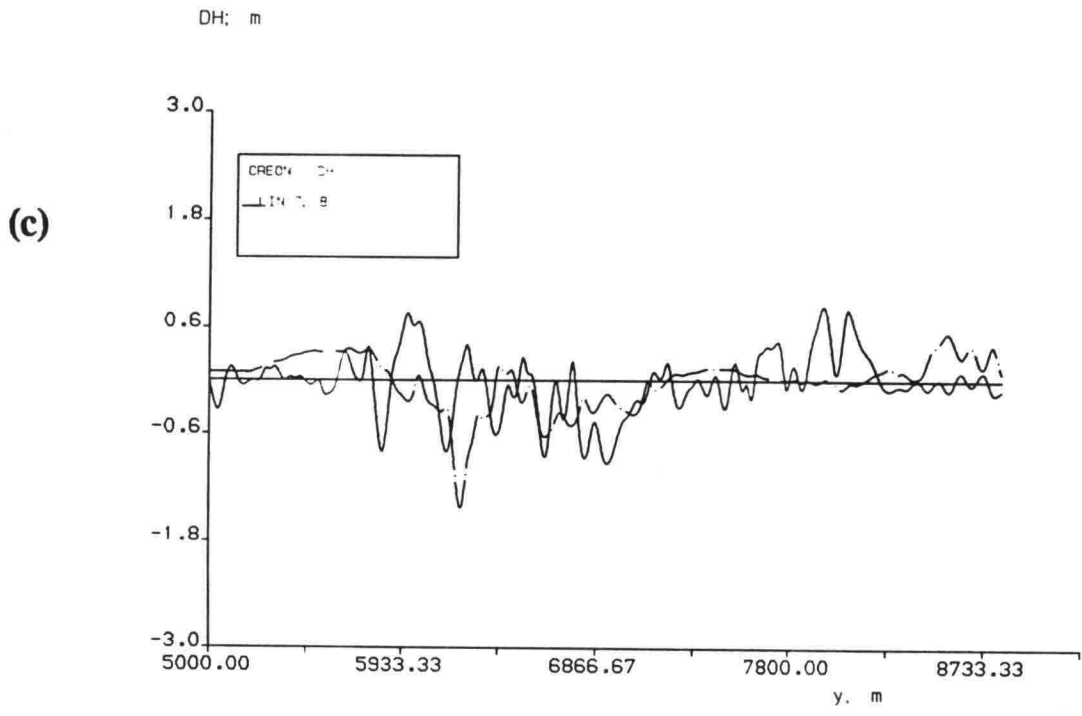
Fig. 4.7(continued) c) the differences along line 7 and line 8,
d) along line 9 and line 10.

(a)

Fig. 4.8   computed waves of case IV, a) wave field, *isolines*

(b)

H: m

(c)

H: m
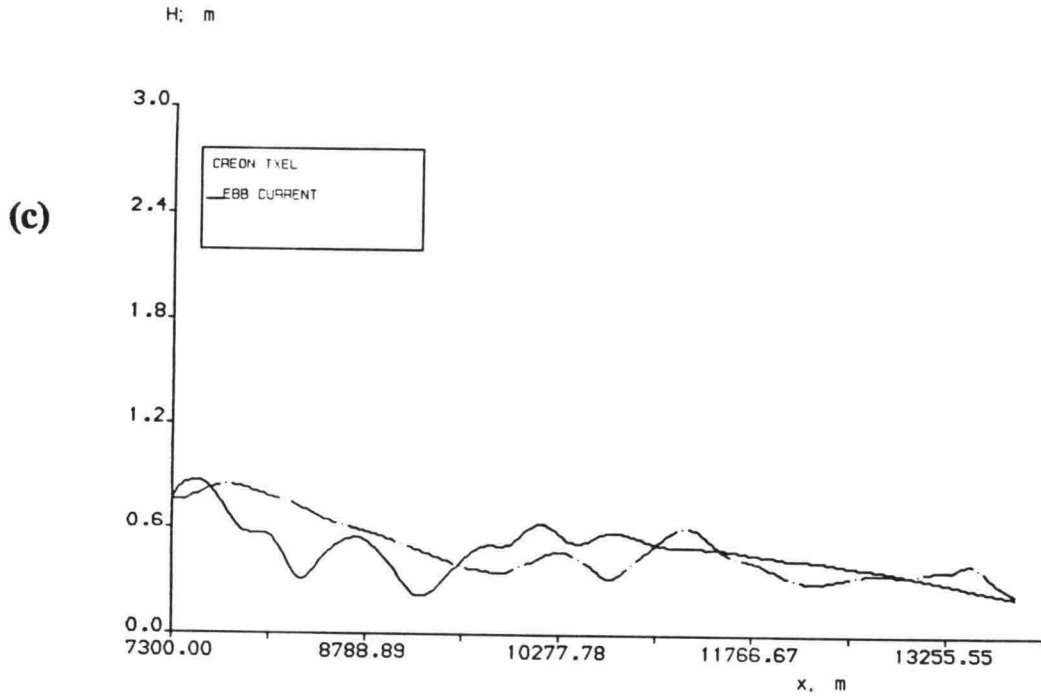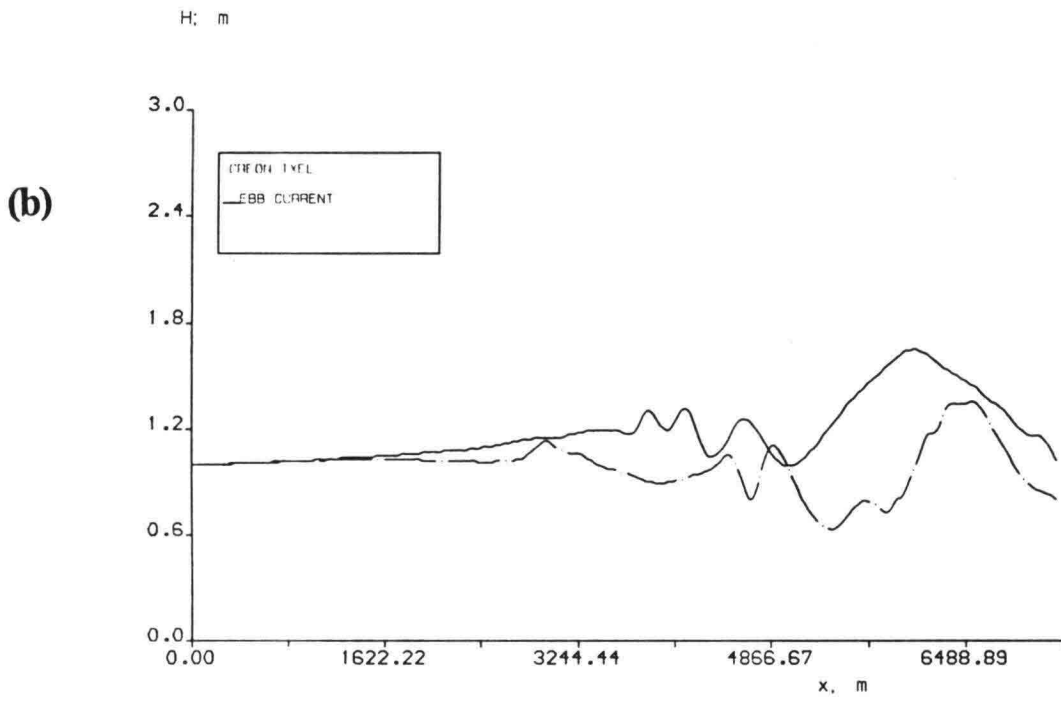
Fig. 4.8(continued) b) wave heights along line 1 and line 2, c)
wave heights along line 5 and line 6.

H: m

(d)

H: m

(e)
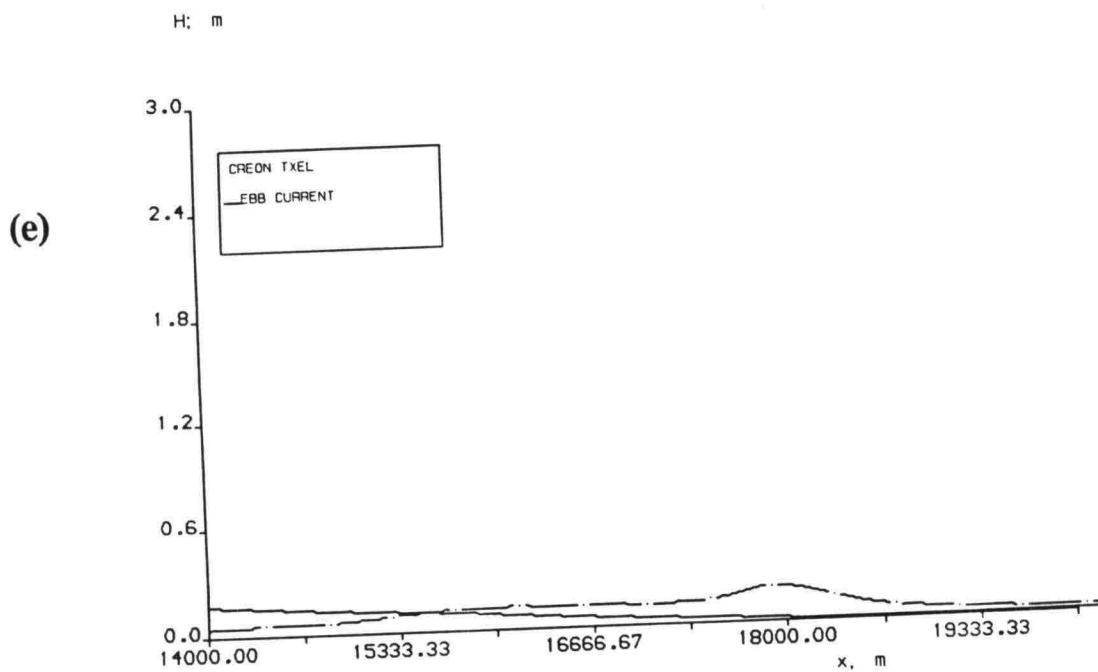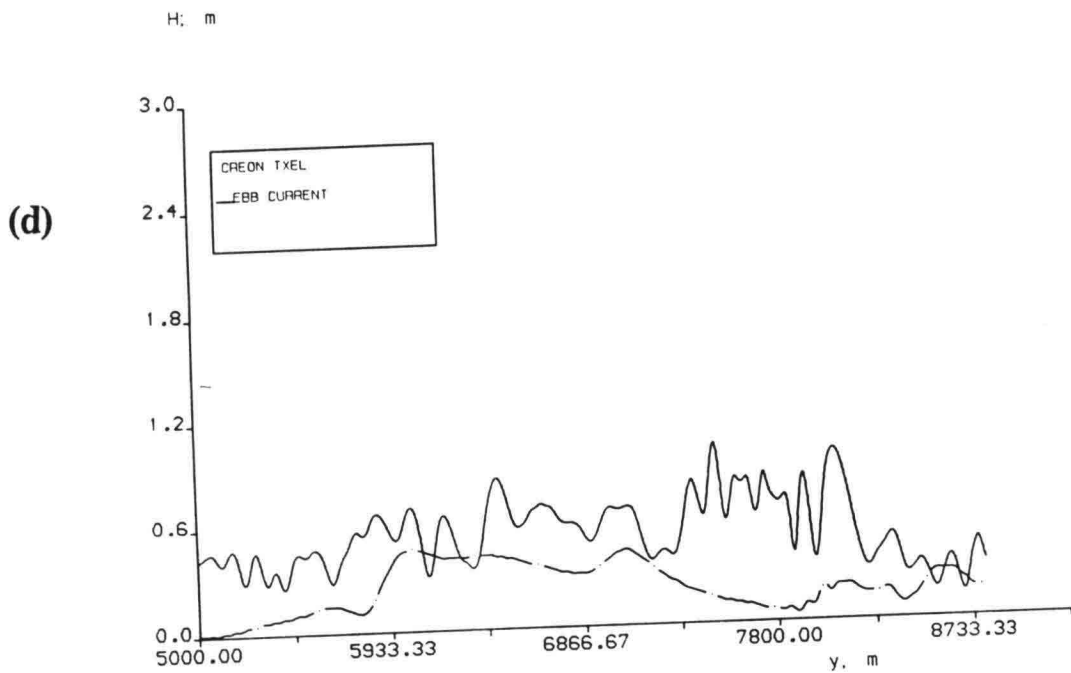
Fig. 4.8(continued) d) wave heights along line 7 and line 8, e)
wave heights along line 9 and line 10

59

DH; m

(a)

DH; m

(b)
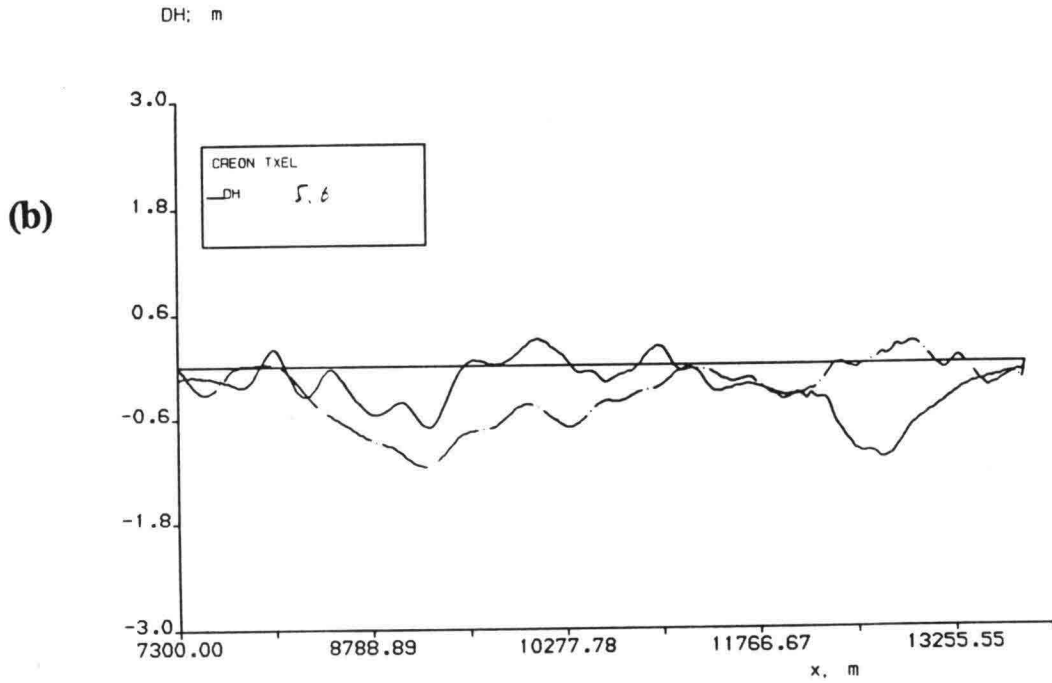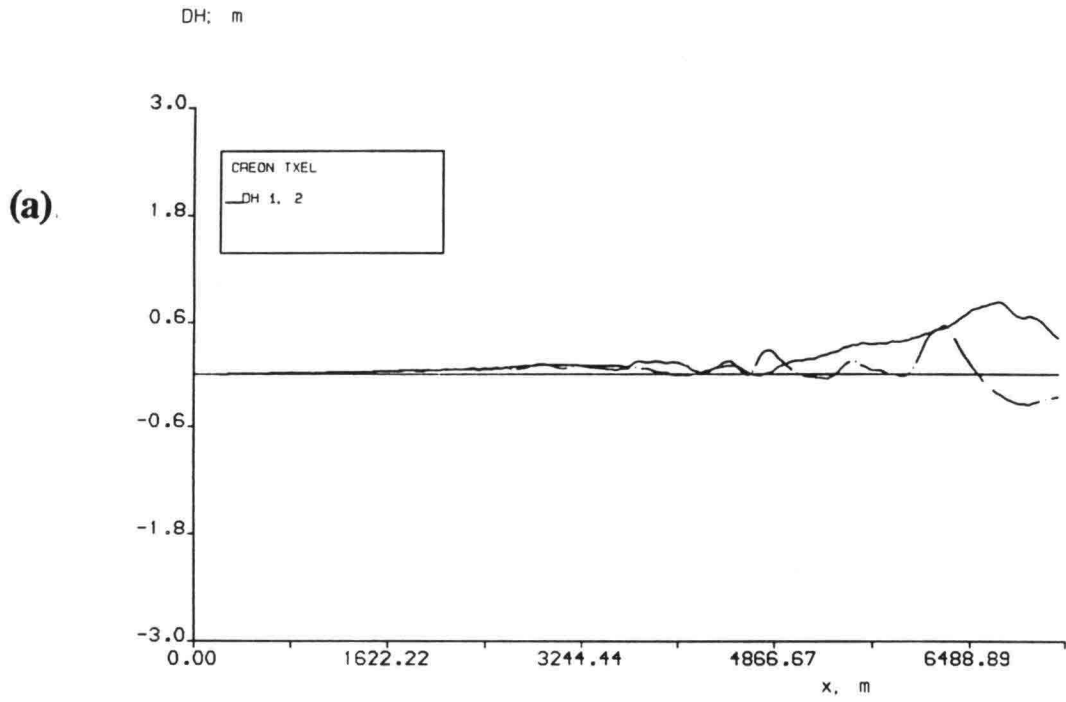
Fig. 4.9 The difference of wave heights between case IV and case II. $\Delta H = H_{iv} - H_{ii}$. a) the differences along line 1 and line2, b), along line 5 and line 6.
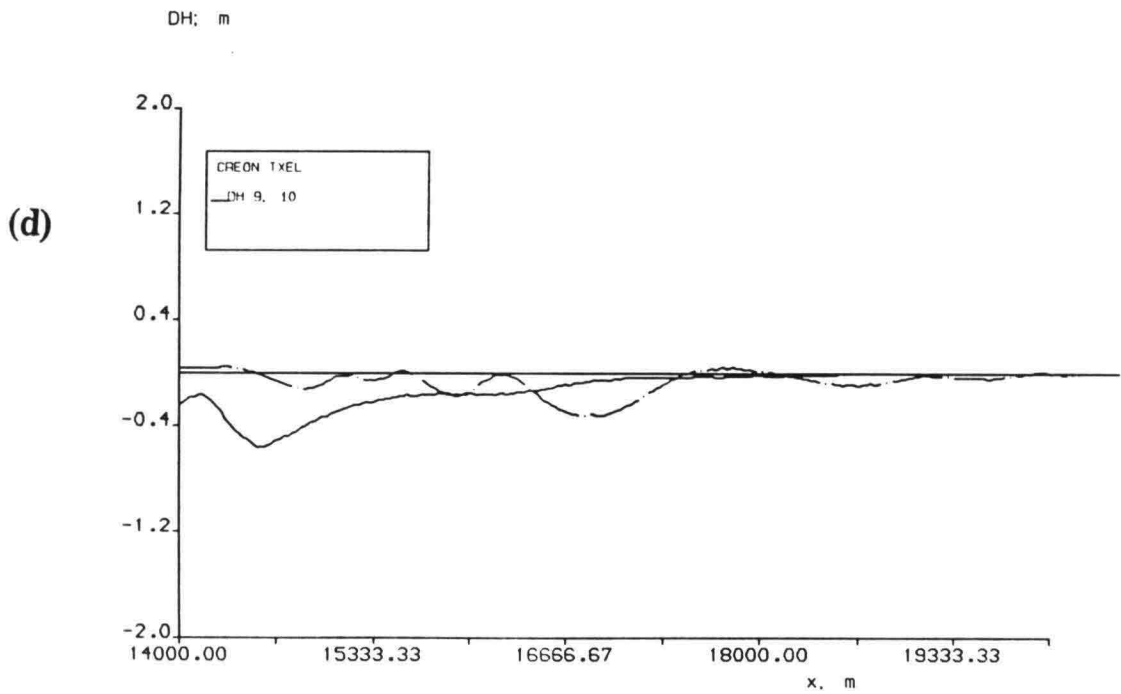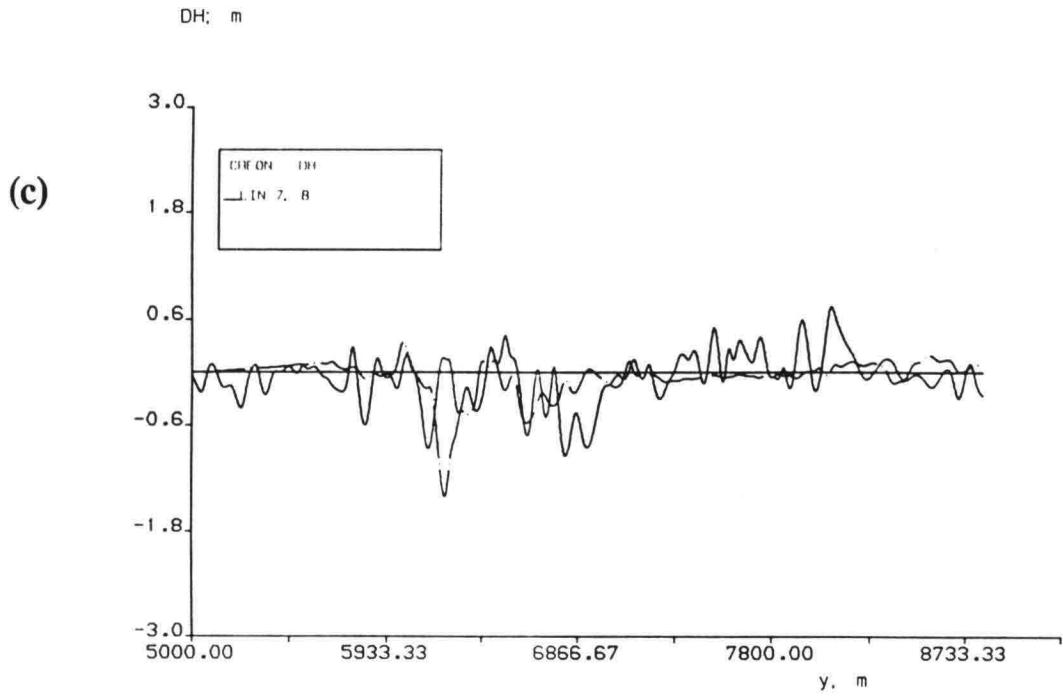
Fig. 4.9(continued)   c) the differences along line 7 and line 8,
d) along line 9 and line 10.
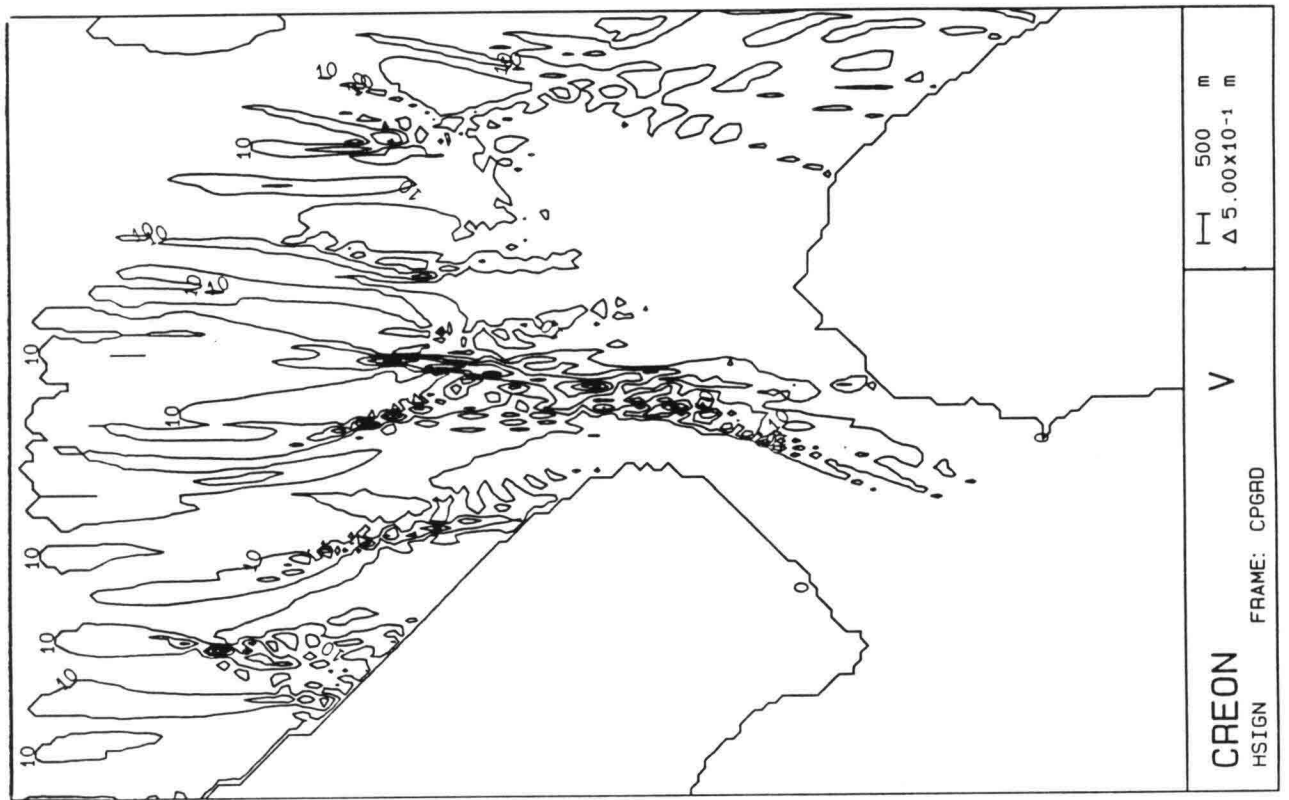
(a)

Fig. 4.10   computed waves of case V, a) wave field, *isolines*
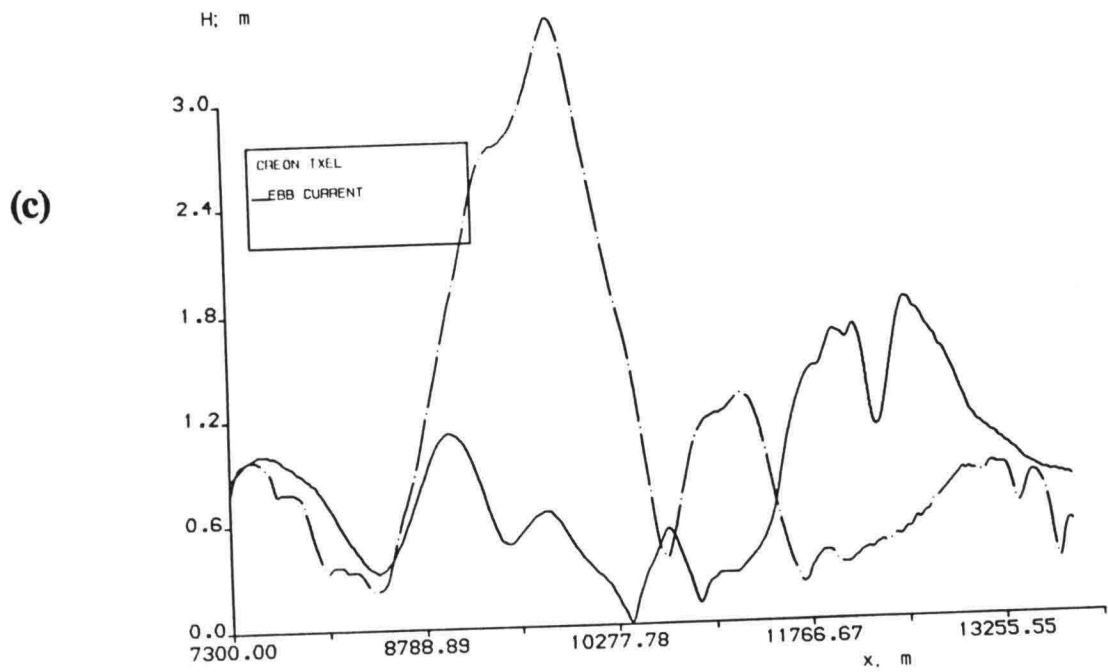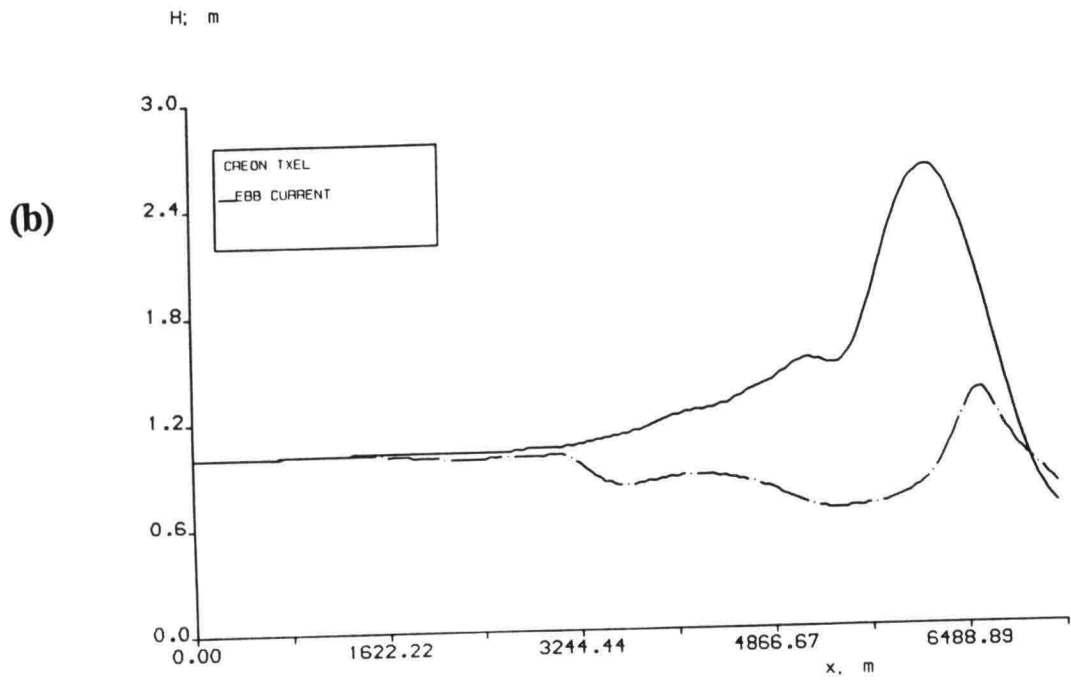
Fig. 4.10(continued) b) wave heights along line 1 and line 2,
c) wave heights along line 5 and line 6.

H: m

(d)

3.50
2.80
2.10
1.41
0.71
0.01

CREON TXEL
EBB CURRENT

5000.00   5933.33   6866.67   7800.00   8733.33

y, m

H: m

(e)

3.0
2.4
1.8
1.2
0.6
0.0

CREON TXEL
EBB CURRENT

14000.00   15333.33   16666.67   18000.00   19333.33

x, m
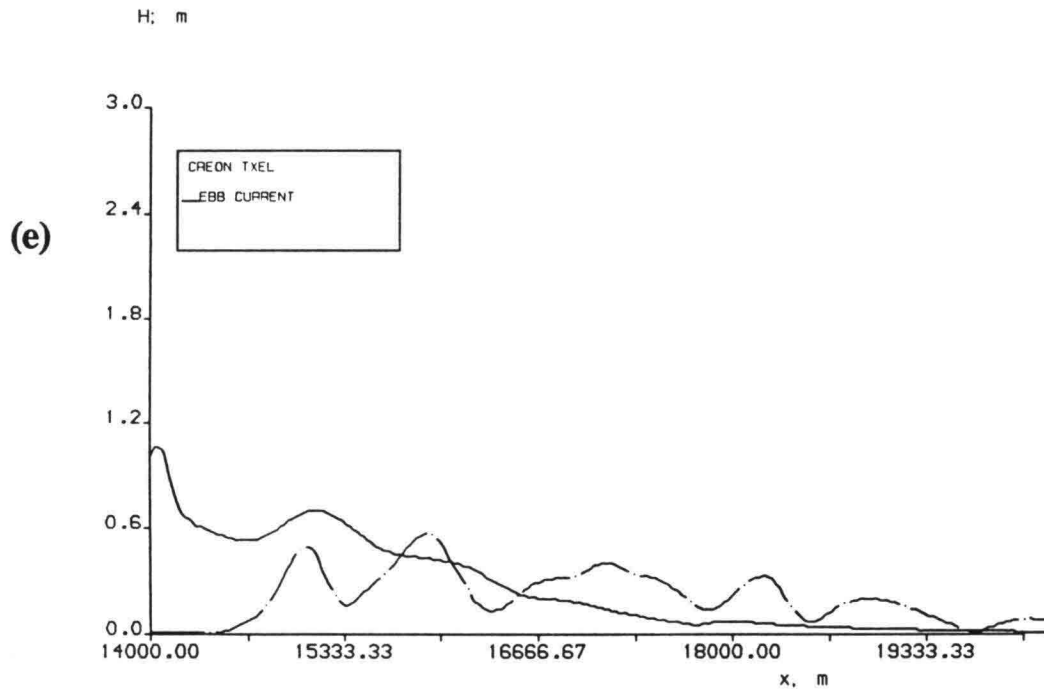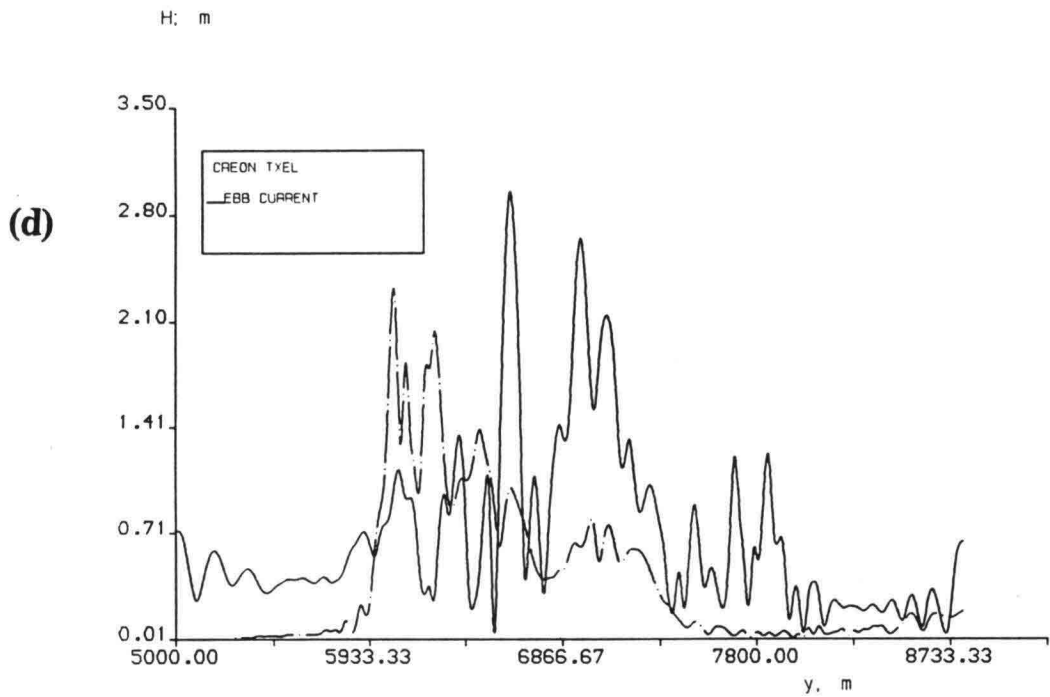
Fig. 4.10(continued)   d) wave heights along line 7 and line 8,
e) wave heights along line 9 and line 10

64

DH: m

(a)

DH: m

(b)
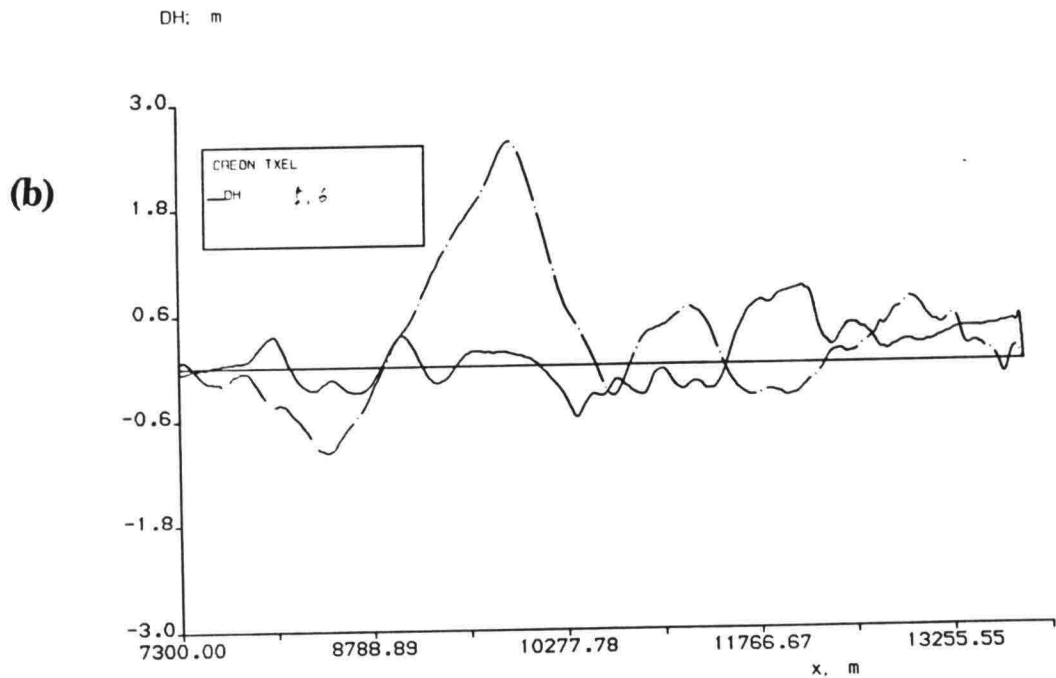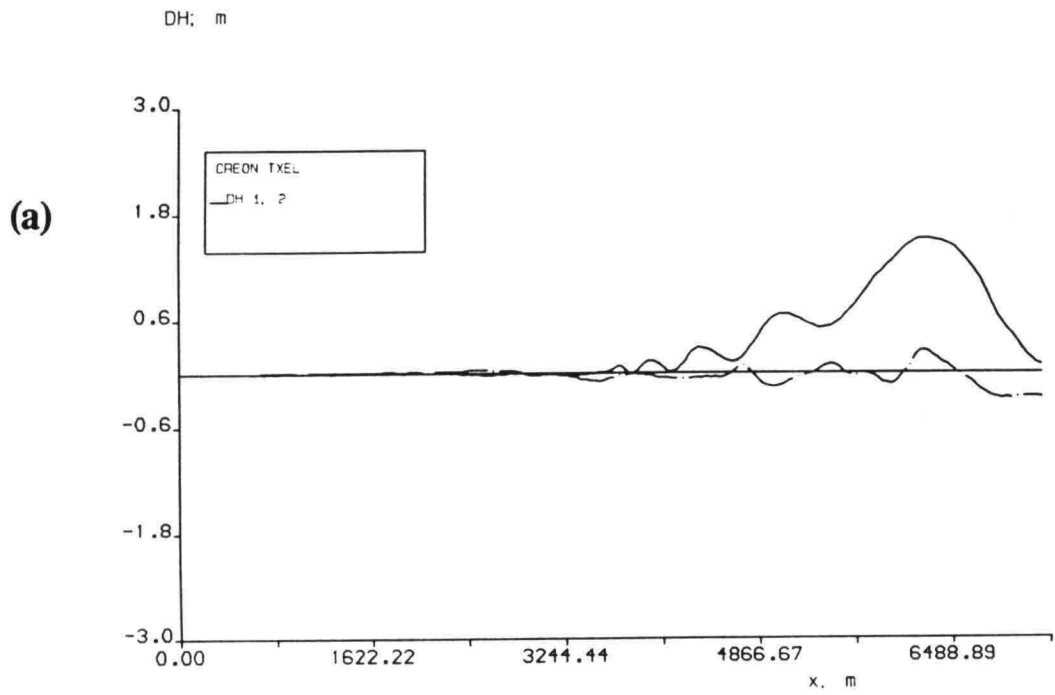
Fig. 4.11 The difference of wave heights between case V and case
II. $\Delta H = H_v - H_{ii}$. a) the differences along line 1 and line2,
b), along line 5 and line 6.

(c)

DH: m

CREON   DH
LIN 7, 8

(d)

DH: m

CREON TXEL
DH 9, 10
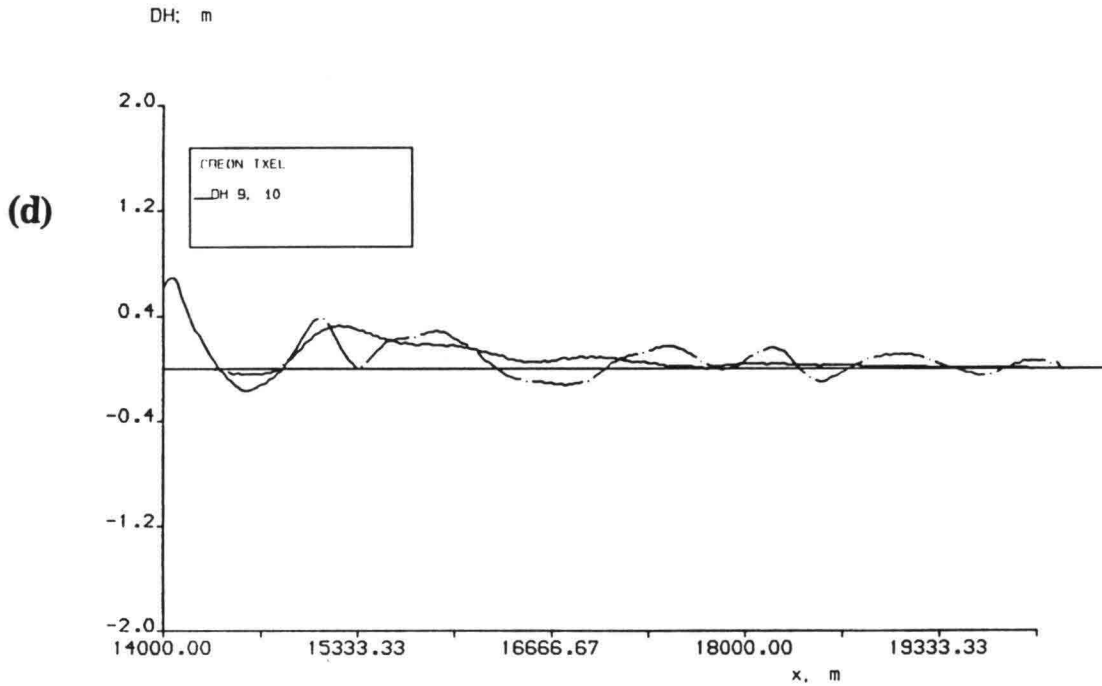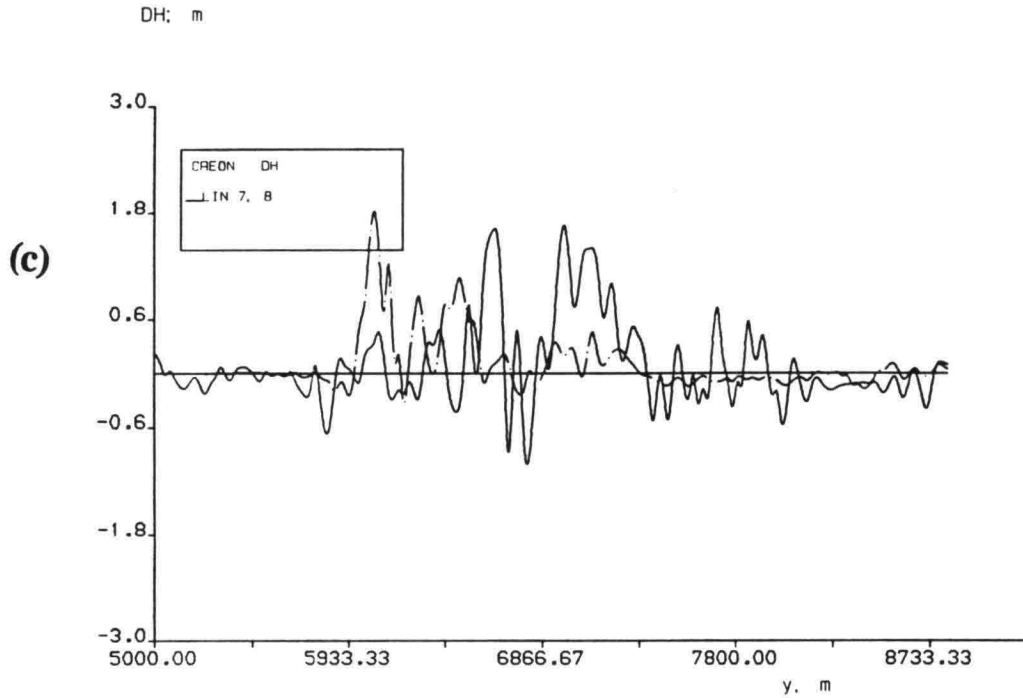
Fig. 4.11(continued) c) the differences along line 7 and line 8, d) along line 9 and line 10.

(a)

Fig. 4.12   computed waves of case VII, a) wave field, *isolines*

(b)

H: m

CREON TXEL
CURRENT

(c)

H: m

CREON TXEL
CURRENT

Fig. 4.12(continued) b) wave heights along line 1 and line 2, c) wave heights along line 5 and line 6.
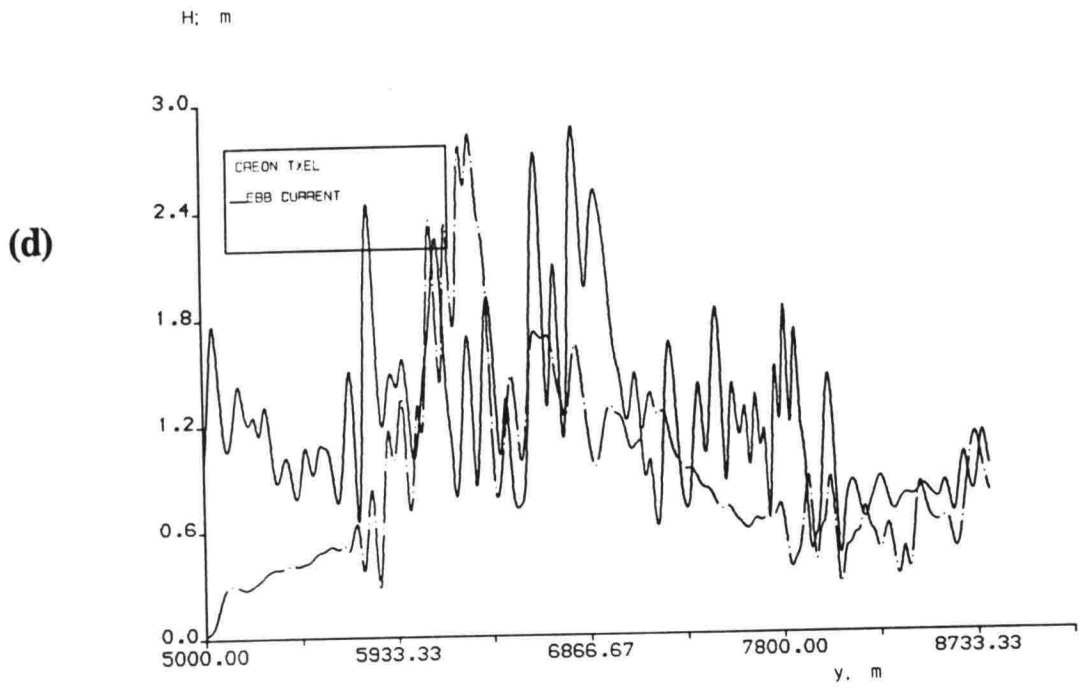
Fig. 4.12(continued) d) wave heights along line 7 and line 8, e)
wave heights along line 9 and line 10
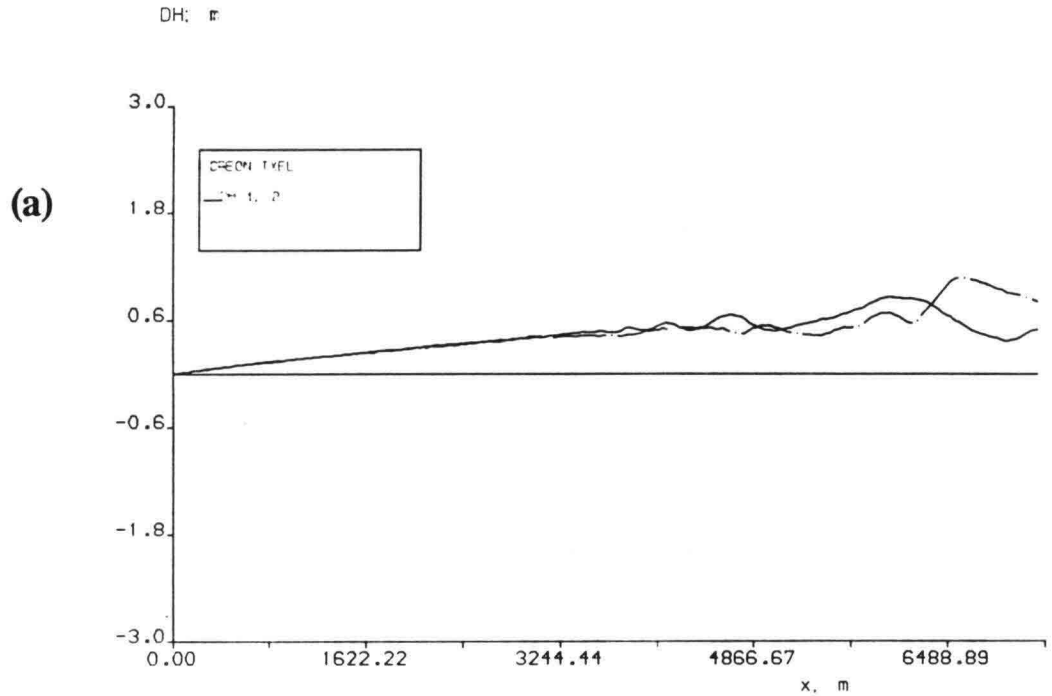
Fig. 4.13 The difference of wave heights between case VII and case II. $\Delta H = H_{vii} - H_{ii}$. a) the differences along line 1 and line2, b) along line 5 and line 6.

DH; m

3.0

CREON DH
_LIN 7. 8

1.8

(c)

0.6

-0.6

-1.8

-3.0
5000.00   5933.33   6866.67   7800.00   8733.33
                                                            y, m

DH; m

2.0

CREON TXEL
_DH 9 10

1.2

(d)

0.4

-0.4

-1.2

-2.0
14000.00   15333.33   16666.67   18000.00   19333.33
                                                            x, m

Fig. 4.13(continued) c) the differences along line 7 and line 8,
d) along line 9 and line 10.

71
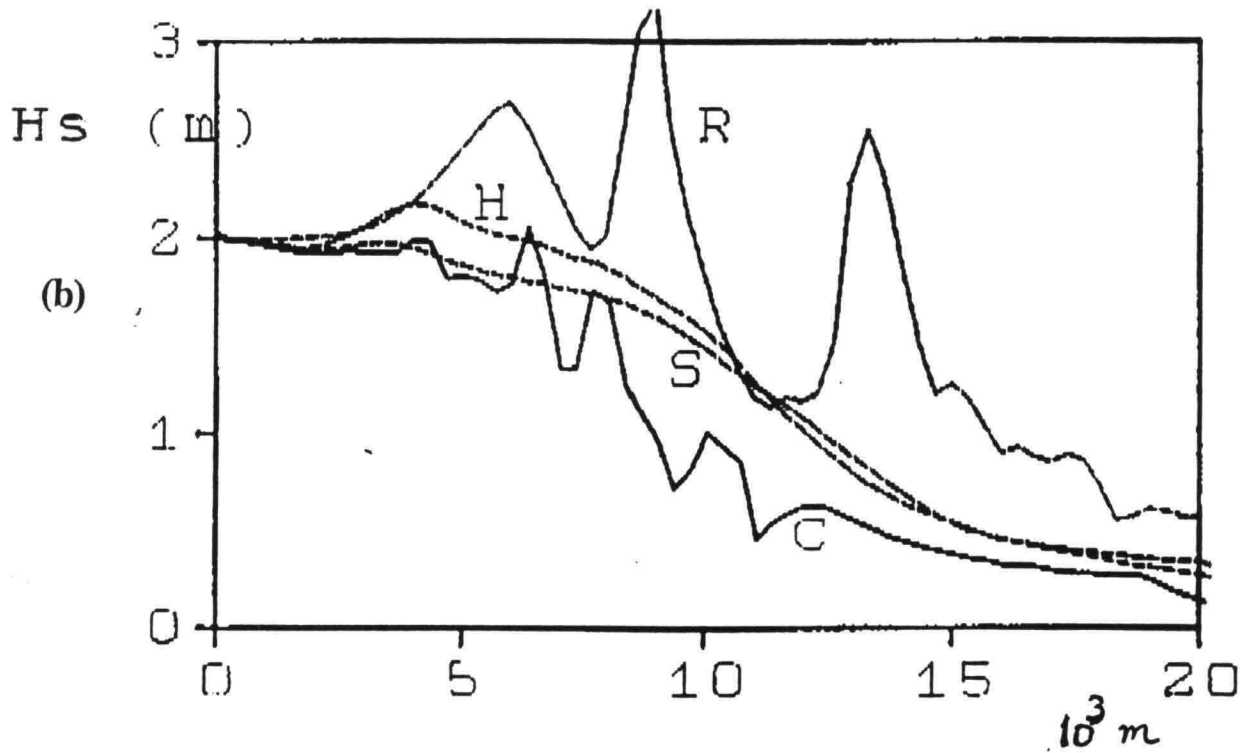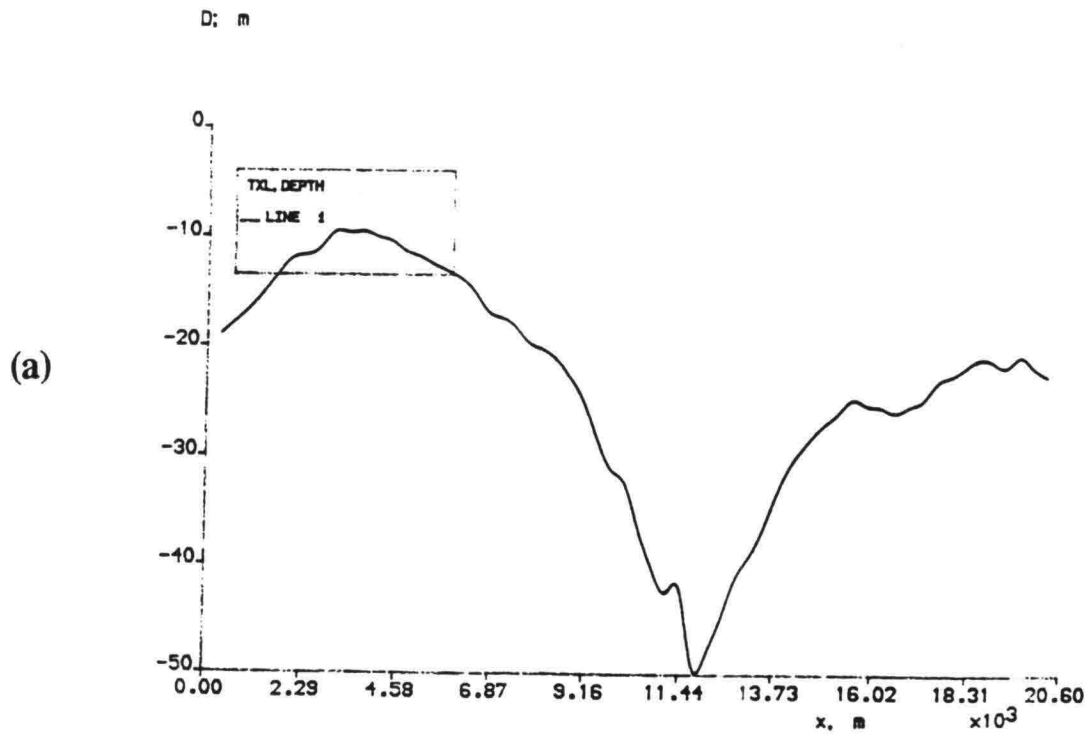
Fig. 4.14. Comparison of wave models.
(a) depth profile along line of main channel.
(b) computed significant wave height (in m)
    for case I (SW waves, wind sea, no current),
    along line (a).

(a)
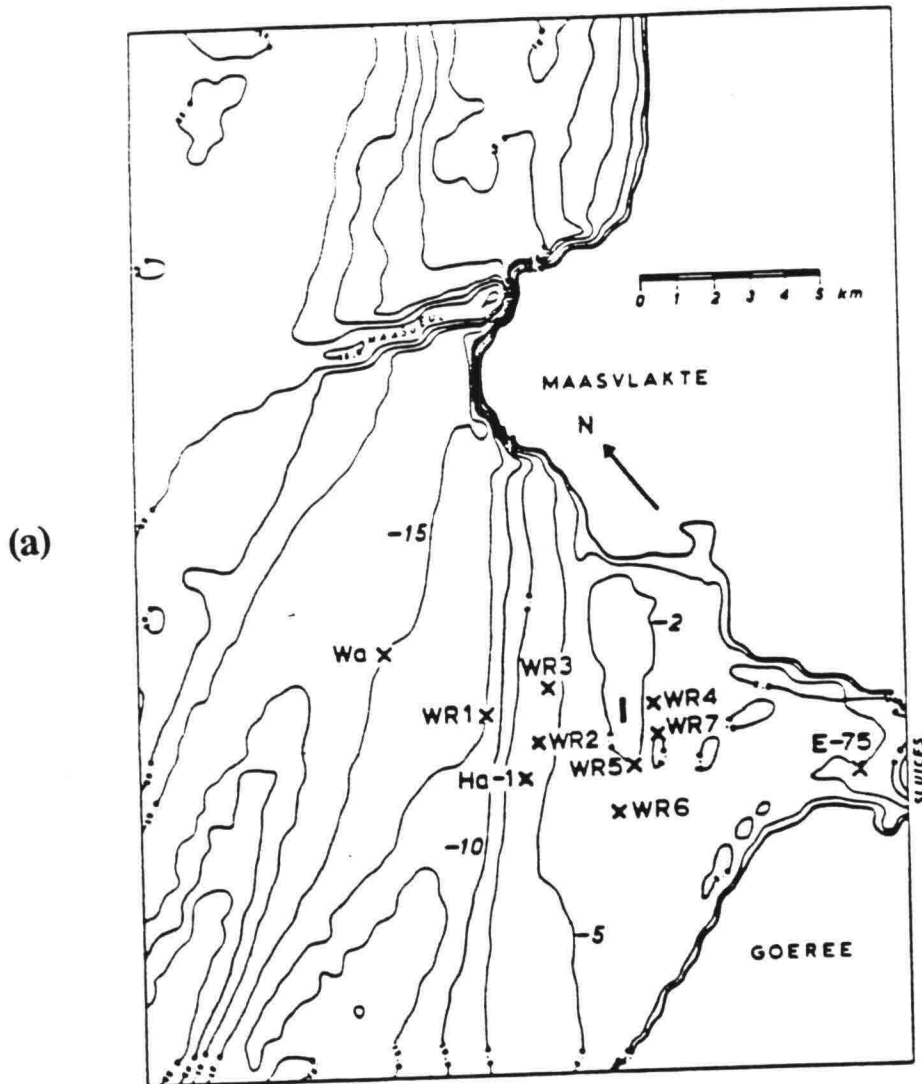
Fig. 5.1 a) depth isolines in the estuary of Haringvliet and measurement locations.
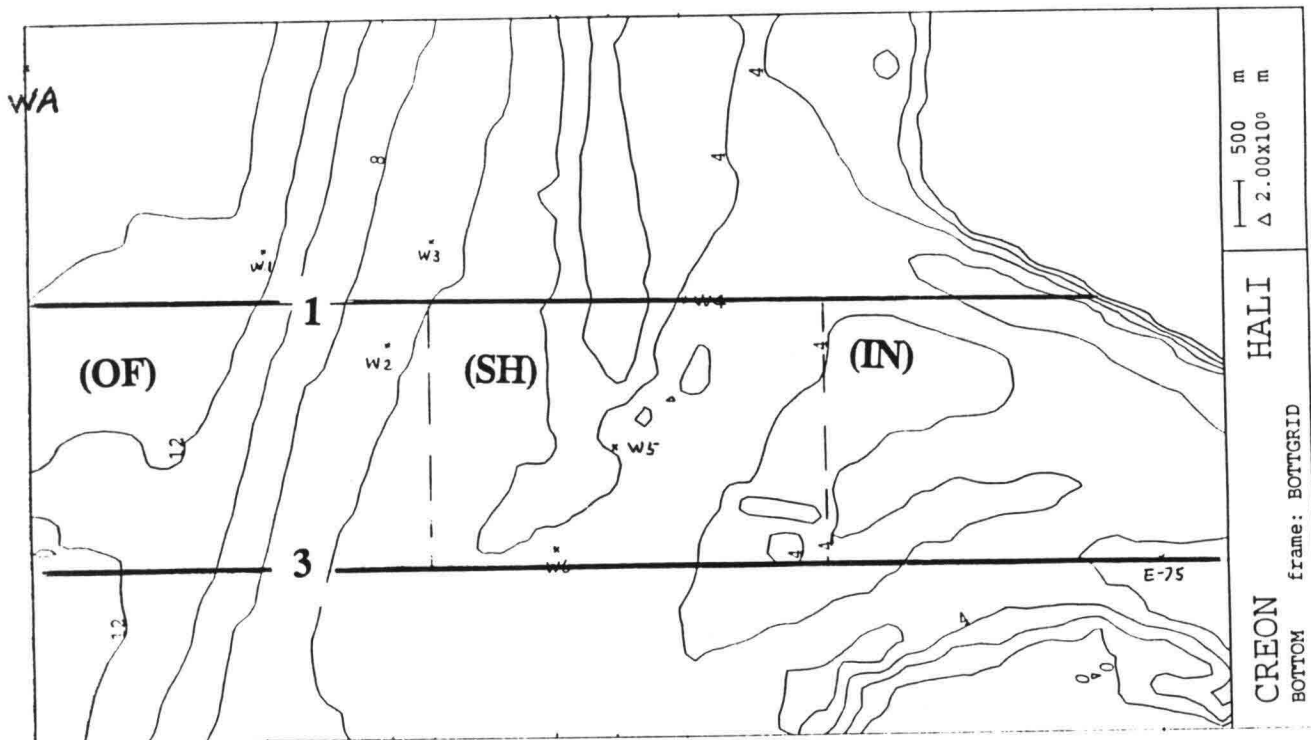
(b)

Fig. 5.1(continued) b) the computational area and the output lines.
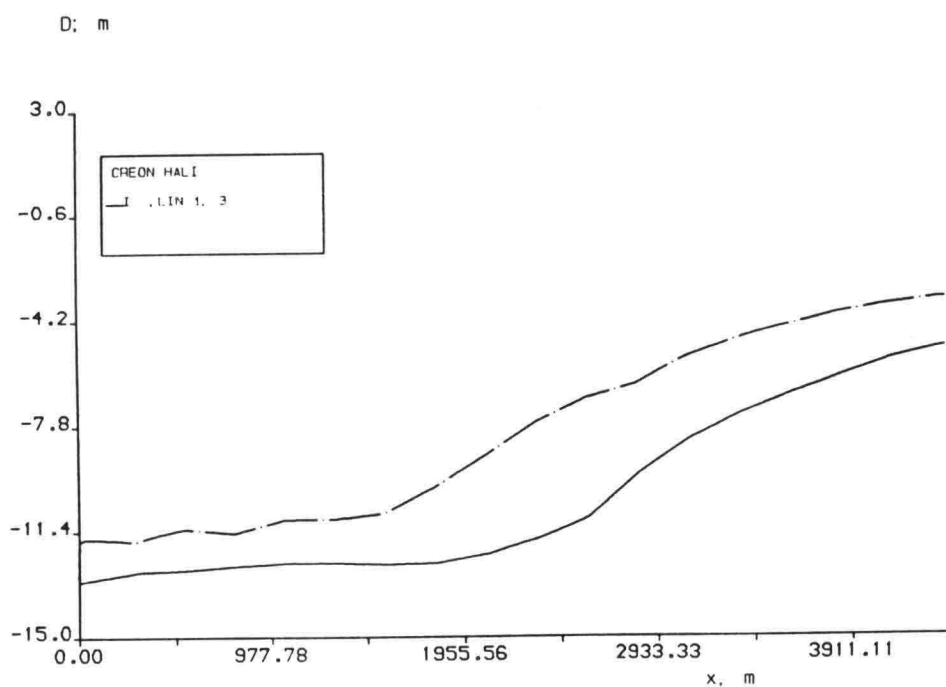
(a)

Fig. 5.2 Depth along the lines. a) line 1 and line 3 in offshore region.
——————: line 1; —•——: line 3. (The same notation for computed wave heights *is used*.)

74
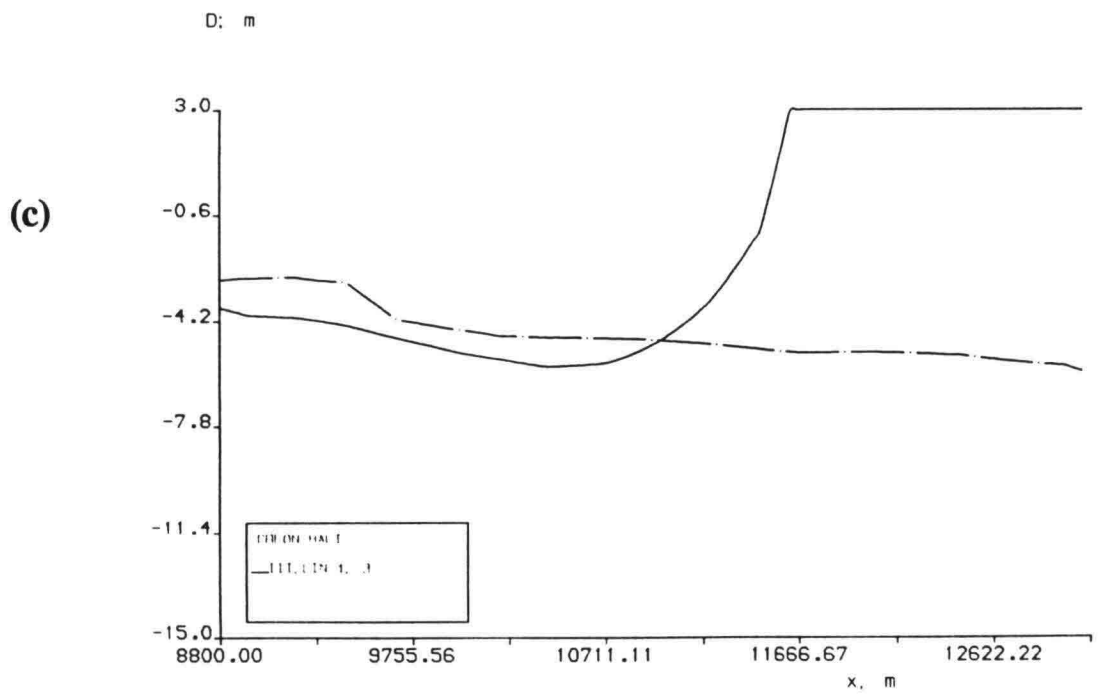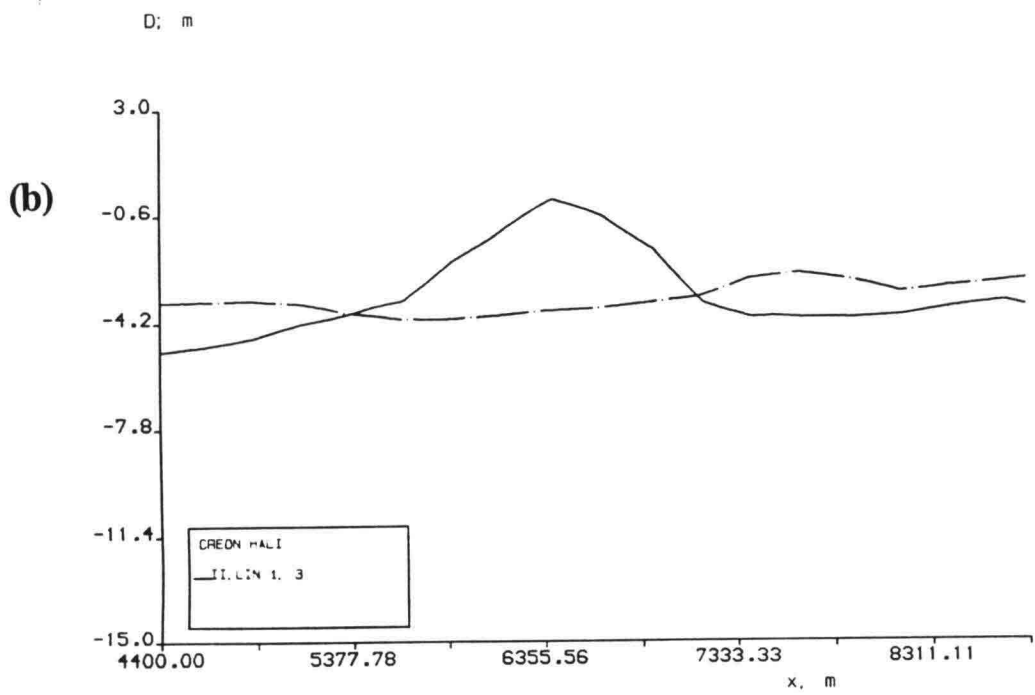
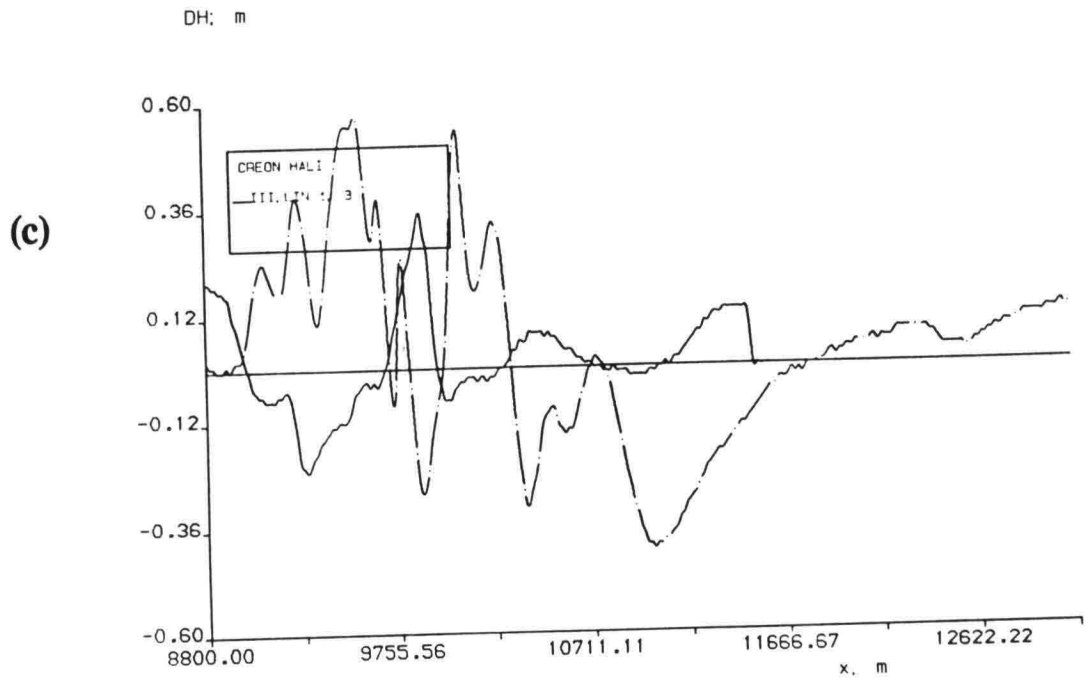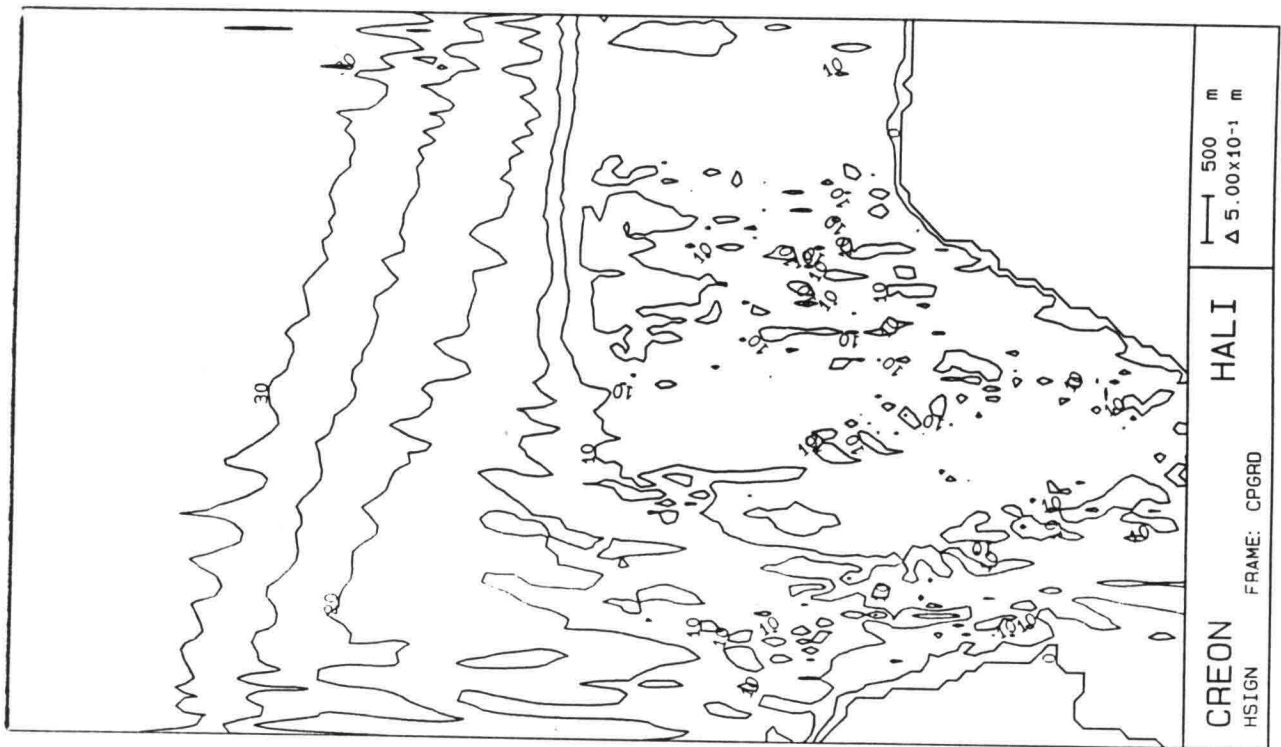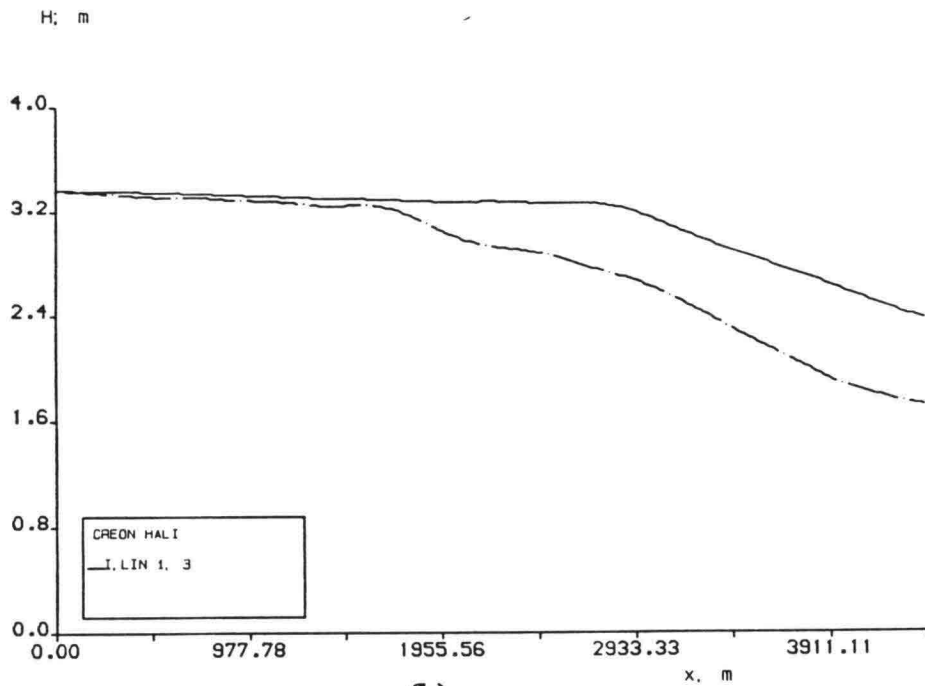Fig. 5.2(continued) b) line 1 and line 3 in shoal region, c)
line 1, line 3 in inshore region.
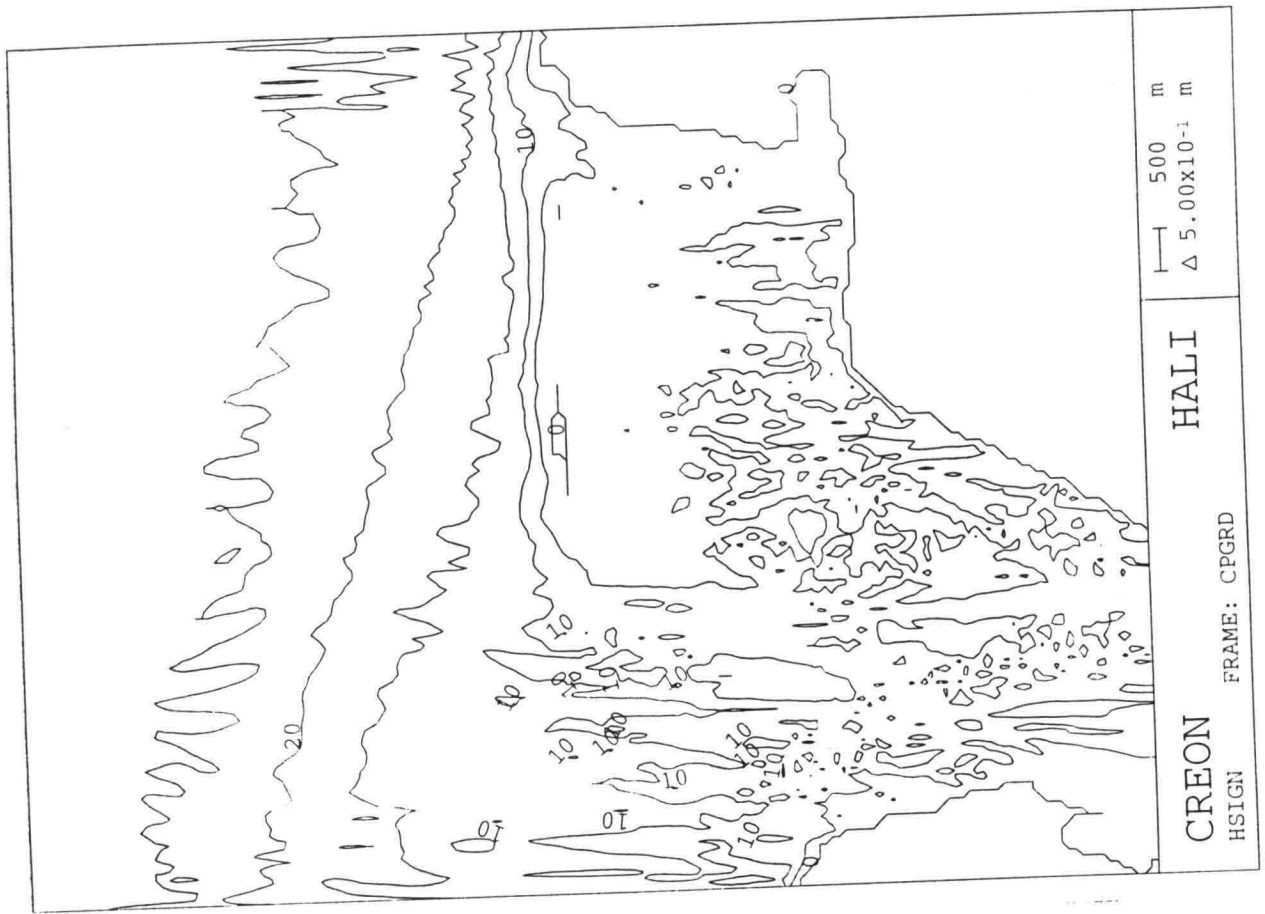
(a)
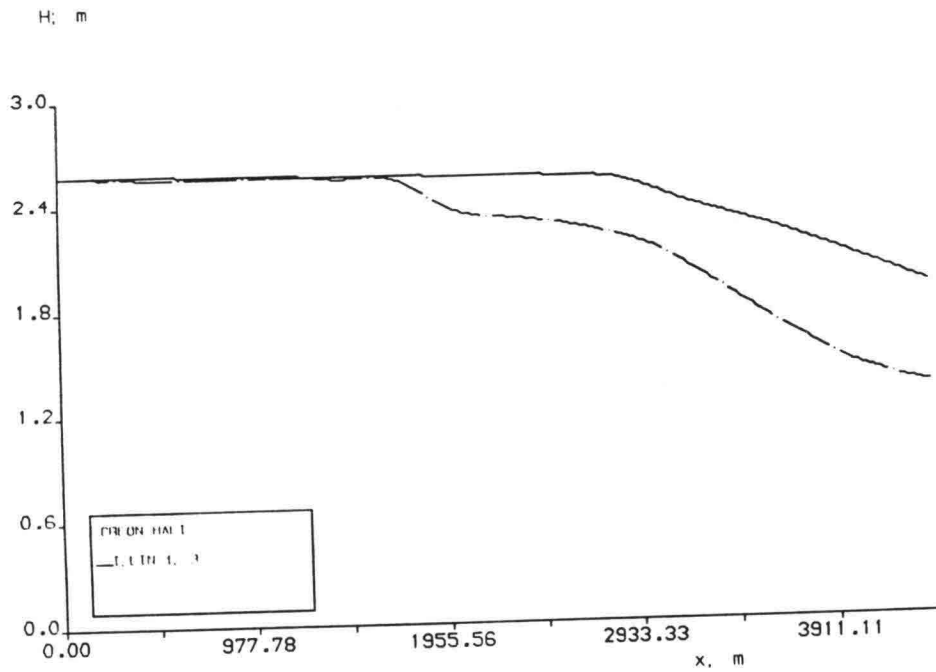
(b)

Fig. 5.3 Hindcast number one at 17:00 Oct. 14, 1982, the incident waves are considered as *irregular*, the computation without 'h$_n$' effect. a) wave field. b) wave height along line 1 and line 3 in offshore region.
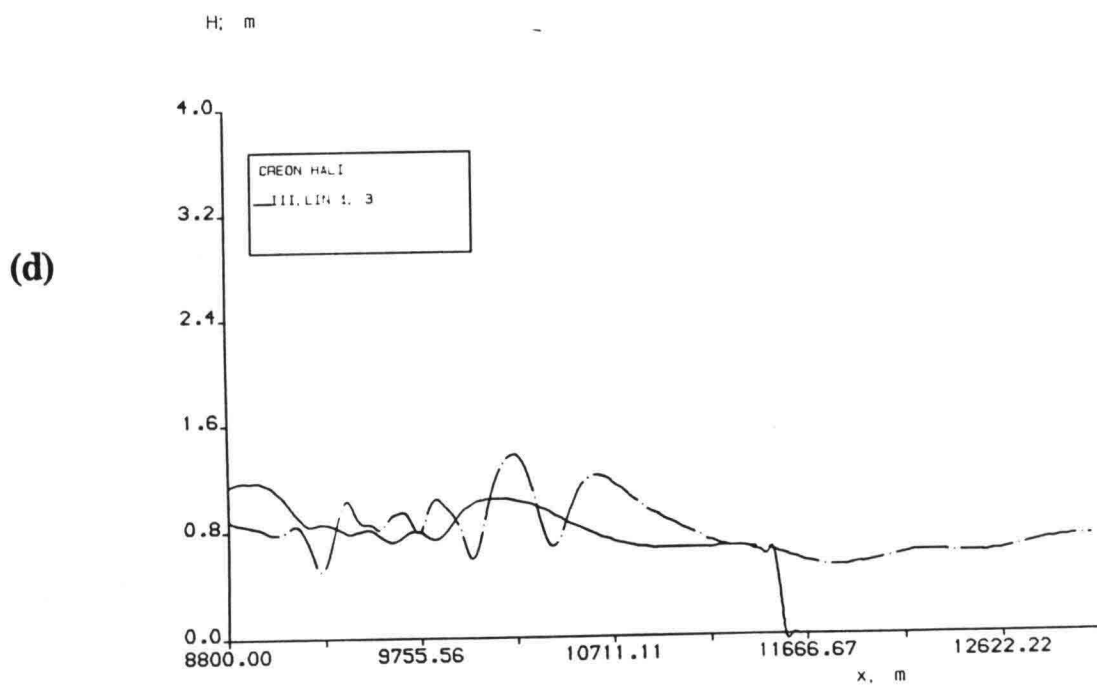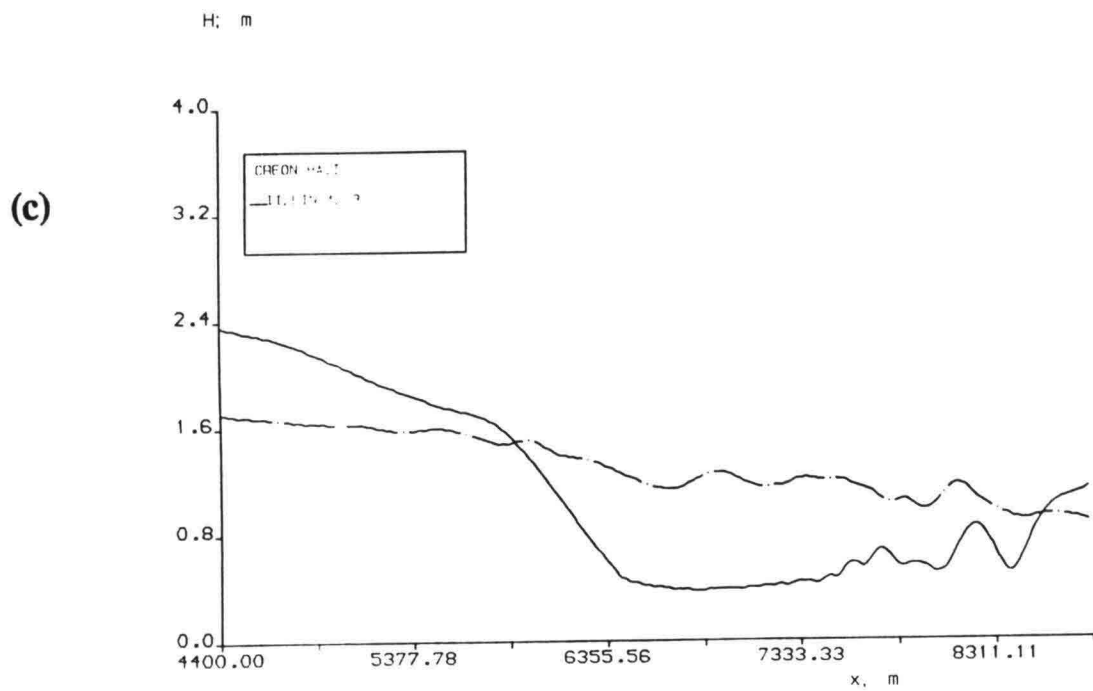
H: m

(c)

H: m
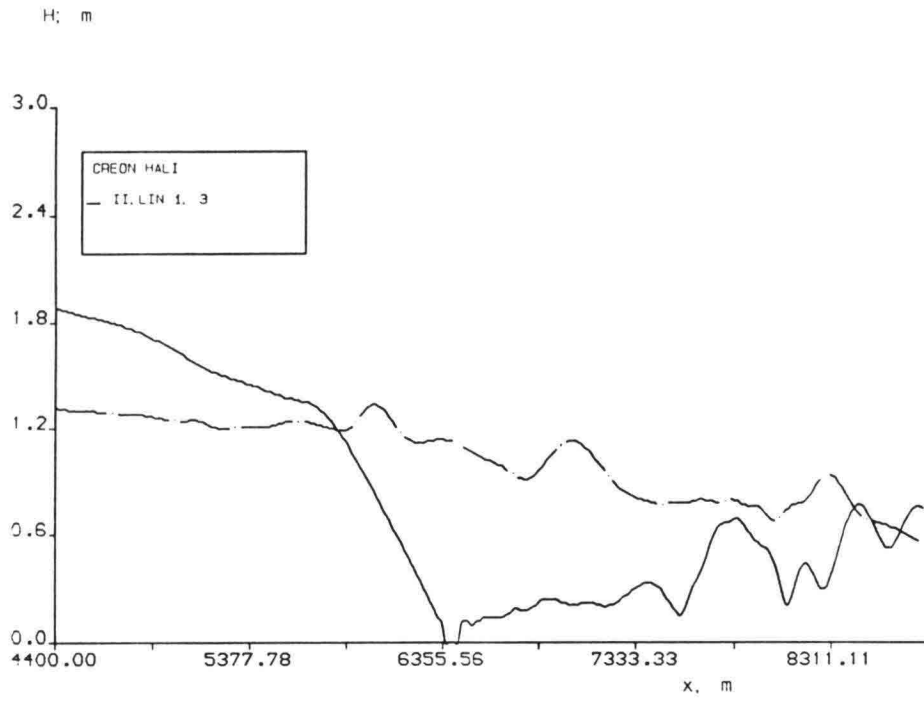
(d)
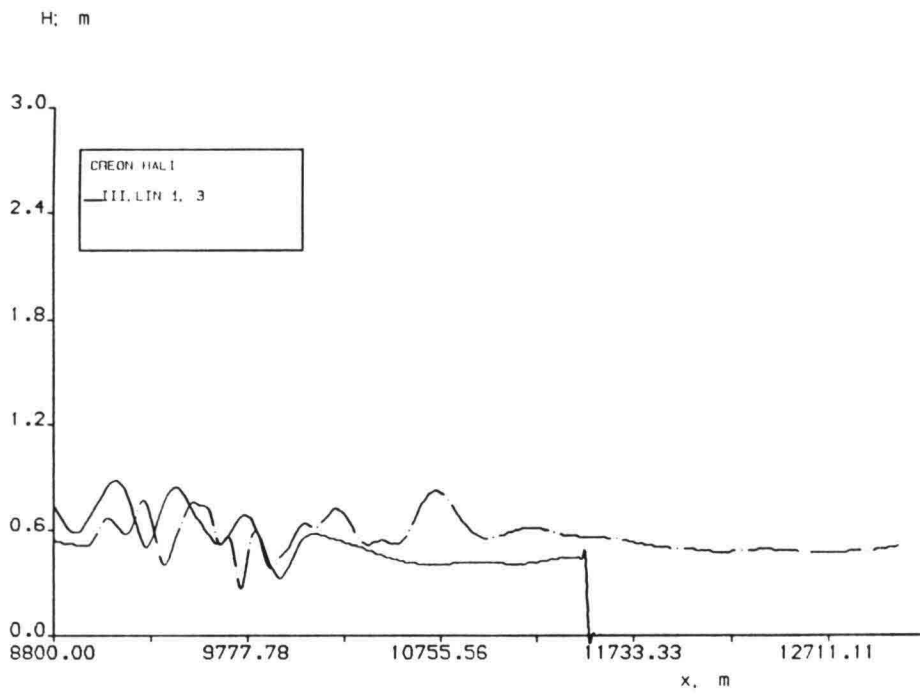
Fig. 5.3(continued) c) line 1 and line 3 in shoal region, d)
inshore region.

(a)
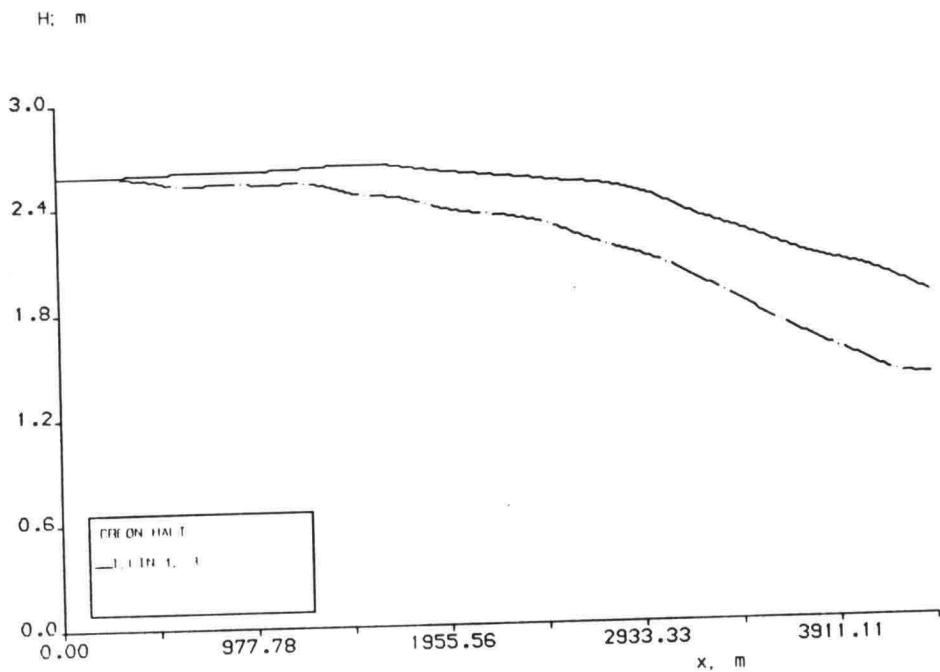
(b)

Fig. 5.4 Hindcast number one at 17:00 Oct. 14, 1982, the incident
waves are considered as monochromatic, the computation without
'h_n' effect. a) wave field. b) wave height along line 1 and line
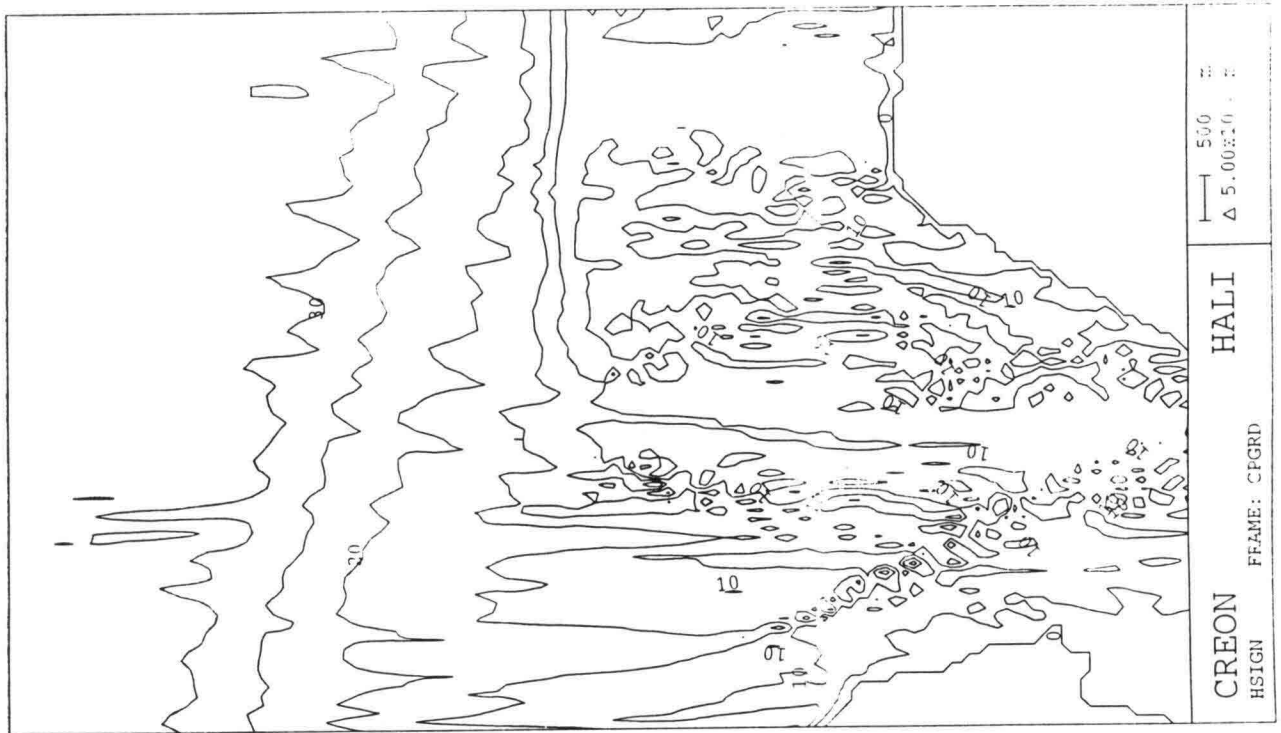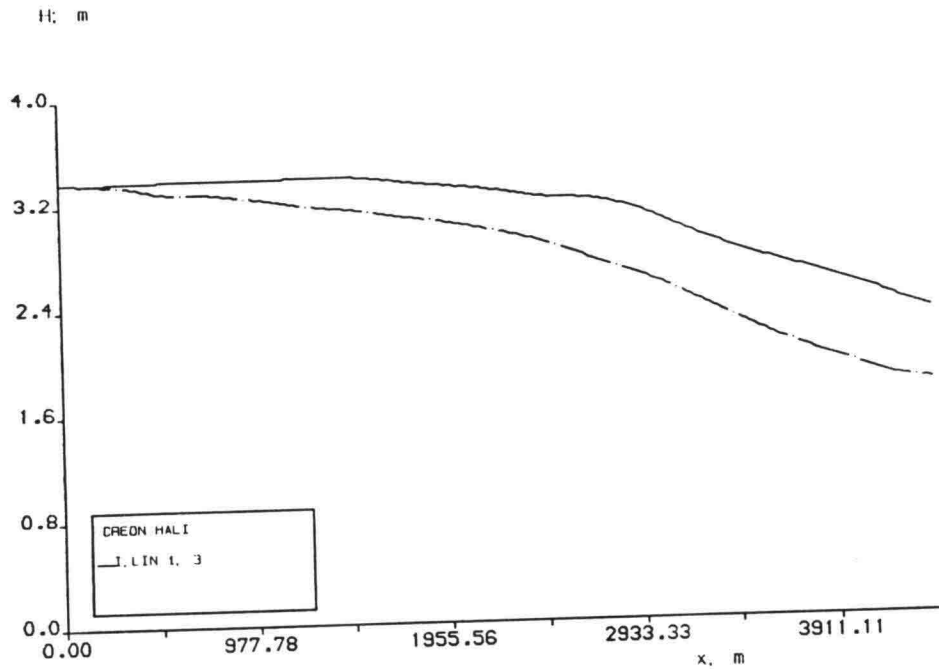3 in offshore region.

(c)

H; m

CREON HALI
II.LIN 1. 3

(d)

H; m

CREON HALI
III.LIN 1. 3

Fig. 5.4(continued) c) line 1 and line 3 in shoal region, d)
inshore region.

DH: m

(a)

CREON HALI
I, LIN 1, 3

DH: m

(b)

CREON HALI
II, LIN 1, 3
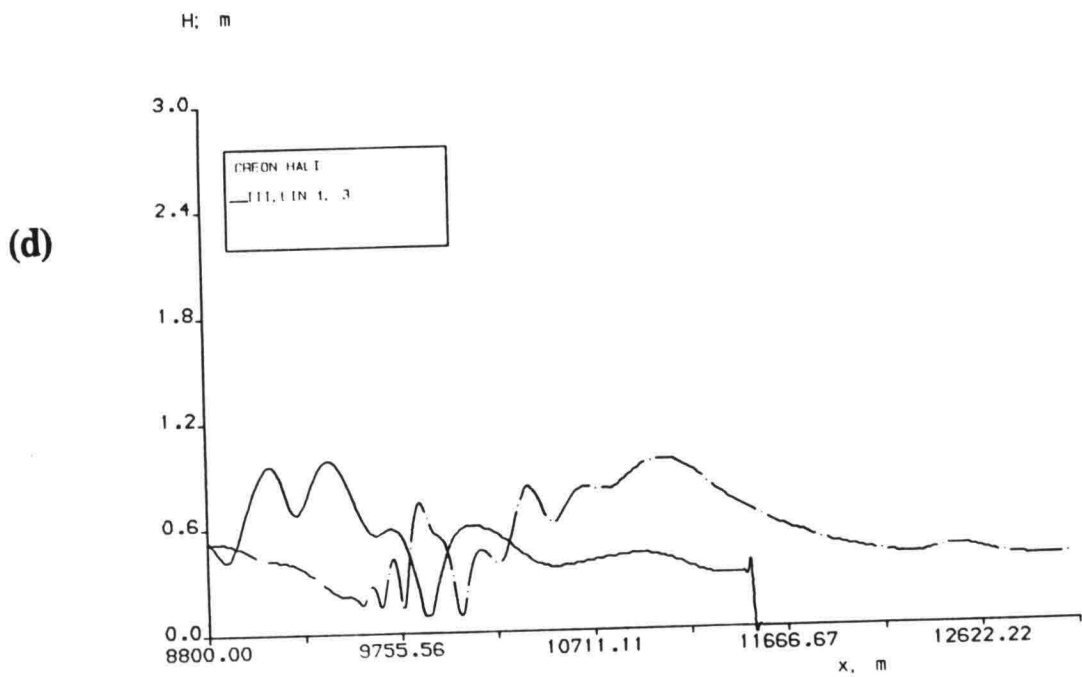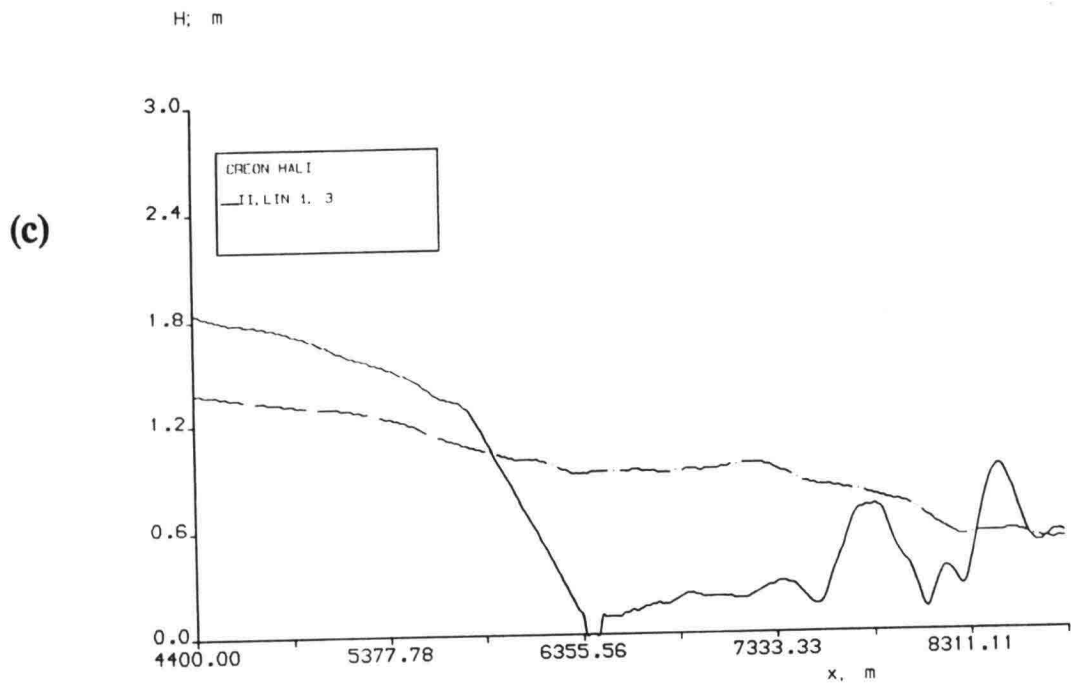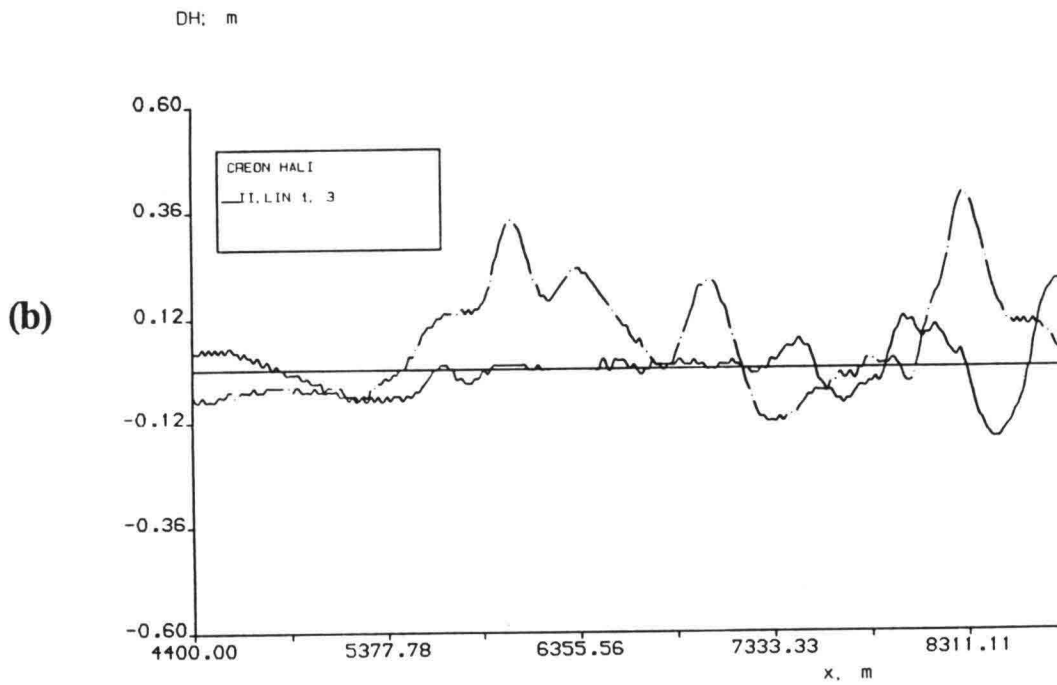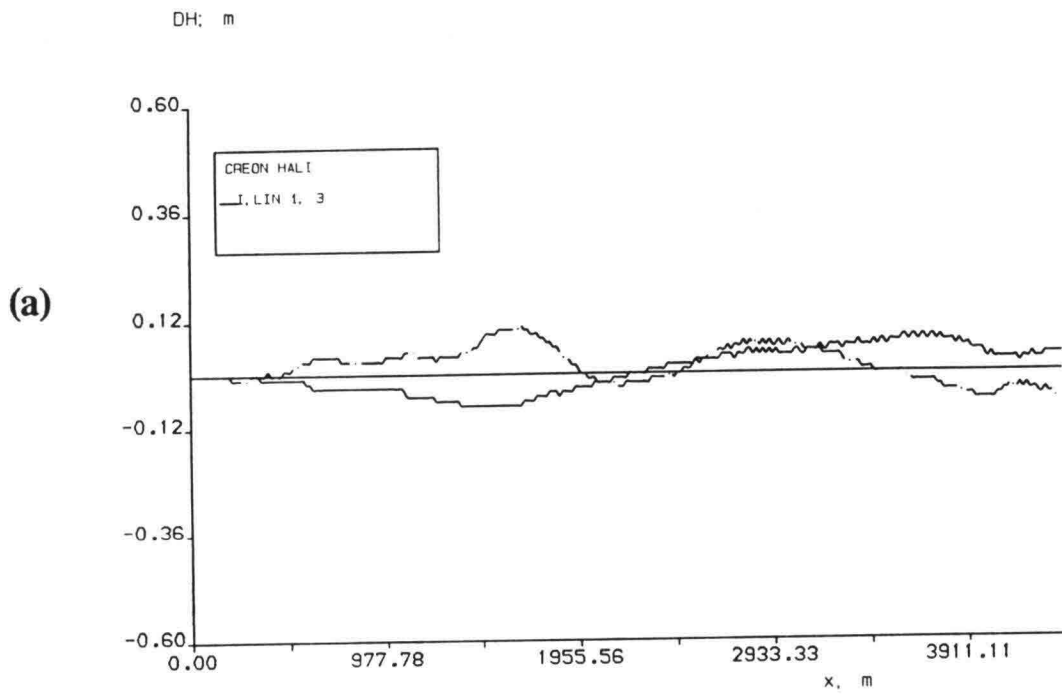
Fig. 5.5 The difference between *irregular* and monochromatic waves $\Delta H = H_{sp} - H_{mo}$, a) in offshore region, b) shoal region.

80

Fig. 5.5(continued) c) inshore region.

(a)

(b)

Fig. 5.6 Hindcast number two at 22:00 Oct. 14, 1982, the incident waves are considered as *irregular*, the computation without 'h_n' effect. a) wave field. b) wave height along line 1 and line 3 in offshore region.

Fig. 5.6(continued) c) line 1 and line 3 in shoal region, d)
inshore region.

83

(a)

(b)

Fig. 5.7 Hindcast number two at 22:00 Oct. 14, 1982, incident waves are considered as monochromatic, the computation without 'h$_n$' effect. a) wave field. b) wave height along line 1 and line 3 in offshore region.
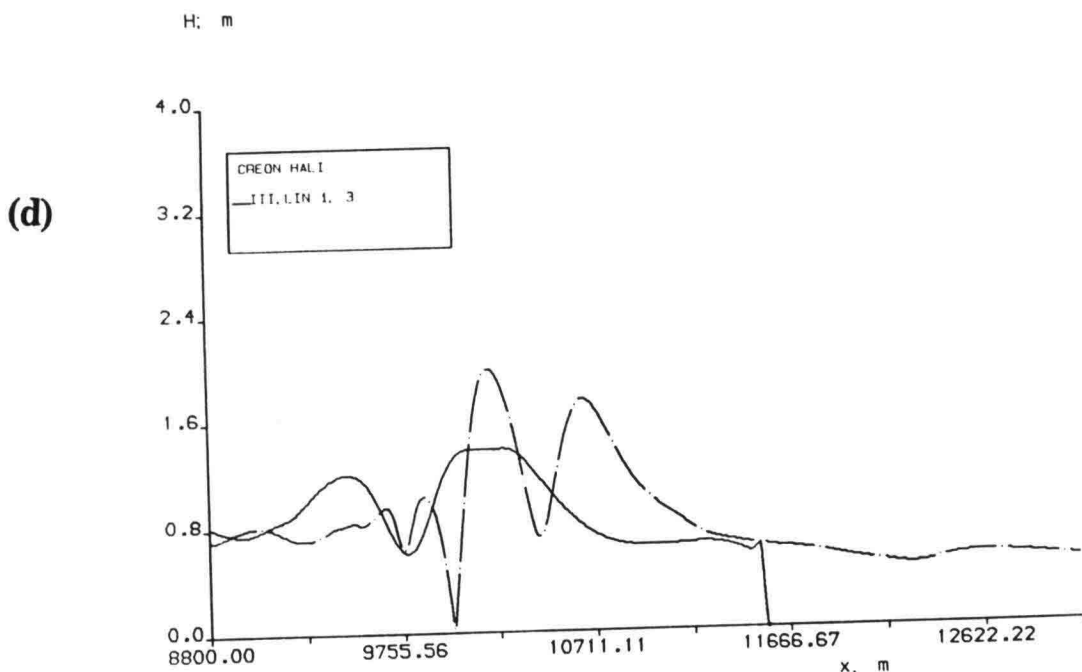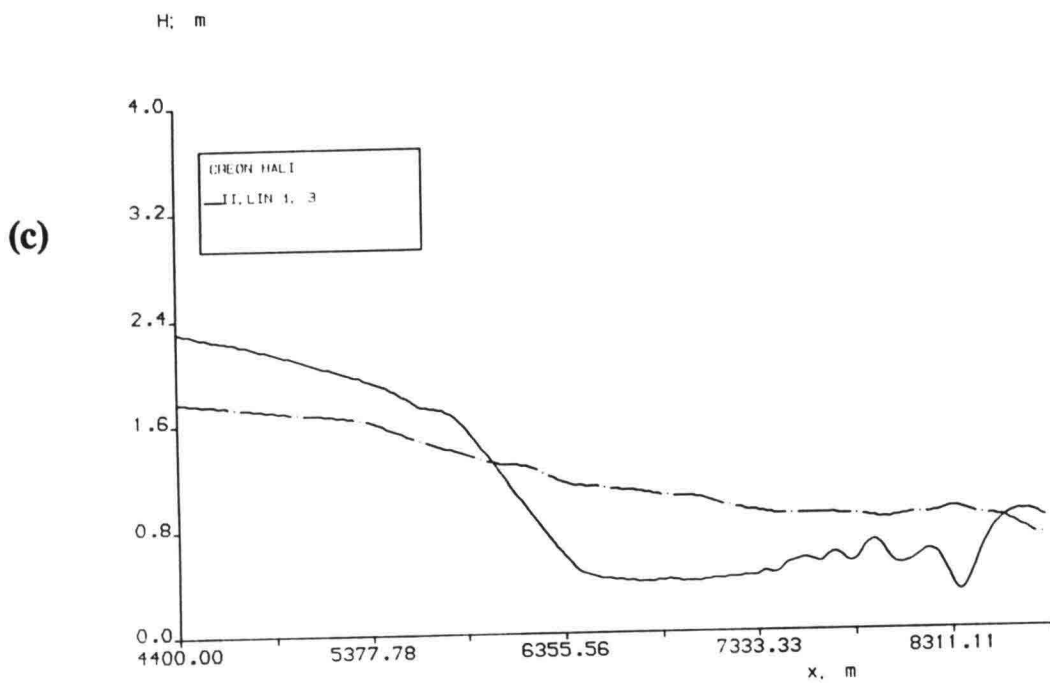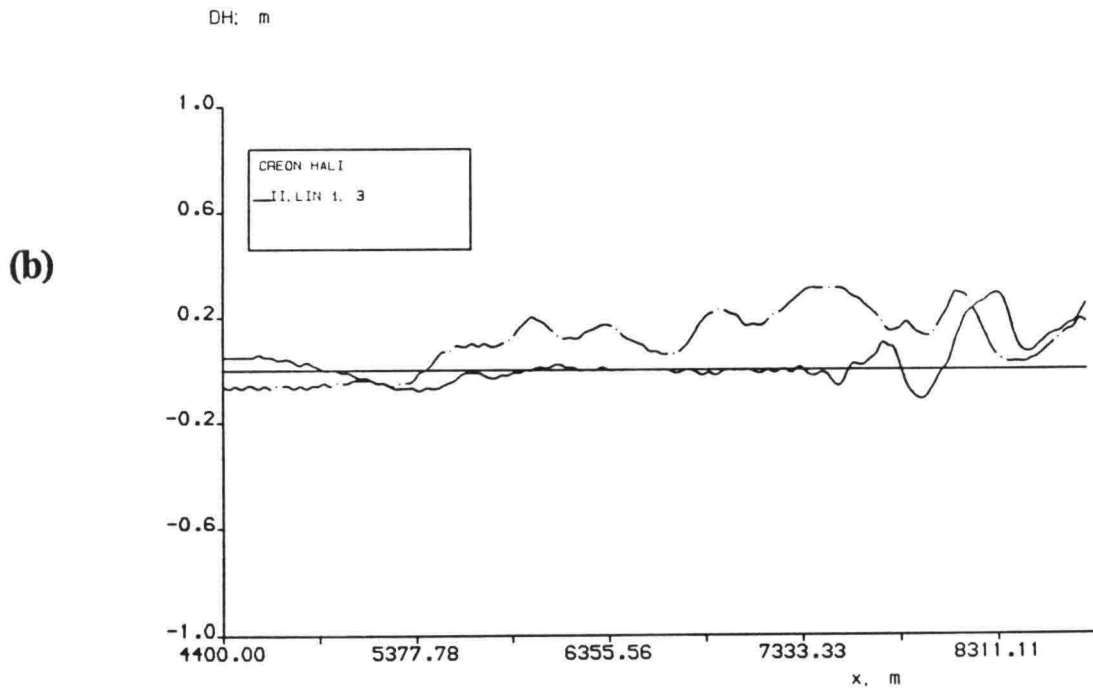
(c)

H: m

(d)

H: m

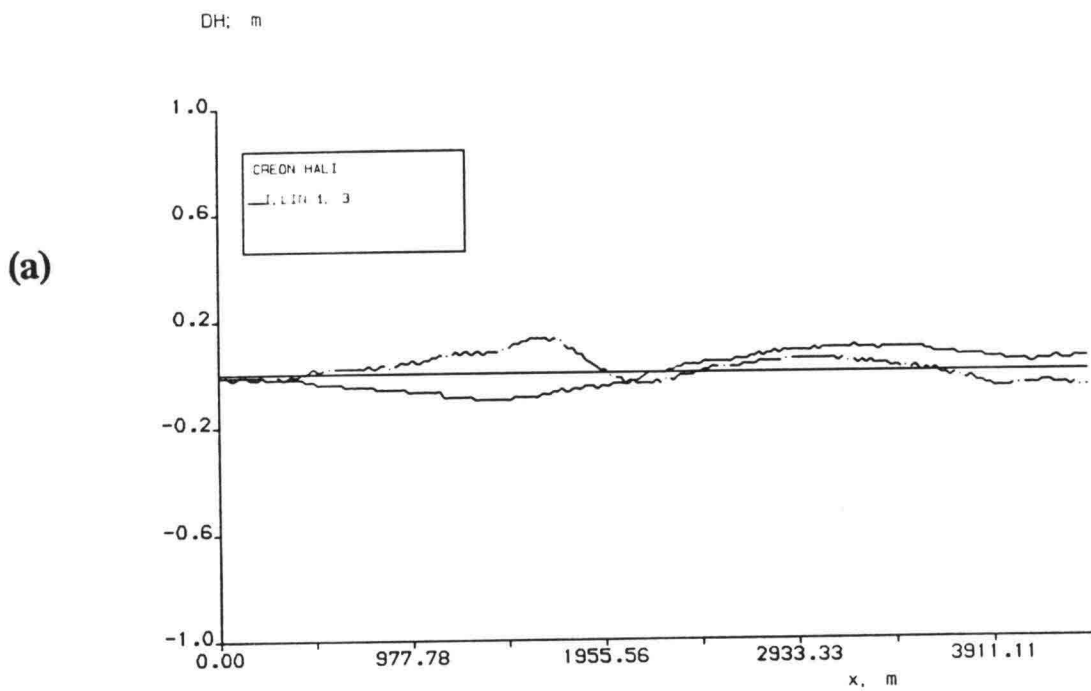Fig. 5.7(continued) c) line 1 and line 3 in shoal region, d) inshore region.

DH: m

CREON HALI
—I.LIN 1. 3

(a)

DH: m

CREON HALI
—II.LIN 1. 3

(b)

Fig. 5.8 The difference between *irregular* and monochromatic waves
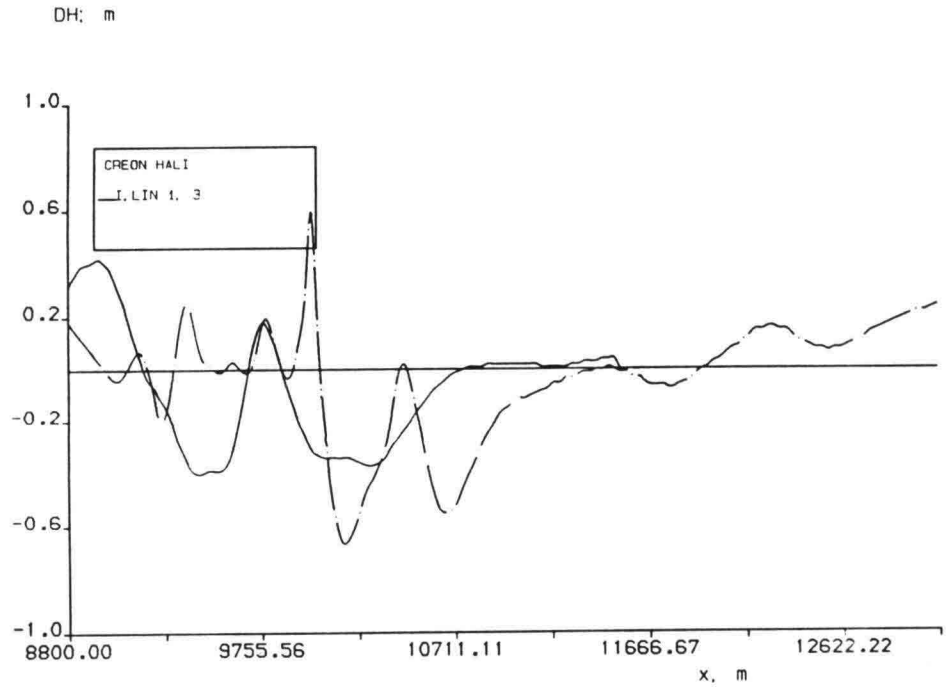$\Delta H = H_{sp} - H_{mo}$, a) in offshore region, b) in shoal region.

86

(c)

DH: m

Fig. 5.8(continued) c) inshore region.